POLITECNICO DI MILANO

Facoltà di Ingegneria Industriale

Dipartimento di Scienze e Tecnologie Aerospaziali

Corso di Laurea in
Ingegneria Spaziale

BURNING AND AGGLOMERATION OF ALUMINISED ADN/GAP SOLID PROPELLANTS

Relatore: Prof. Luigi T. De Luca

Co-Relatore: Dipl. Ing. Volker Weiser

Tesi di Laurea di:

Andrea Franzin Matr. 766210

Anno Accademico 2012 – 2013

To my brother,
whose curiosity has kept alive in me the passion for science

Acknowledgements

The first thank must be given to my professor Luigi De Luca, who instilled in me the passion about its matter, and gave me the possibility to do what I love to do. He open me this world and left to a second person, Volker Weiser, to be my “Virgilio” in this scientific field; so, only one thank to Volker will be not enough. Other really big thanks must be given to the scientists who help me in the writing of this work, Stefan Kalzenberg and Evelin Roth, who, despite their busy schedules, have find the time to take care about my bad English and my scientific gaps.
Big thanks also to the people who work in SPLab, for their availability, and in particular Filippo Maggi and Stefano Dossi for their teaching.
But I have to say a big thanks to everyone in Fraunhofer-ICT, starting from André Lity, Diana Bieroth, and the beloved Heidrun Poth, who help me during the experiments and also out of the laboratory. Thank to Angelika Raab, who try to explain me in a simple way the complicate world of spectroscopy (and computers). Big thanks to Andrzej Koleczko, Erich Walschburger, Heike Schuppler, Karin Wacker and Sebastian Knapp for the weekly lunches together that make me felt like at home. Thanks again to Volker Gettwert and Sebastian Fisher, for the help and the patience to prepare the sample for my experiments, and for the “diligent” reply at my question.
After all, I have to say thank to this entire working group, because I was expected to find colleagues, instead I found friends.

In Italy, first of all I have to say “grazie” to my beloved parents and to my brother, who take care about me despite the distance... and spend their summer with me in the sunny and funny Pfinztal. Other thanks must be done to the friends that did not abandoned me, thank to Marco Pellegrino, Stefano Mazzú, Edoardo Marzi, Emanuele Campagnolo, Carlo Moretti, for their everyday presence.

This work is sponsored within the framework of the European Union Seventh Framework Programme (FP7/2007-2013) under grant agreement number 262099, named as HISP-Project (High performance solid propellants for In-Space Propulsion) and scientific budget of the Fraunhofer Institut für Chemische Technologie (ICT).

Abstract

The aims of this work is to characterize a new type of propellant proposed as part of a research project called HISP-Project (High performance solid propellants for In-Space Propulsion) sponsored by European Union with particular focus to agglomeration. This propellant uses as the oxidizer ammonium dinitramide (ADN), as binder the glycidyl azide polymer (GAP) and different types of aluminium powders. Commercial propellants contain ammonium perchlorate (AP), and the substitution with ADN ensures the absence of chlorine in the combustion products.
For all formulations combustion tests were performed in a pressure range between 0.1 and 13 MPa.
Six formulations containing ADN/GAP/Al with 60% oxidiser, 24% binder and 16% fuel were studied. Four formulations were studied in order to investigate the influence of different types of aluminium particles: aluminium powder of 5 µm and 18 µm, as well as pure nano-aluminium and an activated nano-aluminium. Two further formulations contain ADN of different prill sizes: one with an average particle size of 228 µm, and the other bimodal distribution of 208 µm and 55 µm (70:30). The latter called H32 is the selected propellant used in HISP-project and was investigated in more detail. Both formulations contain aluminium with average size of 18 µm.
The combustion tests results in a ballistic exponent of about 0.58 for all the formulations containing 18 µm aluminium particles and 0.52 for 5 µm. At the operating pressure of 7 MPa, all four formulations show a burning rate between 25 and 33 mm/s. The maximum burning rate was observed for the formulation containing ADN of 208 µm and aluminium powder of 18 µm (33 mm/s) and the lowest was performed by the formulation containing the larger prills (25.3 mm/s).
Emission spectra in UV to NIR range shows temperatures of 2550 to 2650 K over the selected operating pressure range. These temperatures are between the melting point of alumina and the boiling point of aluminium at standard conditions. The proximity of the boiling temperature of aluminium explains the finding of hollow agglomerate, formed only by a shell of alumina.
The size of the agglomerates generated from these four propellants was determined using video analysis and indicate the tendency to form agglomerations larger than the commercially available AP/HTPB/Al propellants.
Another study has been carried out for two further ADN/GAP formulations containing 16% and 28% aluminium hydride, known as Alane. The composition with the larger amount of alane features in an “exotic”

combustion behaviour with formation of agglomerations in the order of two millimetres. The other Alane-based formulation formed agglomerates slightly larger than the aluminized formulations. The hypothesized enhancement of specific impulse replacing aluminium with alane is more than 12 s. But two-phase flow losses may also be large and jeopardize the advantage of this gain.
These studies are preceded by the investigation of pure ADN/GAP formulations. Particular attention was paid to the influence of oxidizer particle sizes on the burning rate. As result the burning rate seems to be lower at high pressure for propellants containing smaller oxidiser size, despite at low pressure they present about the same burning rate. The Vieille's law fitting results in a pressure exponent of 0.49-0.50 for the formulations containing smaller oxidizer grains, and a pressure exponent of about 0.63 for the bigger ones. This is opposite to commercial AP/HTPB propellant.
Parallel to these studies an analysis of the thermodynamic parameters that influences the size of agglomerates was performed by investigating 7 trial propellants formed by AP, GAP and aluminium according to adiabatic temperature, oxygen balance and enthalpy of formation. A correlation between increasing flame temperature and growing of agglomeration size was found.
A further investigation using GA/BAMO as binder instead of GAP indicated lower agglomeration sizes accompanied by better mechanical properties as well.
Four models based on different drag coefficient estimation are investigated in order to better understand the physical behaviour of particle detachment from burning surface. The approximation with 2 phase flow model of drag coefficient results in a trend in accordance with the experimental observations despite it results to be out of its recommended utilization domain.

Keywords: ADN/GAP, HEDM, aluminized solid rocket propellants, agglomeration, Alane, 2P loss

Sommario

Questo lavoro si prefigge l'obiettivo di caratterizzare il nuovo tipo di propellente proposto nell'ambito del progetto di ricerca noto come HISP-Project (High performance solid propellants for In-Space Propulsion).
Questo propellente utilizza come ossidante la dinitroammina di ammonio (ADN), il polimero glycidyl azidico (GAP) come legante e diversi tipi di polveri di alluminio come combustibile.
Il cambio di ossidante rispetto alle normali formulazioni contenenti perclorato di ammonio (AP), garantisce l'assenza di cloro nei prodotti di combustione, generando quindi un propellente "environmental friendly" che non rilascia le notevoli quantità di acido cloridrico rilasciato dai propellenti utilizzati usualmente.
Le polveri di alluminio studiate sono dell'ordine del micrometro e del nanometro, e sarà trattata anche polvere di alluminio attivata attraverso il deposito di acido stearico sulla superfice.
Il totale delle formulazioni contenenti ADN/GAP/Al studiate è sei, tutte contenenti il 60% di ossidante, il 24% di legante ed il 16% di combustibile; quattro formulazioni sono state studiate allo scopo di definire il comportamento di diversi tipi di combustibile, e sono state quindi prodotte formulazioni contenenti polvere di alluminio micrometrico con dimensione media di 5 µm, con dimensione media di 18 µm e due contenenti polveri di alluminio nanometriche, una non attivata e l'altra attivata.
Le rimanenti due formulazioni contengono ossidanti di diversa granulometria, una fornita e lavorata dal FOI in Svezia, con granulometria media di 228 µm, e l'altra lavorata dall'ICT con distribuzione bimodale con rapporto 70:30 per dimensioni di 208 µm e 55 µm.
Entrambe queste ultime formulazioni contengono alluminio micrometrico con dimensione media di 18 µm.
Le formulazioni contenenti alluminio micrometrico hanno mostrato proprietà meccaniche sufficienti alla loro produzione. I test di combustione eseguiti per queste formulazioni hanno evidenziato un esponente balistico attorno a 0.58, a parte per quella contenente polvere di alluminio di 5 µm per la quale è stato calcolato 0.52. Supposta una pressione operativa di 7 MPa, tutte e quattro le formulazioni con alluminio micrometrico si attestano tra i 25 ed i 33 mm/s. Il massimo valore è stato raggiunto dala formulazione contenente ADN di 208 µm e alluminio di 18 µm (33 mm/s), mentre il valore minimo è stato riscontrato per la formulazione con ADN di maggiori dimensioni.
Le misure di temperatura hanno evidenziato che tutte e quattro le formulazioni, a 7 MPa, sono comprese tra i 2550 e i 2650 K. Questa

temperatura è compresa tra le temperature di fusione dell'allumina e di ebollizione dell'alluminio, particolare importante poiché la vicinanza della temperatura di ebollizione dell'alluminio spiega il ritrovamento di agglomerati sferici vuoti, formati di solo guscio di allumina, oppure contenenti un alto grado di porosità. Questi agglomerati sono stati raccolti e analizzati tramite l'uso di SEM solo per il propellente con distribuzione bimodale di ossidante.
La dimensione degli agglomerati generati da questi quattro propellenti è stata determinata attraverso la video-analisi ed hanno rivelato la tendenza a formare agglomerazioni più grandi rispetto ai propellenti commercialmente disponibili.
All'infuori dell'HISP-Project, sono state analizzate due formulazioni contenenti idruro di alluminio, noto come alane; combustibile interessante dato il suo basso peso specifico e la proprietà di abbassare notevolmente la massa media dei prodotti di combustione grazie all'alto contenuto di idrogeno, innalzando notevolmente l'impulso specifico.
Le due formulazioni hanno di differente il contenuto di alane, una ne possiede il 28% mentre l'altra ha la composizione uguale ai propellenti alluminizzati con la semplice sostituzione del combustibile.
La composizione con maggior quantità di alane ha dato origine ad agglomerazioni dell'ordine di due millimetri esibendo una combustione "esotica", mentre l'altra formulazione ha formato agglomerazioni leggermente più grandi delle formulazioni alluminizzate. L'ipotizzato incremento d'impulso specifico ottenibile con la sostituzione del combustibile, più di 12 s.
Questi studi sono preceduti da uno studio della formulazione pura, cioè formata solo da ADN/GAP, nella quale si è posta particolare attenzione all'influenza della granulometria dell'ossidante sul burning rate. È stato osservato un andamento opposto a quello usuale (a valori di pressione superiori ai 5 MPa), poiché la diminuzione del diametro della granulometria viene riflesso in una diminuzione del burning rate invece che in un aumento, come è solito dei propellenti in commercio. Infatti l'interpolazione con la legge di Vieille risulta in un esponente balistico compreso tra 0.49 e 0.50 per le formulazioni con granulometria di ADN di 40-50 μm, ed un esponente balistico di circa 0.63 per le formulazioni contenenti ADN di dimensioni maggiori.
Parallelamente a questi studi è stata effettuata una analisi dei fattori termodinamici in correlazione con la dimensione degli agglomerati, ed in particolare sulla temperatura di fiamma, il bilancio di ossigeno e l'entalpia di formazione, utilizzando 7 propellenti prova formati da AP, GAP, e alluminio.
Lo studio ha rivelato che la temperatura di fiamma gioca un ruolo molto importante nei processi di agglomerazione ed in particolare: maggiore è la

temperatura, maggiore sarà il diametro degli agglomerati formati. Un ulteriore risultato ottenuto é che la sostituzione del legante da GAP a GA/BAMO dà luogo ad agglomerazioni di dimensioni minori, incrementando anche le proprietà meccaniche del propellente.
Tutte le prove di combustione sono state effettuate in un range di pressione almeno tra 0.1 e 13 MPa.
Viene poi proposto uno studio sul distacco delle particelle dalla superficie di combustione, attraverso la considerazione di diverse espressioni del coefficiente di resistenza aerodinamica. Le relazioni ottenute adottando il modello empirico di coefficiente di resistenza aerodinamica valido per il flusso bi-fase si sono rivelate in accordo con le osservazioni sperimentali, nonostante sembra che questo modello non sia valido nell'intorno dell'agglomerato.

Parole chiave: ADN/GAP, HEDM, propellenti solidi alluminizzati, agglomerazioni, Alane, Perdite di flusso bifase

Table of Contents

List of Figures

List of Tables

Nomenclature

Latin Letters

2P	Two-Phase
a	Pre-exponential factor
a_{cc}	Acceleration
Cd	Drag Coefficient
C_x	Concentration
D	Diameter of incipient at the first appearance
d_0	Initial diameter
d_p	Particle Diameter
d_t	Throat Diameter
I_{sp}	Gravimetric Specific Impulse
n	Ballistic exponent
P	Pressure
P_{cc}	Combustion Chamber's pressure
R	Perfect Gas Constant
r_b	Burning rate
Re	Reynolds number
r_p	Particle Radius
S	Exposed surface
T	Temperature
t_b	Burning temperature of aluminium particle
t_{cc}	Residence time in the combustion chamber
T_s	Burning Surface Temperature
u	Velocity of the particle

Greek Letters

α	Constant of burning time equation
ε	Geometric expansion ratio
δ	Substitution Variable
η	Constant of burning time equation
μ	Viscosity
ξ	molar fraction of condensed products

ρ_c	Density of condensed phase
ρ_g	Density of gas phase
ρ_p	Density of particle

Acronyms

ADN	Ammonium DiNitramide
ALEX^{TM}	Nanosized Aluminum obtained by electrical explosion of wires
AN	Ammonium Nitrate
AP	Ammonium Perchlorate
BAMO	Bis-Azide Methyl Oxetane
BPS	BisPropargyl Succinate
CCP	Condensed Combustion Product
DBTDL	DiBuTyltin DiLaurate
EDX	Energy Dispersive Element analysis
FOI	Swedish Defence Research Agency
GAP	Glycidyl Azide Polymer
HDI	Hexamethylene Di-Isocyanate
HEDM	High Energy Density Materials
HISP	High performance solid propellants for In-Space Propulsion
HMX	Cyclotetramethylenetetranitramine
HTPB	Hydrossil Terminated PolyButadiene
ICT	Institute for Chemical Technology
IPDI	IsoPhorone Di-Isocyanate
MIR	Mid-Infrared Range
NIR	Near Infrared Range
PBAN	PolyButadiene AcryloNitrile
PDL	Pressure Deflagration Limit
PU	PolyUrethane
SEM	Scanning Electron Microscope
SRB	Solid Rocket Booster
SRM	Solid Rocket Motor
TAGN	TriAminoGuanidine Nitrate
TMETN	TriMethylolEthaneTriNitrate
UV	UltraViolet Wavelength Range
VIS	Visible Wavelength Range

Chapter 1

Introduction and Objectives

1.1. Motivations of the Work

The growing public awareness toward the environment problem, which has driven the last decades of aeronautical research to find a “green fuel”, could not leave out the scope of rocket propulsion. The solid propellant formulations, commonly used for space access until today, contain mostly ammonium perchlorate in combination with hydroxyl terminated polybutadiene (AP/HTPB). One of the main combustion products is hydrogen chloride (HCl) that should be considered critical under pollution aspects, since it contributes to acid rain and causes environmental damage and corrosion around the launch base. The boosters that contain this type of solid propellants, burn in the order of tons per second, releasing large quantities of HCl, which can reach more than 20% of the reaction products at the nozzle. Also aluminium chloride and other intermediate reaction products, which are not more than 2%, will cause additional serious problems when the huge quantities of expelled mass are considered.
These are the main motivations to develop a new kind of green propellant that possibly will feature better propulsive performance as well.
Ammonium dinitramide (ADN) seems to be a promising substitute to ammonium perchlorate; being chlorine free, one of the main pollution responsible can be eliminated. Due to its lower oxygen balance of +25.8%, instead of +34.04% for AP, an energetic binder is needed to compensate this handicap. The main problem of ADN is his reactivity with some polymeric binders or at least the ingredients of the polymerization process. To overcome this problem, coated ADN prills shall be used.
An appropriate binder is glycidyl azide polymer (GAP), an energetic polymer treated with bis-propargyl-succinate and isocyanates. Even when GAP-diol is a more viscous pre-polymer it needs less oxidiser and allows higher Al filler contents as HTPB.
To achieve a gravimetric specific impulse higher than the commercial available propellants also different type of metal fuels will be investigated.
The proposed fuels are micrometric aluminium, nanometric aluminium, activated aluminium and aluminium hydride.

This kind of propellant has the potentiality to increase of more than 30% the payload mass of the Vega launcher, 17% of payload mass of an apogee motor and 18% of gain in mass for a mars ascent vehicle.

1.2. Objectives

This propellant is intended to be used in in-space applications, and end burning grain will be a common situation. To realize end burning grain is required a burning rate as low as possible and good mechanical properties. So, two requirements must be satisfy:

- Burning rate in the range of 7 to 15 mm/s (at 7 MPa).
- Mechanical properties at a similar level of commercial propellant.

The main objective of the present work is to analyse the combustion behaviour: the burning rate, the temperature and, in particular, the agglomerations of metal particles of this type of new propellants.
A parallel study on formulations based on AP, GAP and aluminium will be performed in order to understand better the influences on the agglomeration behaviour and particle size.
This study intends to analyse what are the thermodynamic parameters that influences the agglomerations as enthalpy of formation, adiabatic flame temperature and oxygen balance.

1.3. Structure of the Work

This work has been performed completely in Fraunhofer-ICT (institute for chemical technology) and will be organised in the following manner:

- **Chapter 2 – State of the Art**: this chapter will be a presentation of the state of the art about the different component of the presented propellant and a brief introduction to the phenomenon of agglomeration;
- **Chapter 3 – Investigated Formulations**: in this chapter will be presented the components used inside the formulations and the methodology followed in order to select the appropriate propellants to test;

- **Chapter 4 – Experimental Technique:** the purpose of this chapter is to explain the instruments and the measurement techniques used for the characterization of the formulations;

- **Chapter 5 – Experimental Results:** it will be a schematic presentation of the obtained results divided by type of formulations;

- **Chapter 6 – Discussion of the Results:** here the results presented in the previous chapter will be discussed and refined;

- **Chapter 7 – Agglomeration Detachment Model:** it would be an analytical analysis of the parameter influencing the detachment of particle from the burning surface, obtained through the consideration of different drag coefficient models;

- **Chapter 8 – Conclusions and Outlook:** it would be a comprehensive conclusion of the results obtained in this work and possible future task.

Chapter 2

State of the Art

The state of the art about the combustion of propellants formed by ammonium dinitramide (ADN, $NH_4N(NO_2)_2$) as oxidizer, glycidyl azide polymer (GAP, $C_3H_5N_3O$) as binder and metal additives is presented in this chapter.

2.1 Overview on ADN/GAP propellant components

Some publications about the combustion and the possible use of investigated mixtures, formed mostly by 60% ADN, 24% GAP and 16% metal, were presented in the course of the project FP7/2007-2013 HISP (High performance solid propellants for In-Space Propulsion) at different conferences and in different journals by the participants involved [1]-[5]. Nonetheless, a huge amount of information about each component of the presented mixture is available both in eastern and western world.

GAP is one of the possible binder candidates for the next generation of solid propellants and hybrid rocket fuels, due to its high energy density, its positive heat of formation (between 960 J/g and 1380 J/g [6]), its high flame and burning surface temperatures (900-1000 K and 700-750 K [8] for pure GAP at 6 MPa, respectively), its steady-state self-combustion (Vieille's law of pure GAP burning velocity $r(cm/s) = 0.14\ (P/P_0)^{0.52}$ [6] (pressure in bar)) and its costs.

GAP is obtained by replacing chlorine atoms of polyepichlorohydrin with azide groups ($-N_3$) and was developed by Guy Ampleman at the end of 1980s in Canada [7].

It is an azide polymer with one azide group N_3 in the structural unit, as shown in Fig. 2.1. The azide group is the most important group since it gives the property of self-burning to this polymer without oxidizer. Starting at 0.3 MPa, it precisely releases this energetic group in the area of the first combustion zone.

A lot of investigations were made about this energetic polymer and a big amount of experimental results, most of the time discordant, are available in literature. The work of Kubota in [9]-[11] deserves special attention. He makes a comprehensive study about the burning behaviour of this energetic polymer. Especially [10] shows that the combustion of pure GAP is mostly governed by the release of nitrogen and a huge amount of heat. This first

reaction affects the plastic nature of the polymer creating small fragments on the burning surface, and from this fragments, the real "oxidation" takes place releasing a smaller amount of heat as a second step of reaction. This model is explained in detail by Hori in [8].

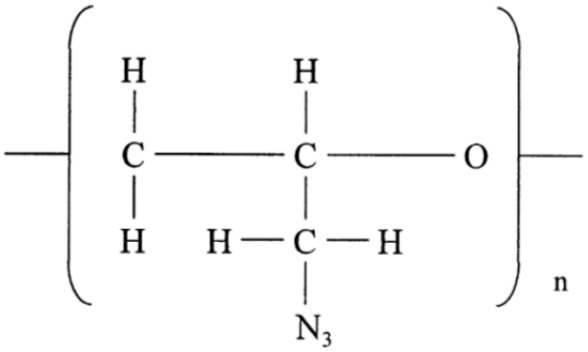

Fig. 2.1. Chemical structure of Glycidyl Azide Polymer [10]

The huge amount of gases created by the pyrolysis of GAP makes it attractive for gas generation purposes, and in fact, its common use is in airbags [13].
Further investigations for the use of GAP as a monopropellant for low cost rockets were made. But on the one hand because of the strong amount of soot created, and on the other hand the combustion that sometimes leave a carbon structure as inert mass, it does not find big success for space application.

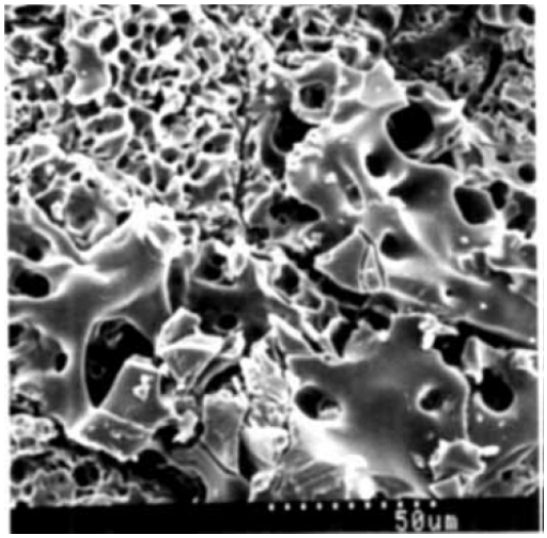

Fig. 2.2. Quenched burning surface of GAP [8]

The importance of the combustion behaviour of GAP lies in the type of burning surface with pores above and below it created by the decomposition of the azide group releasing nitrogen gas, as shown in Fig. 2.2.

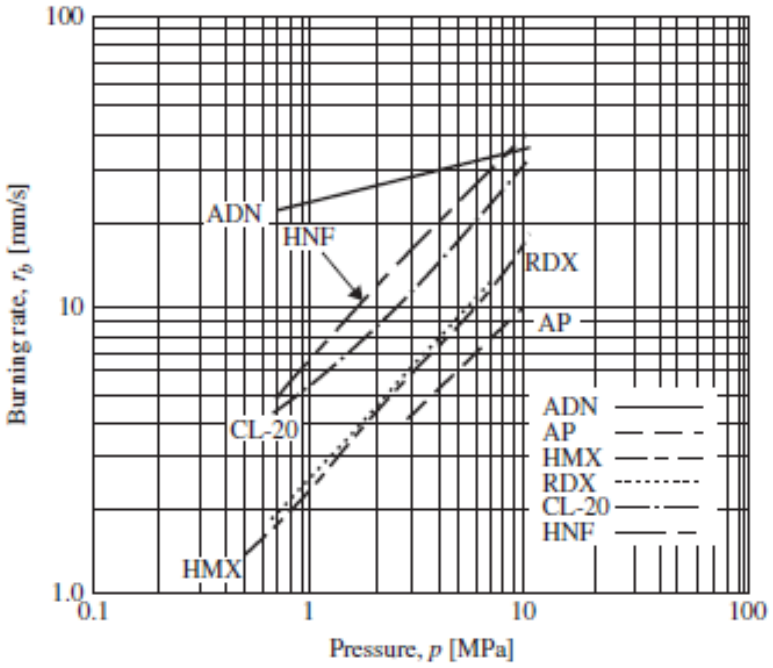

Fig. 2.3. Steady burning rate of pure ADN in comparison with other monopropellants at ambient temperature [15].

ADN was first synthetized in Russia (Zelinsky Institute of Organic Chemistry, Moscow,1971), then independently in USA (Strategic Resource International Inc., 1988) during the years of the cold war, and it was proposed as a monopropellant [6][14][15][17] (I_{sp}=216.9 s under shifting equilibrium assumption, expansion ratio 70:1 calculated by ICT Thermodynamic code [18]). But due to its complex synthesis and resulting expensive production costs, high hygroscopicity [16], complex burning behaviour [20], high self-deflagration rate [15] (Fig. 2.3), low melting point [17] (365–367 K), low decomposition temperature (408 K), and strong initial temperature sensitivity [17] (Fig. 2.4), it did not find a wide spread use in civilian space applications. ADN monopropellant has some unique features, like the superior ballistic properties (high burning rate and low pressure sensitivity, low impact and friction sensitivity), low signature, and full environmental respect (the only combustion products are nitrogen, oxygen and water) and unique physical and chemical properties compared to other solid oxidizers, such as high condensed phase heat capacity of 2.5 J/g/K, low surface temperatures, good oxygen balances (25.8% [9]) and

a pressure deflagration limit (PDL) around 0.2 MPa. Further information about combustion of ADN monopropellant is reported in [3] as an interesting review, [19] for a detailed model on chemistry point of view and [20]-[21] as a complete description of burning behaviour in dependence of pressure.
For these reasons the research and development of this kind of oxidizer was carried on. In fact during the following years, mostly FOI (Swedish Defence Research Agency) and Fraunhofer Institute for Chemical Technology (ICT) have dedicated research and have also developed different technologies to prill ADN starting from the raw material, generally salt crystals as shown in Fig. 2.5.
The synthesis path which lead to the raw ADN crystals pass through a very complex chemical process, better discussed in [22], in which the last step includes potassium dinitramide (KDN, $KN(NO_2)_2$) and ammonium sulfate, as shown in Eq. 2.1.

$$2KN(NO_2)_2 + (NH_4)_2SO_4 \rightarrow 2NH_4N(NO_2)_2 + K_2SO_4 \qquad (2.1)$$

The solid product K_2SO_4 at the end can be filtered. The synthesized ADN can be extracted from the solution by washing with solvents and drying to obtain the white ADN salt crystals [23][23].

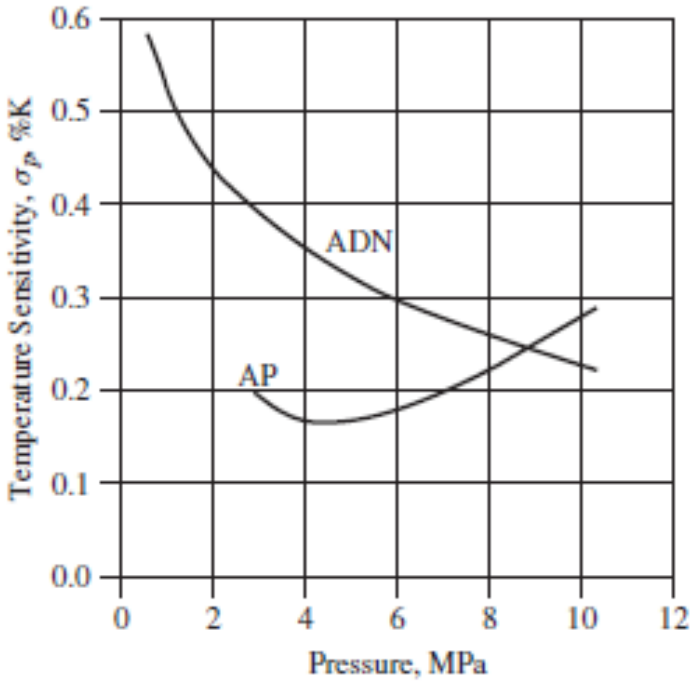

Fig. 2.4. Initial temperature sensitivity vs. pressure of ADN in comparison with other propellants [17].

From this reaction path, it is possible to understand why potassium is one of the main impurities of ADN, which have, in general, a high purity level (around 99%). But potassium shows up during combustion because of its high-intensity atomic lines in the spectrum and its colour.
Particular attention has to be dedicated to the prilling process because it is a key factor to obtain propellants with the necessary oxygen balance and a good combustion process.

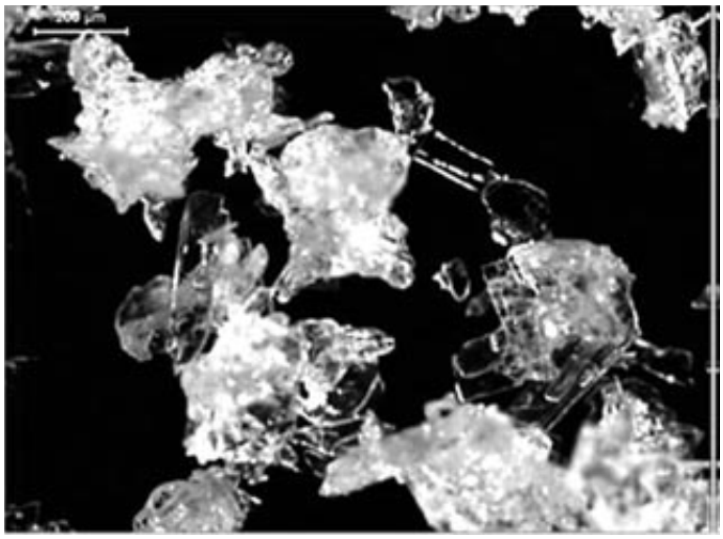

Fig. 2.5. Raw ADN salt crystals [24].

The technologies developed by FOI and ICT to prill ADN are based on different physical principles ([3]) though both processes are operating with molten ADN. The main difference of the two processes is the way to generate the molten droplets. At ICT the complete process is performed in the liquid state and the generation of the droplets is performed in a hot emulsion. The cooling of this emulsion starts the nucleation and crystal growth. The recrystallization creates quite homogeneous and round prills [24][25].
At FOI, molten ADN is pumped to a spray nozzle, where the molten droplets are generated by pressure atomization. The recrystallization behaviour of ADN makes it necessary to collect the molten droplets in an anti-solvent for recrystallization [26].
Afterwards, the prills (Fig. 2.6) are separated, washed and dried in both cases.
Both of the two presented ingredients were separately used in the past in the western world, sometimes proposed as monopropellants, but most of the time they found some application as oxidizer and binder independently from each other.

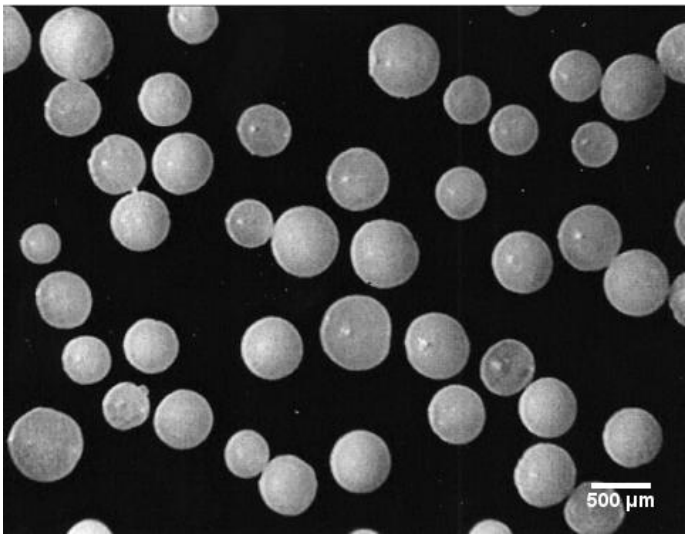

Fig. 2.6. Recrystallized ADN prills (emulsion crystallization process) [25].

2.2 Composite Solid Propellants

The smokeless property of ADN, in addition to its non-pollutant combustion products has driven the research to use it as a component of the gas generators in automotive airbags.
The importance of the prilling procedures of ADN salts reported before lies in the fact that the raw material does not guarantee a loading level sufficient for the purpose of creating an ADN-based propellant with good mechanical properties and good oxygen balance. An Increase of the available amount of ADN inside the solid propellant, which can be reached using bimodal prills distribution, can lead to a mixture with a sufficient amount of oxygen to oxidize enough metallic and non-metallic components to achieve maximum specific impulse, in accordance to Pak [27]. Obviously, this huge amount of oxidizer, which should be around 90% in mass, is not achievable, but starting from the "environmentally friendly" purpose of these ADN-based propellants, and from the presented advantages previously shown, the research and development was encouraged to test ADN oxidizer with various quantities of different binders during the last fifteen years.
The first published work about ADN-based propellant in western world was done by Price (1998) in [14] and then by Weiser, in [28], who use a very small percentage of paraffin (9% in mass) as binder. They compared the obtained results with the results obtained using ADN as monopropellant. This study revealed plateau behaviour around a burning rate of about 18-20 mm/s in a pressure range between 2 and 5 MPa. This result is partially in agreement with the findings of Sinditskii in [20][21]

five years later. The main difference between the two studies is the interpretation of the result: Sinditskii (only 0.2% of paraffin in mass) interpreted the high scattering behaviour in this pressure range as the typical mesa-burning behaviour of ADN ([19]), instead the data shown by Weiser outline a plateau with high scattering for ADN/paraffin propellant and almost plateau behaviour without scattering for ADN.
ADN-based propellants were extensively studied with different kinds of binder also in USA, mostly by Price [14], who observed a liquid layer on the burning surface (a liquid layer of the same type as created by AN-based propellants) for mixtures containing ADN and polyurethane (ballistic exponent n=0.32); the luminous flame of ADN/PU propellants appears detached from the burning surface, as in the case of double based propellants, but that was not observed in the propellants evaluated in the present work.
Some further investigations with some energetic binders have been performed on ADN. But mostly due to its cost and its incompatibility with most of the classical binders caused by their acidic nature [29], which makes a complex coating process of the ADN prills necessary to avoid undesirable reactions, it was preferred to use a binder, for which the compatibility was tested, precisely GAP.
Since the azide polymers, like GAP or BAMO (bis-azide methyl oxetane) are energetic materials with the property of self-burning, their use as a binder in a propellant formulation can increment the gravimetric specific impulse by more than 10% with respect to inert binders ([9]). Thanks to this aspect their use is well investigated and some of them found current application. Formulations of ammonium perchlorate (AP) and GAP were tested due to the theoretical specific impulse gain (about 12%) caused by the change of binder with respect to HTPB (hydroxyl terminated polybutadiene) and a higher loading level of oxidizer that the new binder allow (formulation loaded up to 86% of AP).
Some studies confirm that the addition of AP and in particular its combustion products, as oxygen rich components, interact with fuel rich decomposition products of GAP, producing a heterogeneous flame structure [9][10] (behaviour not observed during experimental campaign).
Other noteworthy types of High Energy Density Materials (HEDM) used in conjunction with GAP for propellants are octogen (HMX or cyclotetramethylenetetranitramine), ammonium nitrate (AN) and triaminoguanidine nitrate (TAGN), investigated by Kubota in [9]-[10][11][30].
As an overall rule found by Kubota, the different oxidizers burn as monopropellants at the surface of the propellant, and only the reaction products interact with the gaseous decomposition products of GAP.

The HMX/GAP propellant (80:20) features an adiabatic flame temperature of 2574 K that increases rapidly with increasing the amount of HMX in the mixture. The combustion behaviour shows a flame stand off-distance which exponentially decreases when pressure increase. So it is possible to state that the increase in temperature due to HMX governs the combustion behaviour and in particular the burning rate (n=0.82 and thermal sensibility σ_p=0.002 K^{-1}[9]) of this propellant.
The adiabatic flame temperature of TAGN/GAP (60:40) propellants is quite low, 1470 K, but the particularity of this HEDM is that the burning rate does not change also using different polymeric binders.
The low loading is due to the high amount of hydrogen contained in TAGN, that makes it, when mixed with GAP, a high energy density composite (n=0.79 and thermal sensibility σ_p=0.0042 K^{-1}, trend that degenerate rapidly reducing the amount of energetic filler to 20%: n=0.95 and thermal sensibility σ_p=0.01 K^{-1} [9]).
When GAP is mixed with AN, a completely different behaviour is observed. The exothermic decomposition reaction of GAP dominates the combustion process and supports the AN particles in their burning. The burning rate drastically decreases with the addiction of AN, in opposition to what is presented for HMX and TAGN, but a lower content of AN returns a combustion instability (n=1.05 for 30:70).
The burning rate at 70% AN is measured to 3.7 mm/s despite an adiabatic flame temperature of about 1950 K (n=0.55).

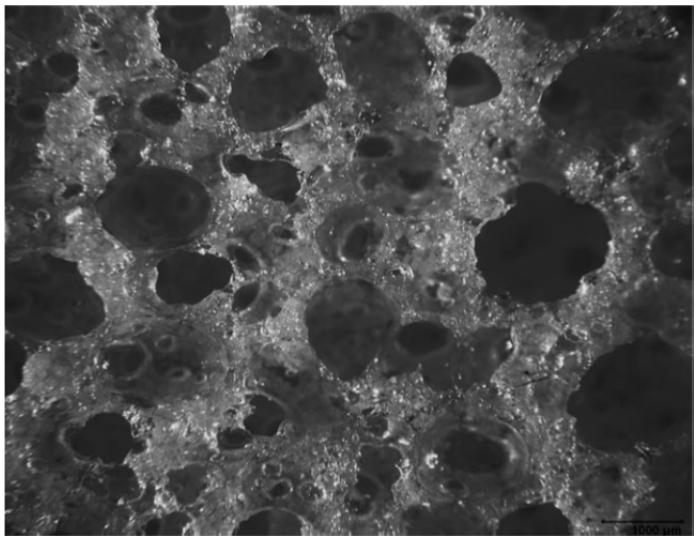

Fig. 2.7. Magnification of foam from ADN/GAP [31].

Without the use of an adequate catalyst the presented propellants seems to be far from finding an application, partly due to their performance, partly due to their instability.

For these reasons, for the compatibility with oxidizer and for the less-pollutant combustion products, a mixture was proposed formed by ADN/GAP with addiction of HMX and trimethylolethyltrinitrat (TMETN) as plasticizer [31].
The problem of this mixture was the high reactivity of ADN with the isocyanates used as curing agent, which creates a "foam propellant" showed in Fig. 2.7.
The problem of the reactivity of ADN with isocyanates was not resolved and up to now a solution for this inconvenience is still under research. Some steps forward are done in Fraunhofer ICT by Gettwert [32], who prepared a propellant, without HMX and without TMETN but with metal additives, for which the porosity is around 2-3%, so aligned with the normal level found in most known propellants as AP/HTPB. These ADN/GAP/metal propellants are precisely the ones characterized in the following chapter.

2.2.1 AP/HTPB Formulations

Several books (as example [9][32][34][35]) about this type of propellant are available in literature, and even more publications are available for the interested reader, since formulations containing AP/HTPB/metal are the most used ones around the world for space access and for in-space manoeuvres with solid rocket motors (SRM). It is the most known formulation, in particular with aluminium and different kinds of burning catalysts.
Famous examples of application are the European heavy launcher Ariane V (the boosters), the more recent Vega (first, second and third stage), the Apogee motor STAR-27, and many other's.
Several combinations of AP/HTPB/metal were investigated with addiction of microsize aluminium, nanosize aluminium, boron, magnesium, zirconium etc., and with different oxidizer/binder ratio with respect to the different missions for which the propellant is optimized.
It is possible to say that the most used metal as fuel is aluminium (30 μm certified for space), with a mass fraction between 12% and 18%. HTPB percentage is generally higher than 12% to reach very good mechanical characteristics, and the remaining part is mostly AP.
Generally the complete sum of curing agent, catalyst, plasticizer and cross linker is around 4% and it is worldwide accepted to include it into the binder fraction.
Since it is the most known propellant mixture, it should be useful as a reference to be compared with the different formulations under characterization, so, the general characteristics will be presented when necessary.

2.2.2 Green Propellants

Green propellants have been studied for many years to achieve an "environmentally friendly" alternative to the very pollutant agents released by the combustion of the common propellants.
In civilian space applications, the research on green propellants has done very big steps forward, and to make a brief review on that a dedicated chapter will be not enough (so only the main motivation that concerns our topic would be exposed). In spite of this, the mainly used propellants are always the same with all the serious environmental consequences they entail.

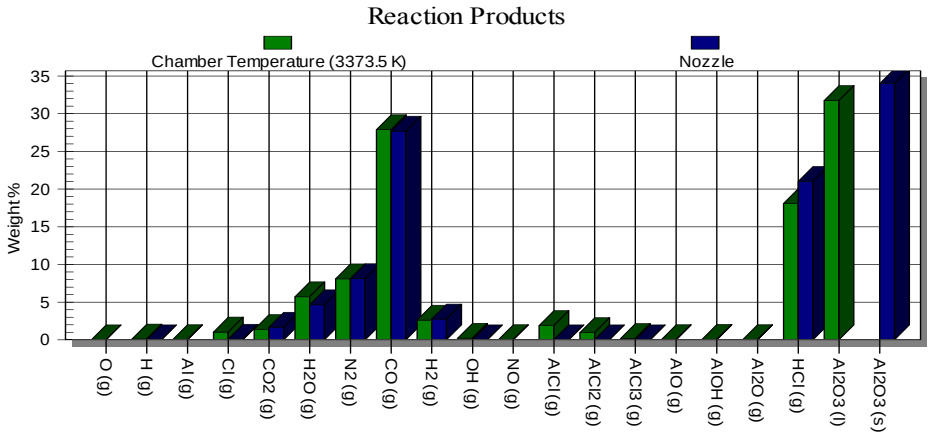

Fig. 2.8. Reaction products at nozzle level of typical AP/HTPB/Al Propellants [1]

The ubiquitous use of AP (NH_4ClO_4), which contains chlorine, in every SRM for space access is extremely dangerous for the atmosphere; in fact, a high amount of hydrochloric acid (HCl) is released by the solid boosters of the modern launchers that should be considered critical under pollution aspects, since it contributes to acid rain and causes environmental damage and corrosion around the launch base.
It has been calculated that during the first atmospheric phase of its launching trajectory, the retired space shuttle, released 220 tons of hydrochloric acid from the Solid Rocket Booster (SRB) which burns only 2 minutes; The SRB of the European launchers Ariane V, and P-80, the first stage of Vega, which contain this type of solid propellants, burn in the order of tons per second, releasing large quantities of HCl, which can reach more than 20% of mass of the reaction products at the nozzle (Fig. 2.8).
Also aluminium chloride and other intermediate reaction products, which are not more than 2%, will cause additional serious problems when the huge quantities of expelled mass are considered.

For this motivation, and not only for the evaluated increase of specific impulse (with the natural increase of deliverable payload), the HISP Project has been pushed to develop a new kind of propellant ([35]) based on components which does not present chlorine, or other severe pollutants, inside its formulation.

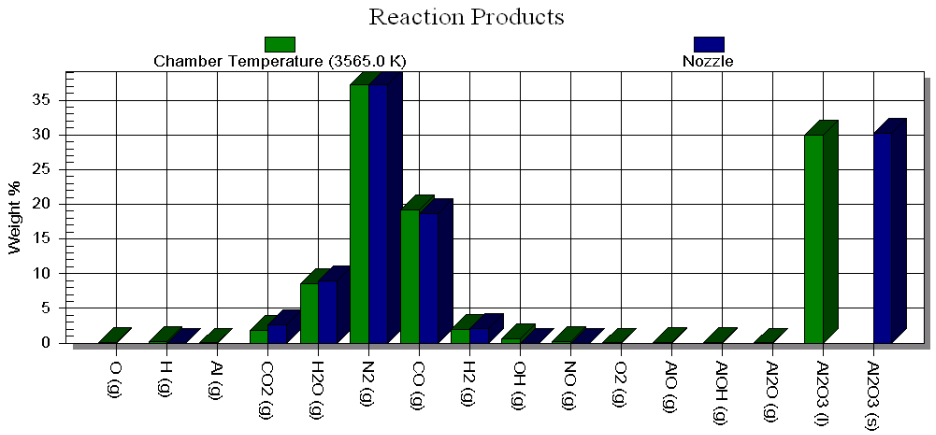

Fig. 2.9. ADN/GAP/Al (60:24:16) combustion product (ICT-Code)

The mixture ADN/GAP/metal fits very well with all of these requirements, since no serious polluting agents are present in the formulation of each component and the main combustion products are normal components of air, for ADN, and normal combustion products for GAP.
When Aluminium is used as a fuel for this formulation, mostly water, hydrogen, nitrogen, aluminium oxide and carbon monoxide and dioxide (the last two are the only pollutant products) are created, as shown in Fig. 2.9.

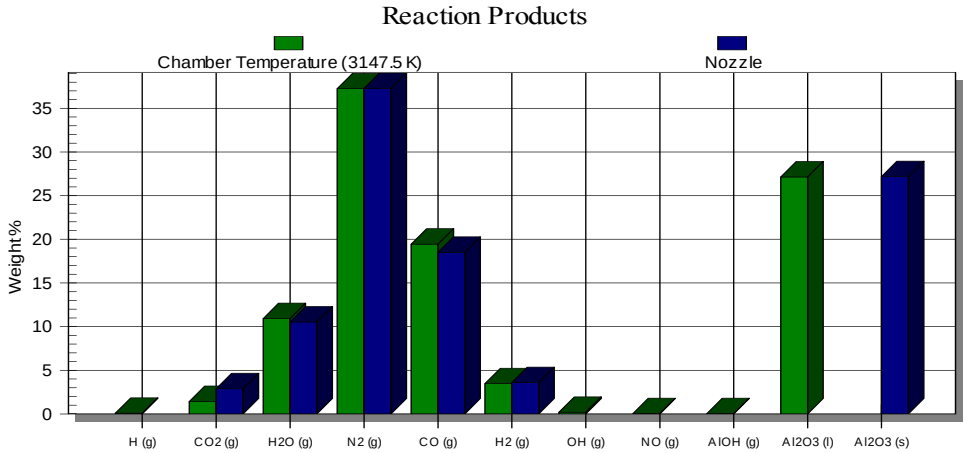

Fig. 2.10. ADN/GAP/alane (60:24:16) combustion products (ICT Thermodynamic Code)

The high percentage of alumina (Al_2O_3) in liquid state in the chamber and in solid state at the nozzle exit is the focal point of the agglomeration problem.
The introduction of alane in the examined formulation leads at a not so different chart (Fig. 2.10), with less monoatomic combustion products due to the lower adiabatic temperature.
Again, it is possible to see the absence of extremely dangerous combustion products.

2.3 Aluminium and Aluminium Hydride Combustion

Aluminium is the most abundant metal on earth and is also the most used. In astronautics it is widely used in the structural field because of its high strength to weight ratio, but also in the propulsion field, since it is an optimum fuel for space propellants. The increase of adiabatic flame temperature, due to the high enthalpy released during combustion of this metal, is reflected in a strong increase in gravimetric specific impulse, and its density occur also to increase the volumetric specific impulse.
For this reason, aluminium is used in most composite solid propellants for space applications, and its burning behaviour, its properties inside a mixture and its reaction inside the combustion chamber have been investigated deeply.

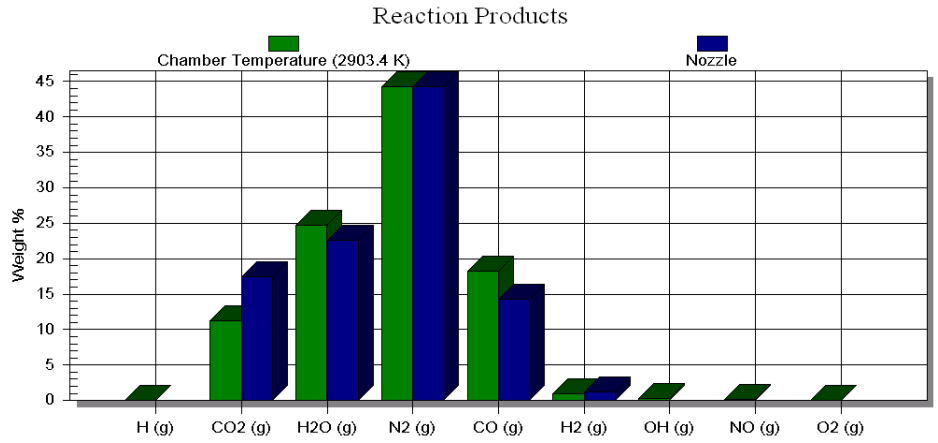

Fig. 2.11. ADN/GAP (70:30) combustion products (ICT Thermodynamic Code)

Some models of combustion of aluminium inside and outside the condensed phase of propellants are available in literature, starting from the 1970s with the Gremyachkin model for metal droplet combustion [37], very interesting under the aspect of agglomeration treated in the next

paragraph, to arrive to the comprehensive and interesting review made by Beckstead in 2002 [38]. Nevertheless, combustion of aluminium is extremely complex and not well understood up to now.
Every scientist agrees that the main oxidisers of aluminium during combustion are primarily oxygen (if available), then water and carbon dioxide and in minor parts also NO, HCl, Cl_2.
Most of these molecules (except oxygen) will largely be present in the reacting gas over the burning surface, because they are the main combustion products of the reaction, as shown in the combustions products chart of the non-aluminized ADN/GAP formulation in Fig. 2.11.
Looking at this chart, it is possible also to note that the main combustion product is nitrogen, which is estimated to be over 45 % in mass of the total combustion products, and to find water (25%) as the second most product which will be the main oxidation reaction partner of aluminium. With this huge amount of water vapour present in the reacting gas, an enthalpy of about +945 kJ/mol [38][39] is freed.

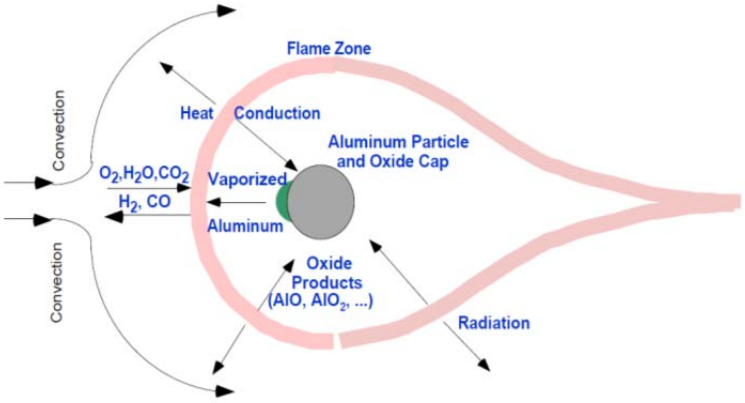

Fig. 2.12. Scheme of the combustion of aluminium droplets [38].

Unfortunately, it seems that up to now no one has investigated the pressure effect on the melting and boiling temperatures of aluminium in the pressure range of interest for the rocket propulsion (1-10 MPa), which can be a determinant factor for a better understanding of the aluminium particle combustion and the aggregation/agglomeration of aluminium droplets on the reacting surface of solid propellants.
It is commonly accepted ([40][41]) that the aluminium particles, which emerge from the propellant because of the regression of the burning surface, are mostly the melted aggregates of the initial aluminium contained inside the propellant itself. So the melting point should be very useful to understand the heat condition of the condensed phase.

In composite solid propellants used for space applications, the amount of aluminium added to the mixture is between 12% and 20% in mass, and it is added as a powder which can be classified in three different types (as space certified aluminium powder): Type I with an average diameter of 7.5 μm, Type II with 15 μm and the largest Type III with 30 μm [39]. Often, bimodal mixtures of two of these three types of particles are present in the same propellant, with respect to the performance required from the mission as well as for better production and mechanical properties.
There are also new types of aluminium powder under investigation like the well discussed nano-aluminium, mostly produced by wire explosion, which has the potential to drastically increase the burning rate because of the high specific surface exposed to oxidation, to enhance the combustion, to increase the combustion temperature which can be much closer to the adiabatic flame temperature, and to decrease the tendency to agglomeration of the liquid aluminium droplets on the burning surface, so reducing the two phase flow loss [42]-[44]. But on the other hand high peroxidation value, health and safety aspects and processing problems for dispersion are serious disadvantages of this kind of energetic powder.
Other interesting research is dedicated to the so called "activated aluminium", which is a kind of micrometric aluminium for which the surface is treated with some activating solutions containing a complex fluoride in different concentrations. The surface treated in this way has a reduced melting temperature and allow a better diffusion of oxidizer molecules through the oxide layer that covers the normal aluminium particles. In this way the aluminium is more reactive increasing the combustion efficiency of the entire mixture and the burning rate of the propellant [45][46][47].
Other important steps forward in the characterization of aluminium powder are under research and in particular some interesting work is done in SPLab by Dossi about the activation of aluminium powder by mechanical processes [48].
Aluminium is not the only metal fuel that can be used for space applications, in fact also others like lithium, titanium, zirconium etc. have been proposed during the years. However, none of these metals has found wide use as fuel, once for the too high sensitivity, others for the high costs and not least because of the environmental problems. So, the attention is moved to another type of fuel, the hydrides, for which the main interesting property is not the increment of the adiabatic flame temperature, but the reduction of the molar mass of the combustion products, which is another focal point in the direction of the specific impulse increment, as shown in Eq. 2.2, where M is the mean molecular mass of the combustion products.

$$I_{sp} = \frac{1}{g_0}\sqrt{\frac{2k}{k-1}R\frac{T}{M}} \tag{2.2}$$

Again, the most popular hydride is the aluminium trihydride, AlH_3. Since it is presumed that the hydrogen dissociates at temperatures reached inside the condensed phase (125-160°C) or near the burning surface, so the main combustion characteristic should be equal to the well-known aluminium metal without passivation layer. This is partly true, since the aggregation/agglomeration give rise to particles which are visible different and the combustion behaviour sometimes is closer to the one observed for mixtures containing nano-aluminium [49]. Aluminium hydride, known also as alane (CAS Registry Number of alane AlH_3: 7784-21-6) is usually available as α-AlH_3, which is the thermally most stable polymorph, with respect to the seven possible crystalline structures that this hydride can potentially create [50].

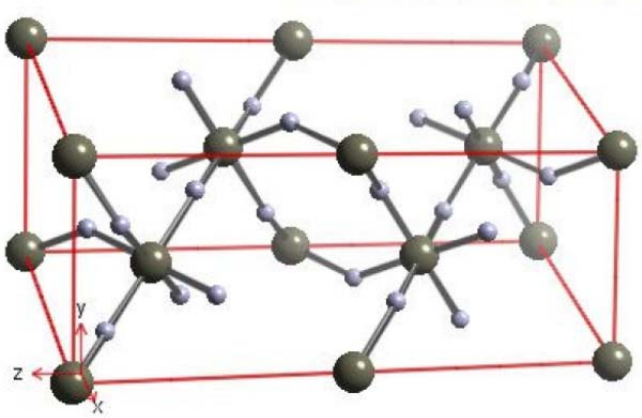

Fig. 2.13. Structure of α -AlH_3; black spheres are Al, grey spheres are H [50]

In this configuration the aluminium atoms are surrounded by six hydrogen atoms that bridge to six other aluminium atoms. The quantity of hydrogen encapsulated inside this hydrate makes alane also interesting as hydrogen storage, because it provides a higher density of hydrogen (0.148 g H_2/cm^3) than pure hydrogen in liquid state (0.071 g H_2/cm^3). This is also the main driving factor of choice for the reduction of mean molecular mass of combustion products to enhance the specific impulse.
Up to the present, only some work is published on the combustion characteristics of rocket propellants containing alane, but it is well known that it has been used for many years by Russians.
Until now Russia is the only state which can provide stable alane with good characteristics and very low aging effect.

Their way to synthesise alane is not public, but the work of De Luca in [50] is a very interesting summary about the chemical procedure to synthesise alane and about its combustion behaviour. The work is complemented by the same author in [51], with much deeper investigations on the combustion of mixtures formed by AP/HTPB/alane. About the stability of the Russian alane it has to be remarked that the hydride used for the burning experiments on ADN/GAP/alane, presented later in this work, is the same used by Weiser in experiments more than seven years before reported in [49]. By comparing the two images of alane (Fig. 2.14), visual inspection already shows that size and shape is maintained, and direct observation shows that also the colour is exactly the same.

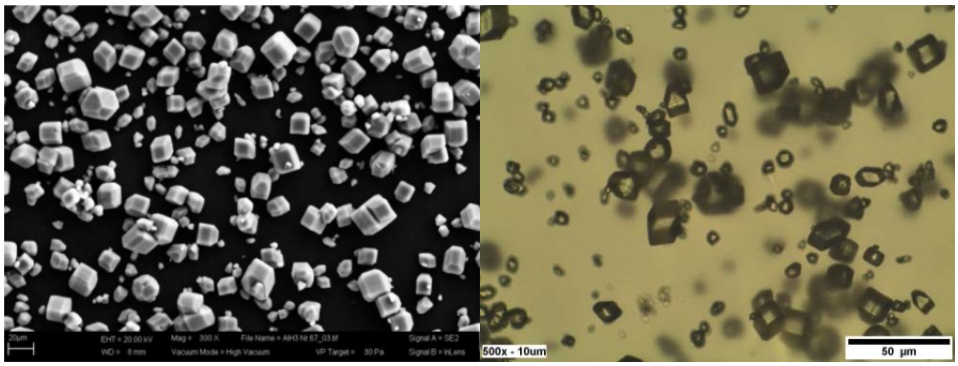

Fig. 2.14. SEM image of alane [49] (left), and microscope image of the same alane 7 years later (right).

This work will treat the combustion of both ADN/GAP/Al and ADN/GAP/alane for the first time in open literature though it is known that ADN/GAP propellants mixed with some percent of alane are probably used for military purpose.

2.3.1 Aggregation and Agglomeration

The biggest loss in specific impulse for SRM is due to two phase flow (2P loss). This loss mostly depends on the size of the solid particles contained in the gaseous products of the combustion and results from the interaction between the solid particles and the gases.
The behaviour of a two phase flow is extremely complex and to estimate the losses with some accuracy is very difficult.
The 2P loss, which can generally be estimated to be around 3-4% of the gravimetric specific impulse, represents only one third of the total loss of an SRM. This is mostly due to the non-equilibrium conditions between the exhaust gases and the particulates, and can be divided into three main aspects: lack in kinematical equilibrium between gas and particulates,

incomplete phase transition of the particulates, and lack in thermal equilibrium between particulates and gas.
The Condensed Combustion Products (CCP) tend to move slower than the gaseous phase and also to release their thermal energy slower. This is traduced in an excess of temperature and in a defect of speed through the nozzle.
All of these non-equilibrium problems are mainly influenced by the character of the CCP, by its nature, by its shape, and, most important, by its size and distribution.
The most important loss is due to the kinetics lag, the velocity non-equilibrium between the two phases. It has been demonstrated that it increases with growing size of CCP, and decreases with a decreasing throat diameter. Other effects as the angle of divergence of the nozzle are perceptible but not so strongly determinant as the throat dimension ([34]). This means that the diameter of the throat is the main important parameter for the evaluation of the velocity lag, and also for the 2P loss.
This could be understand thinking on the principle functioning of a nozzle: the highest velocity and the highest temperature are reached at the throat, so it is obvious that the main non-equilibrium problems find their main effect in this region.
This non equilibrium cannot be recovered in the divergent part of a nozzle, since the temperature decreases (hindering further combustion of CCP) and the velocity of the gases increases (other factors, combined with the previous one, leads to an increase of loss).
Within these considerations, these losses are attributed not to the divergent part, but the convergent part of the nozzle, which must be in the same conditions as the combustion chamber.
Then it becomes of utmost importance to know what the conditions are and in particular what is the size of the metal particulates in the throat.
Researchers agree in that particulates burn completely before reaching the nozzle, and then re-condensate in the divergent part.
However, it is not likely to leave out the "initial condition" in which the particle leaves the burning surface, the more as it can be considered as the worst condition, from which the optimization of the propellant starts.
Further motivation can be find in the usual steps of the development of a propellant: In a preliminary study, without medium or large scale experiment, it is quite difficult to estimate the CCPs acting inside the nozzle. Therefore, it is generally preferred to study the particulates leaving the burning surface of a propellant using strand burner experiments, combining investigations of burning behaviour, and burning rate, with the studies on the temperature and the particulates in only one experiment (if non-intrusive methods are used).

Generally the way of formation of these particles is quite standard: first an emergence of aluminium particles from the burning surface can be seen and after melting a tendency to aggregate in a bigger particle or droplet can be observed. This particle, normally after the first ignition, becomes quite spherical and leaves the propellant.
De Luca in [34], extensively describes the agglomeration process on the burning surface of a propellant, and divides the agglomerates in two different types basing on the way they aggregate: agglomerates of the first type are those for which the emergence, aggregation, ignition, transition to agglomerates and the detachment from propellant happen in the same position, on the other hand agglomerates of the second type are the agglomerates for which the aggregation occurs by the moving of one agglomerate on the propellant burning surface where it interacts with other agglomerates and grows because of the collisions.
Babuk, in [52], make a further distinction according to the structure of agglomerates: he elaborates a first concept of agglomerates made by different ingredients more than aluminium and his oxide, like pieces of unburned binder, degradation products and pieces of oxidizer, which create a non-spherical particle; the second concept only concerns agglomerates made by aluminium and his oxide. They are quite spherical but it is possible to identify metal droplets where a classical "oxide cap" mostly made by alumina (Al_2O_3) is attached.

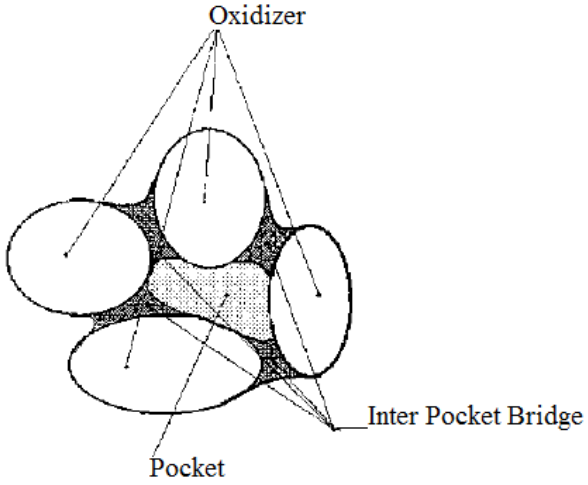

Fig. 2.15. Structure of Pocket [52].

According to the literature [34][52]-[55], the aggregation process for micrometric aluminium powder inside a solid propellant can be divided in different steps: first is a pre-aggregation within the space left free by the bigger oxidizer particle, called "pocket" and "bridge". The pockets are

connected together by the bridges. The bridges are littler line of aluminium between oxidizer prills (shown better in Fig. 2.15).
The second step begins when the burning surface reaches these pockets.
Could be possible that the pockets are in melted state alone creating directly the agglomerate, or there is a possibility that the entire structure of pocket and bridge appear on burning surface. Babuk calls this structure skeleton layer in [52].
Then, this structure collapsed in a bigger metal sphere, the agglomerates.
Most of the emerged aggregates are in liquid state, and the aggregates continue their growth attaching themself to other pockets that emerge in the neighbouring. As a third step the aggregates (that are not yet spherical, but like a coral), reach the temperature of ignition, showing the first inflammation and conclude the transition between aggregate and agglomerate (exhibiting the typical structure represented in Fig. 2.16).

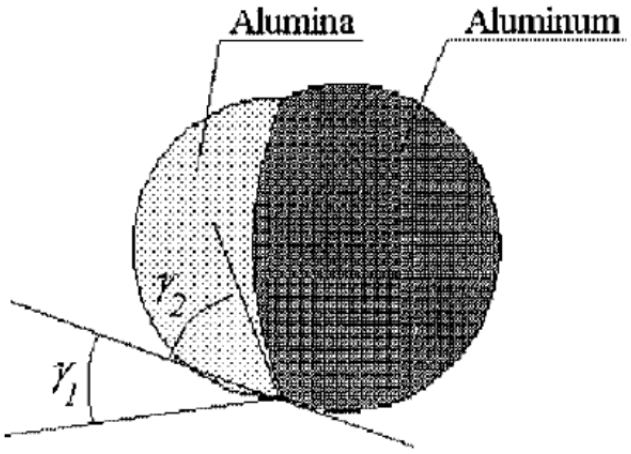

Fig. 2.16. Structure of agglomerate [52].

Then they can detach, or begin moving on the burning surface where they collide with other agglomerates.
Collisions between agglomerates can be considered as the main growing factor. In general, the agglomeration effect depends on the pressure [39] (higher pressure means smaller agglomerates), the temperature, the oxygen balance of the propellant (which influences the burning), the type of burning surface (a liquid layer impedes the detachment with the consequence of further growing of the agglomerate [3]), the mean size of the original metal particles, the size of the oxidizer prills (which directly influences the size of the pockets) and the residence time on the burning surface before the detachment [34].

When the agglomerates detach the determination of the maximum diameter is possible.
According to Glotov ([55]), the maximum diameter is reached closest to the burning surface. So it is regarded as worst case parameter for the evaluation of the loss in specific impulse.
Once the distribution of the diameter of the particles, and consequentially, the average diameter of the agglomerates is obtained, it is possible to evaluate the losses in gravimetric specific impulse using the empirical Eq. 2.3, utilized by AVIO S.p.A., which is recommended in [56] as an international standard for 2P flow losses

$$(\Delta I_{sp})_{2\mathrm{p}} = C_3 \frac{\xi_{cc}^{C4} d_p^{C5}}{p_{cc}^{0.15} \varepsilon^{0.08} d_t^{C6}} \tag{2.3}$$

where, ξ_{cc} is the molar fraction of the condensed products in the combustion chamber (mol/100g), a thermodynamic parameter characteristic of the propellant, d_p is the measured average diameter of the condensed particles (μm), P_{cc} the pressure in the combustion chamber (psi). In addition and two nozzle parameters are used: the geometric expansion ratio ε and the throat diameter d_t in inches, which are important for the reasons expressed above.
The constants C_3, C_4, C_5, and C_6 are correlation constants dependent on the throat diameter and particle dimensions, as reported in Tab. 2-1.

Tab. 2-1 Correlation Coefficients for 2P loss for molar fraction of condensed reaction products greater than 0.009 mol/100g [34].

Throat Diameter d_t [in]	C_3	C_4	C_5	C_6
$d_t < 1$	9	0.5	1	1
$1 \leq d_t \leq 2$	9	0.5	1	0.8
$d_t > 2$ e $d_p < 4$	13.4	0.5	0.8	0.8
$d_t > 2$ e $4 \leq d_p \leq 8$	10.2	0.5	0.8	0.4
$d_t > 2$ e $d_p > 8$	7.58	0.5	0.8	0.33

To estimate the diameter of the agglomerates without the procedures shown in [39], which require a lot of time, some empirical and semi-empirical equations have been proposed [57] (and [34] for a complete overview). The most used one in conjunction with the previous Eq. 2.3 is Eq. 2.4.

$$d_p = 3.6304 \cdot d_t^{0.2932}[1 - \exp(0{,}0008163 \cdot \xi_{cc} \cdot p_{cc} \cdot t_{cc}^*)] \tag{2.4}$$

where t_{cc}^* is the residence time of the particles in combustion chamber.

In general these equations result in diameters which deviate, sometimes a lot, from the results obtained experimentally, and, most important, are tested only on propellants based on AP/HTPB/Al. So, a change in composition invalidates these equations (same discussion can be done on Eq. 2.3).
Agglomerations are not only the origin of losses, but they also have a strong influence on the burning stability inside the SRM; as an example it has been demonstrated that aluminium inside a propellant reduces drastically the high frequency instability increasing the safety of the entire system.
Other kinds of metals have been tested [58], but aluminium has always played the most important role.
Another material that can be interesting for the discussion is definitely alane.
Some experiments have been conducted on propellants for which the formulation was AP/HTPB/alane, and the main result can be summarized as particles of lower mean dimension and drastical change in shape of agglomerates, as shown in [50][51].

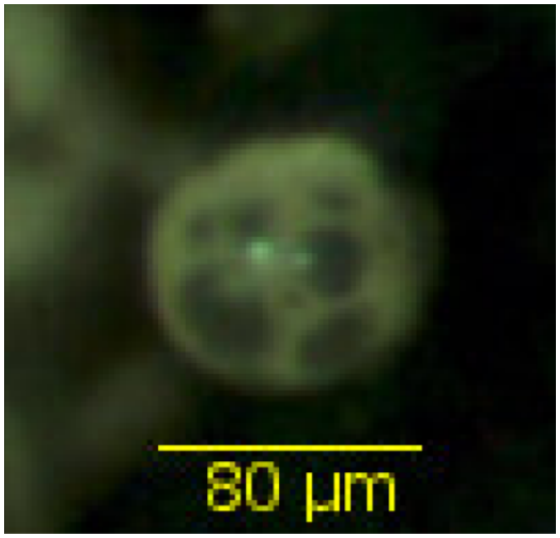

Fig. 2.17. Typical agglomerate of propellants containing alane [50]

The agglomerates, in this type of propellant, present sometimes a “leopard skin”, known as “matrix agglomerates”; the way to build aggregations/agglomerations is, in accordance to De Luca, of the second type. But the collisions of the particles do not form a common aluminium droplet- oxide cap shape, like in Fig. 2.16, but have the characteristic shape represented in Fig. 2.17. This behaviour is known as matrix type of agglomerate, where the darkest parts are aluminium droplets drowned in a matrix of aluminium oxide.

All the discussion presented above, are valid also for propellants different from the classical AP/HTPB/metal formulations, but up to now the only investigated materials, are based on AN or AP as oxidizers, and different types of inert binder, like PU, HTPB, and polybutadiene acrylonitrile (PBAN), for some kind of metals.
This study investigates for the first time the combustion of aluminized ADN/GAP propellants including particle agglomeration in comparison to other types of binder and oxidizer.

Chapter 3

Investigated Formulations

In order to characterize the ADN/GAP-based propellants, several different formulations have been selected and tested. Different sizes and size distributions of oxidizer prills and different sizes of aluminium powder have been tested. In this work only results of formulations and samples will be presented for which problems like high porosity or difficult production were only marginal. Samples with such problems are described with particular relevance.

The main path follows the proposal of Max Calabro given in the first HISP project report [59] that contains ADN/GAP with aluminium particles.

Additionally, formulations of ADN/GAP without metallic particles, ADN/GAP/Al with aluminium particle diameters of micro and nano size, and ADN/GAP/alane were investigated.

Calabro searched for an applicable formulation with the maximum possible theoretical specific impulse, based on the theoretical increment of payload gained by the substitution of used propellants.

These formulations only base on thermodynamic calculations without an experimental background. Despite of this, they are very interesting: an increase of payload masses of 17% just by changing the propellant type in the apogee motor of the upper stage for the newborn VEGA launcher, and an increment of 14% of payload mass for the Mars Ascent Vehicle (in-loco launchers for return travel from Mars).

The main problem of the calculation performed by Calabro is the hypothesis of reduced losses that the introduction of new propellants should return.

Starting in the same way, several calculations, using a different thermodynamic code (ICT-Thermodynamic Code [18]), were performed in order to have an overall picture of the new propellants, to better understand its properties, and to make a quantitative comparison with the omnipresent AP/HTPB/Al.

Comprehensive information about the thermodynamic aspect of ADN and GAP used in the experiments will be presented, with a brief excursus about AP, and also some additional information about the metals used.

3.1 Frozen Chemistry Performance Evaluations

The results obtained using ICT-Thermodynamic Code are in agreement with the ones obtained by Calabro with the "code Isp2001" [5], however, it has been chosen a more intuitive graphical visualization (using OriginPro 8.5) similar to the one used by Boyars in [60]. The choice of graphical representation has the disadvantage of exhibiting only data under frozen equilibrium assumption. All the performed calculations were done assuming an expansion ratio of 70:1 MPa and an adapted nozzle.
The amount of component will be always expressed in mass percentage.

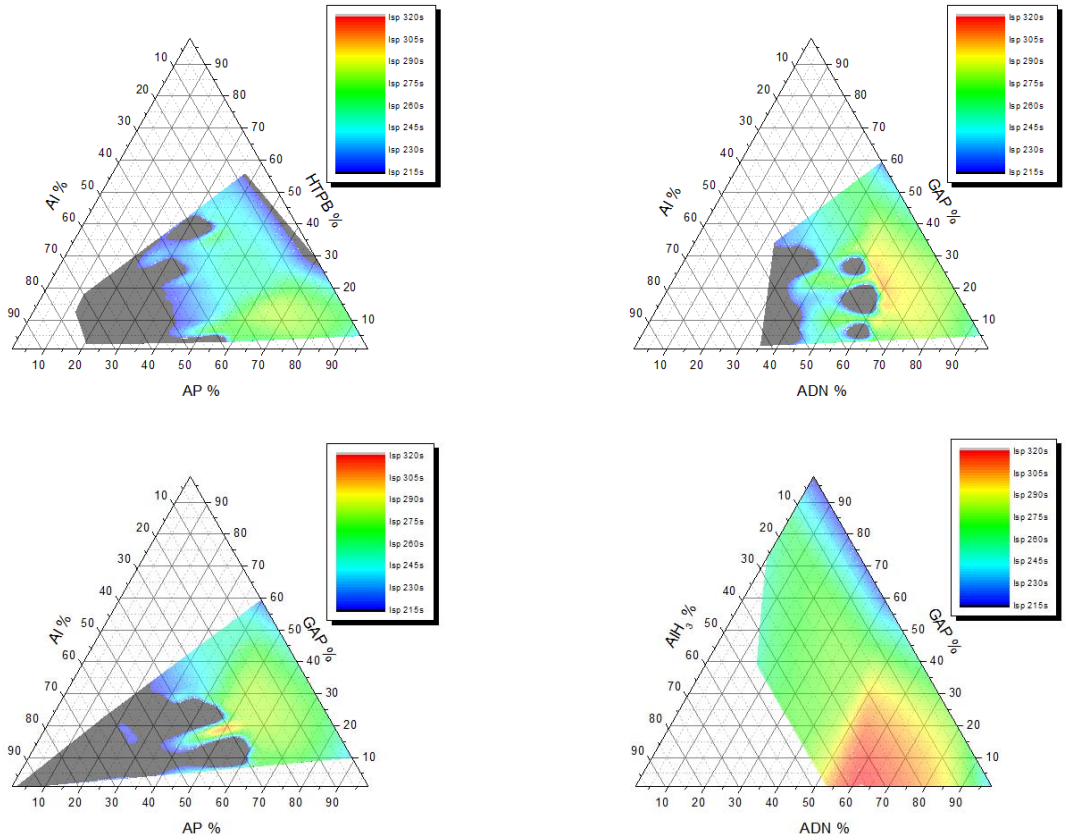

Fig. 3.1. Thermochemical results of the theoretical gravimetric specific impulses (frozen equilibrium in vacuum) calculation for three compositions including metals (AP/HTPB/Al for reference)

From the comparison between the four triangles in Fig. 3.1 it is possible to see that the maximum specific impulse is reached by the mixture containing alane, at the lower right position. This could be expected because this system contains an energetic oxidizer in an energetic binder with an energetic fuel (all of them are HEDM), followed by the

formulation ADN/GAP/Al (above the first) and AP/GAP/Al (bottom left), respectively.
The calculated maximum specific impulses are 315 s for the composition 60/12/28 of ADN/GAP/alane, 296 s for 59/20/21 for ADN/GAP/Al, 284 s for 56/24/20 AP/GAP/Al with respect to again 284 s for AP/HTPB/Al reference at the ratio of 68/12/20. If shifting equilibrium is assumed, the maximum is still maintained for the same composition, but with a common enhancement between 4.7 and 5 s in specific impulse.
The introduction of the new formulation substituting AP/HTPB/Al, at least at thermodynamic calculation level, will give an increment of 31 s for the gravimetric specific impulse if alane is considered as fuel , or "only" 12 s if the mixture contains aluminium.

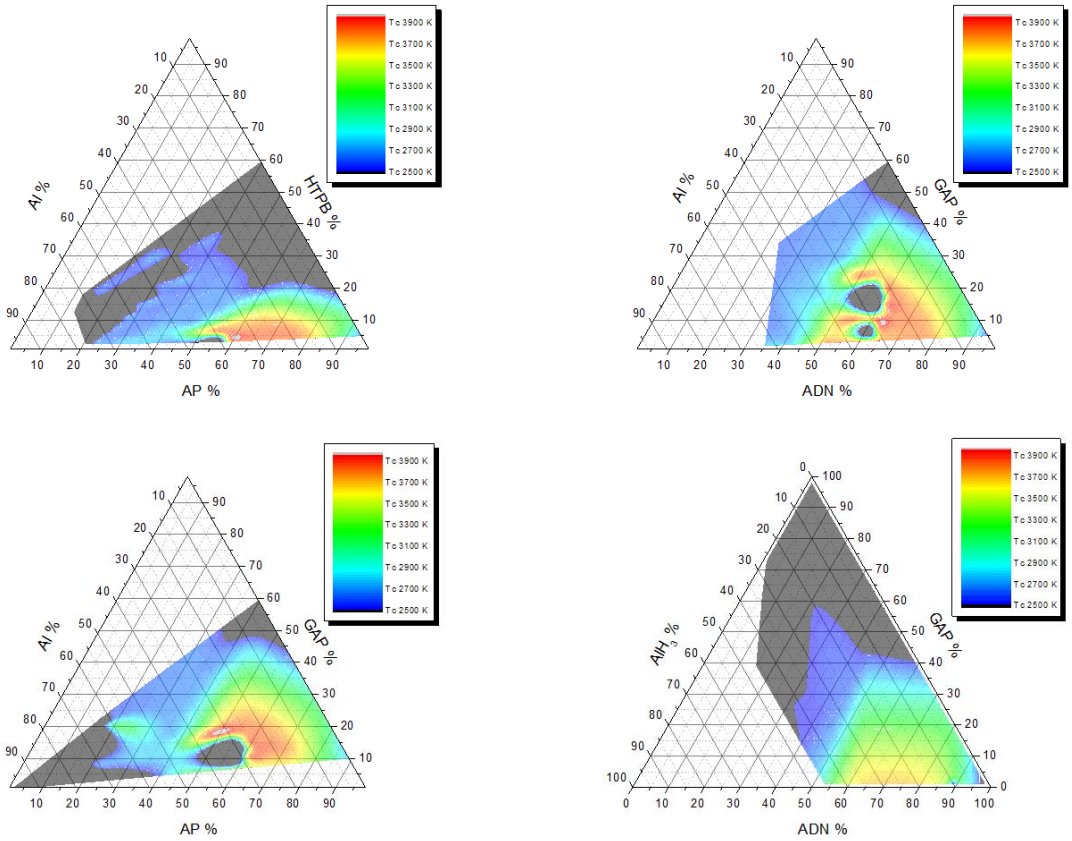

Fig. 3.2. Adiabatic flame temperature of the compositions

It is notable that the calculated specific impulse for the formulations of ADN/GAP has definitively higher specific impulse in a wider region of metal content with respect to the formulations containing AP.
The increment of the ADN/GAP/Al formulations is mostly due to the growth of adiabatic combustion temperature (which is shown in Fig. 3.2),

in concomitance with the widest range of lower mean molecular mass of combustion products considered in the combustion chamber, because the variation of the specific heat ratio presents a not so marked difference with respect to AP/HTPB/Al.
At the point of maximum specific impulse, considering AP/HTPB/Al and ADN/GAP/Al formulations, there are no marked differences between the mean molecular mass of the combustion products, so the increment of 12 s in specific impulse is mostly due to the difference of 220 K between the two adiabatic flame temperatures (3550 K for AP/HTPB/Al and 3770 K for ADN/GAP/Al).
The composition including alane shows a growth in specific impulse mainly due to the reduction of molecular mass of combustion products, as stated in Chap. 2.2. In fact, the adiabatic temperature at maximum specific impulse reaches a value of 3530 K, which is even lower than the 3550 K of the estimation for AP/HTPB/Al.

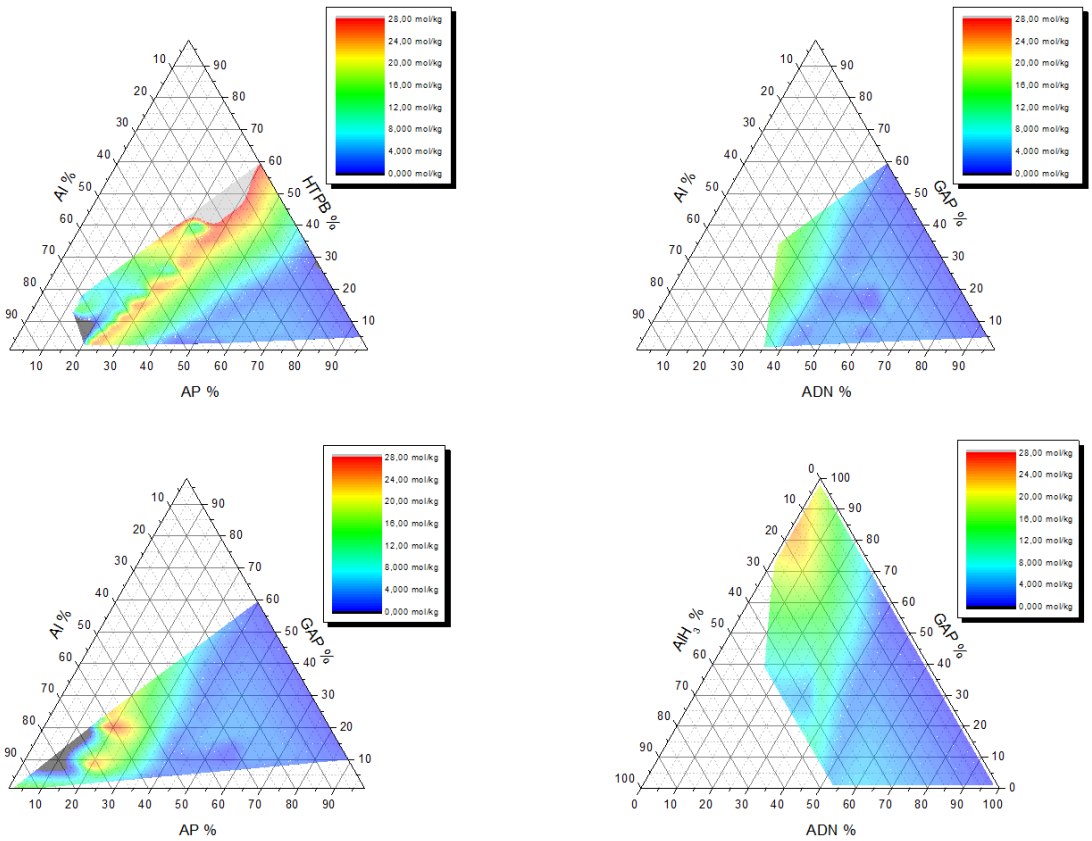

Fig. 3.3. Condensed combustion products of the compositions (mainly Al_2O_3)

In Fig. 3.3 are reported the evaluation of the combustion products that are considered in condensed phase, which are of particular importance since

they give a preliminary indication of the expected amount of solid particles released by each propellant. These condensed products are practically always aluminium oxide (alumina, Al_2O_3) and it is possible to see that under perfect thermodynamic conditions at the maximum specific impulse of each composition, the value does not substantially change and remains stable around 4-6 mol/kg.
The evaluation used in order to select the propellants to be tested does not include the formulation based on AP/GAP/Al, because this composition was used as a trial propellant for better understanding of the combustion behaviour and the determinant factors that influence the creation, the proliferation and the growth of the agglomerates. For this reason the path followed was to try to maintain only one thermodynamic aspect of propellants constant for each type of composition (i.e. firstly maintaining the same temperature of ADN/GAP/Al, then maintaining the same oxygen balance, then maintaining the same heat of formation and then completely change the adiabatic temperature of combustion).
The last formulation to test was the pure ADN/GAP composition, without metals.

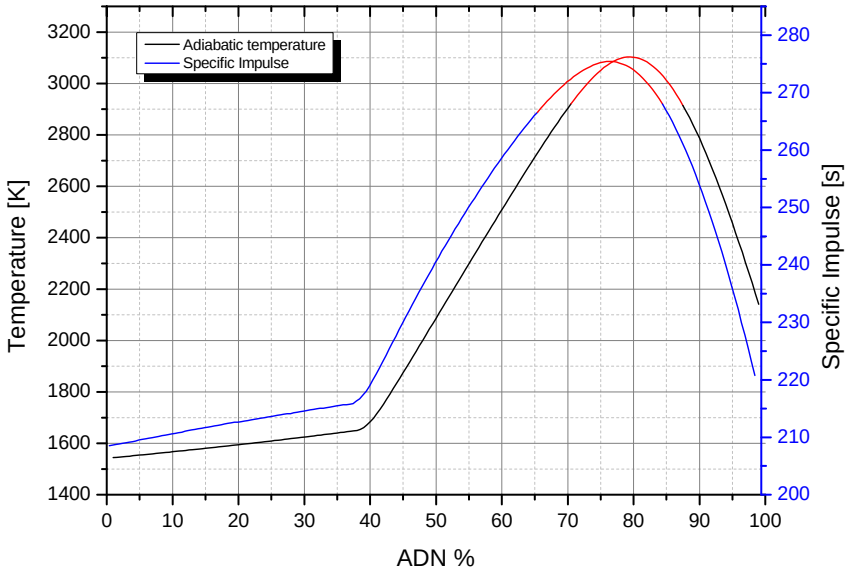

Fig. 3.4. Adiabatic Temperature and gravimetric specific impulse under frozen equilibrium in vacuum assumption for ADN/GAP formulation

Also for this formulation a thermodynamic calculation was performed using ICT-Thermodynamic Code and it is presented in Fig. 3.4 resulting in a maximum gravimetric specific impulse of 275 s which corresponds to an

adiabatic flame temperature of 3060 K for a mass ratio of 76:24 for ADN/GAP.
In general thermodynamic calculations do not take into account size and distribution of oxidizer and metal particles.
For this reason further information about each component of the formulations will be given in the following paragraphs.
Particular attention must be paid also on feasibility and mechanical characteristic of the propellant, which can determine the final product.

3.2 Oxidizers

The oxidants used are ADN and AP. Both are very powerful oxidizers and react also as monopropellants. Both components include ammonia and decompose below the melting point releasing nitrogen, water, oxygen and, in the case of AP, also chlorine.

3.2.1 Ammonium Dinitramide (ADN)

Different sizes of ADN prills were used from two suppliers, who prepare prills using different anti-caking agents and prilling technologies starting from neat ADN delivered by Eurenco Bofors (Chap. 2).
Only one formulation includes prills delivered by FOI with an average dimension of 228 μm.
All the other prills were produced by ICT in two batches in order to get different average prill sizes: the first batch results in average prill diameters of 208 μm and 55 μm, and the other one achieve average diameters of 272 μm, 212 μm, 153 μm, 55 μm, 40 μm.Also raw ADN was used as reference with maximum dimension of about 300 μm.
The thermochemical data of the used ADN are summarized in Tab. 3-1.
ADN shows a strong incompatibility with normally used polyfunctional aliphatic isocyanates like IPDI, HDI or polyisocyanates for the curing of GAP. So another curing methodology based on different isocyanates was used.
The mass percentage of ADN is often 60% and varies only in the case of pure ADN/GAP propellant and for one of the compositions of ADN/GAP/alane.

3.2.2 Ammonium Perchlorate (AP)

Ammonium Perchlorate is the most used solid oxidizer in space propulsion (an old but complete investigation can be found in [62]) and here it will be only used as a reference to compare the behaviour of new propellant, and as oxidizer for the trial propellant AP/GAP/Al used for the analysis of the parameters that influence the development of agglomerations. The AP used

in the mixture investigated has a monomodal distribution of particle size with an average diameter of 192 µm, synthetized and produced at ICT. The thermochemical aspects are resumed in Tab. 3-1.

3.3 Binder - Glycidyl Azide Polymer (GAP)

The investigated binder is the same for all formulations and is produced by the reaction of the GAP-diol prepolymer (molecular weight 1160 g/mol), purchased from Eurenco Bofors, using a curing agent.
Generally GAP is cured with an alkyne curing agent and this curing system approved to be compatible with ADN, but, in order to increase the length of the chains of the GAP molecules, another method has been preferred, the dual curing system [32]. The dual curing system consists in a "pre-cure" with different isocyanates and then in a crosslink reaction with bispropargyl succinate (BPS).
These are the "isocyanates which leads to a chain elongation of the GAP molecules which are cross-linked through an azide-alkyne cycloaddition and subsequent formation of triazole crosslinks" ([32]).
The incompatibility of ADN with isocyanates was solved using GAP-diol because the isocyanates will mainly react with butanediol (chain extender) to create butanediol-based polyurethane which will be integrated inside the GAP-diol by a secondary reaction and then, all of this structure will be cross-linked by the reaction between the azide groups and BPS.
The advantage of the dual curing is to avoid the isocyanates in the final product (and so their reaction with ADN).

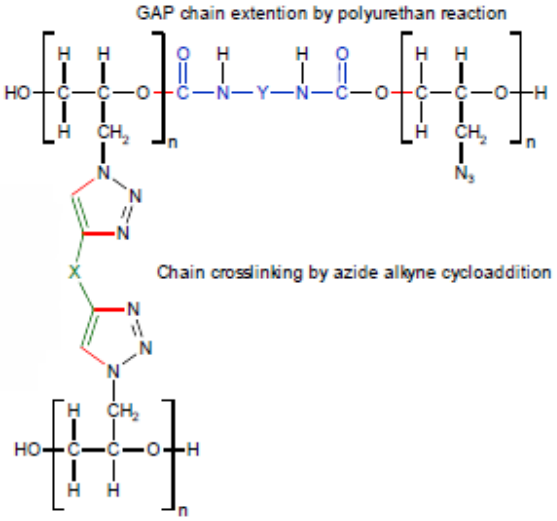

Fig. 3.5. Structure of cured GAP [32].

The mass percentage of GAP is mostly 24% for the ADN compositions but it varies for the AP compositions.

Tab. 3-1 Thermochemical data resuming

	Chemical Formulation	Oxygen bal. [%]	Molar Mass [g/mol]	Density [g/cm^3]	ΔH_f [kJ/mol]	Self-Ignition temperature [K]
ADN	$NH_4N(NO_2)_2$	25.79	124.056	1.1812	-134.6	425
AP	NH_4ClO_4	34.04	117.489	1.95	-295.77	623 [63]
GAP[a]	$C_{10}H_{16.56}N_{8.51}O_{3.38}$	-128.48	310.074	1.28	239.9	593 (monomer)

[a] Cured GAP-binder.

3.3.1 Curing Agents and Catalysts

The word "additives" is used improperly here since no ballistic modifier was introduced in the formulations studied; however, all reagents used to obtain the binder are considered as additives.
The isocyanate used as curing agent is Desmodur E305 (equivalent weight 328 g/mol) from Bayer Material Science and the alkyne curing agent is BPS (equivalent weight 97g/mol), synthesized from succinic acid and propargyl alcohol in ICT. The curing catalyst is dibutyltin dilaurate (DBTDL) from Merck Schuchardt in a dose of 400 ppm at 328 K.
Despite the methodology utilized, the porosity of the final product was always between the 3.7 and 4.5%, probably because of further reactions between E305 and ADN.

3.4 Metals

Since the sixties of the last century space propulsion field is mainly focused on micrometric aluminium. This does not mean that other fuels were not considered; hydrides of light metals, zirconium, boron and more were investigated as a possible replacement with fruitful results. Comparative analyses performed during the last three decades shows that these potential substitutes can give also higher gravimetric specific impulse. On the other hand, problems like lower density, reduced castability, compatibility and compounding problems made this substitution unfeasible. Final formulations must be a compromise between combustion quality, mechanical properties and physical aspects in order to meet the requirements of each mission.
For these reasons, aluminium is once again the ideal candidate in the characterization of propellants based on ADN/GAP.
Since the scope of the HISP project is to discover a high specific impulse propellant, two main strategies has been followed: from one side the use of aluminium in the form of nanoparticles or activated particles, in order to

reduce the agglomerations problem, and consequently, the two phase loss, and on the other side the use of energetic ingredients which grant higher ideal theoretical specific impulses, like alane.

3.4.1 Aluminium

The most used type of aluminium for space propellant purpose is in the form of a spherical powder with an average diameter of 30 μm.
For the ADN/GAP/Al propellants, four types of aluminium have been proposed: two have sizes in the micrometre range and two belong to nano-field. The two micrometric types of aluminium powders used are ALCAN 400 (average size of 5 μm) and A1X-81 (average size of 18 μm), both purchased from Toyal.
The two nanometric powders were both obtained by the aluminium wire explosion technology (ALEX^{TM}) with an average diameter of 100 nm.
One was only covered with the natural alumina passivation layer; the other was activated using a coating of stearic acid before air exposure.
The amount of aluminium in each composition is always 16% and the mixing and forming of propellants with A1X-81 and ALCAN 400 do not show any problem. In all cases the sheets were prepared through the distension inside a former shape of the slurry and not by casting.

3.4.2 Alane (AlH_3)

Aluminium trihydride used as energetic fuel grants the overall ideal performance if compared to standard aluminium, because of the lower molecular weight of the exhaust gases, lower thermal load for the motor, limited density, an expected higher burning rate and observed limited agglomeration attitude (for AP/HTPB propellants).
alane has relatively low density (1.477 g/cm^3) with respect to aluminium, and metal content of 88.2%.

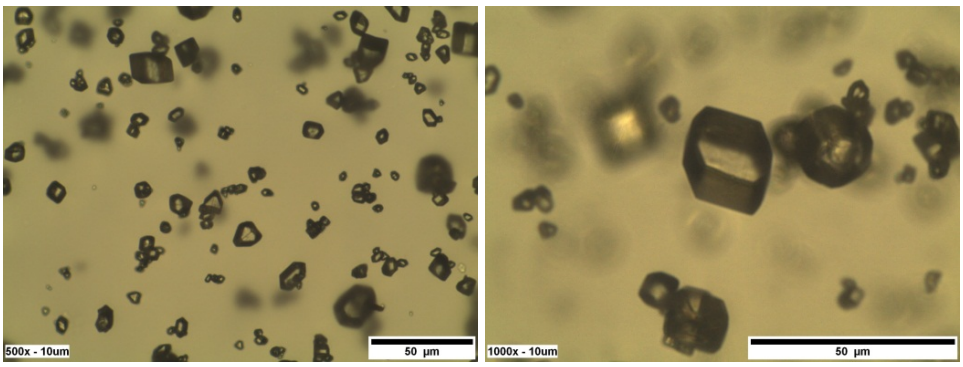

Fig. 3.6. Microscopic observation of the utilized alane.

The alane used to prepare ADN/GAP propellants was supplied from Tomsk, Russia, more than 15 years before this characterization (average size 9 μm). For this reason it was also possible to evaluate the quality of this ingredient, that appears, under microscopic evaluation, with its original shape and without the characteristic pores due to the release of hydrogen (Fig. 3.6).

3.5 Investigated Formulations

All the above described ingredients were mixed in a planetary centrifugal vacuum mixer, the Thinky ARV-310, with 1600 cycles per minute at a pressure of 35 mbar for two minutes. This kind of mixer is generally not used for the preparation of small amounts of propellants, because the dispersion of the oxidizer and metal powder inside a high viscosity binder takes place without contact and without shearing, but with a possible formation of bubbles.

Fig. 3.7. Thinky mixer ARV-310 and mechanism of mixing [1].

On the other hand, the production of small amounts of propellants, which is of interest for the characterization, proceeds much faster with this kind of mixer (2-5 minutes for 30-150 g) if compared with the classical kneader. Fortunately, no formation of bubbles was observed during the mixing.
The formulations obtained are mainly made by 60% of oxidizer, ADN (with monomodal or bimodal distribution) or AP, 24% of GAP and 16% of fuel.
Also configurations without fuels have been considered and their formulation is always 30% GAP and 70% ADN of different prill sizes.
The 21 formulations prepared are reported in Tab. 3-2.
All ADN, if not specified, was prilled at Fraunhofer-ICT by emulsion nucleation [25].
The propellants formed of pure ADN/GAP were produced in order to understand better how the size of oxidizer prills influences the combustion behaviour and in particular the burning rate.

The guideline followed for the metallized propellants for obtaining the maximum specific impulse has to deal with the mechanical properties and machinability of the mixtures obtained.
Looking at the formulations, they are quite far from the one obtained by thermodynamic calculation in Chap. 3.1 where the maximum specific impulse is obtained for 59% ADN, 20% GAP and 21% Al (296 s) for the aluminized formulation, 60% ADN, 12 % GAP and 28% alane (315 s) for the formulation containing aluminium hydride, and 76% ADN, 24% GAP (275 s) for the formulation without fuel.

Tab. 3-2 list of investigated propellant (mass percentage)

Label	Oxidizer	GAP	Fuel
H31D	60% ADN 208 µm	24%	16% Al 5 µm
H31E	60% ADN 208 µm	24%	16% n-Al 100 nm
H31F	60% ADN 208 µm	24%	16% act-Al 100 nm
H31G	60% ADN 208 µm	24%	16% Al 18 µm
H32	60% ADN 208 / 55 µm (70:30)	24%	16% Al 18 µm
H27	60% ADN 228 µm (FOI)	24%	16% Al 18 µm
H53	60% ADN 208 / 55 µm (70:30)	24%	16% alane
H54	52% ADN 208 / 55 µm (70:30)	22%	26% alane
H55	70% ADN 212 µm	30%	-
H56	70% ADN 153 µm	30%	-
H57	70% ADN 55 µm	30%	-
H58	70% ADN 272 µm	30%	-
H59	70% ADN 40 µm	30%	-
H60	70% ADN raw 300 µm	30%	-
A1	58% AP 200 µm	26%	16 % Al 18 µm
A2	39% AP 200 µm	45%	16 % Al 18 µm
A3	48% AP 200 µm	36%	16 % Al 18 µm
A4	43% AP 200 µm	41%	16 % Al 18 µm
A5	-	84%	16 % Al 18 µm
A6	69% AP 200 µm	31%	-
A7	58% AP 200 µm	26% GA/BAMO	16 % Al 18 µm

The problem mostly lies in the viscosity of the obtained mixture.
The two propellants containing nano-aluminium were incredibly viscous, and the distension inside the former shape creates cracks inside the propellant (Fig. 3.8 and Fig. 3.9). Decreasing the amount of aluminium in the formulation can be a possible solution for this problem.

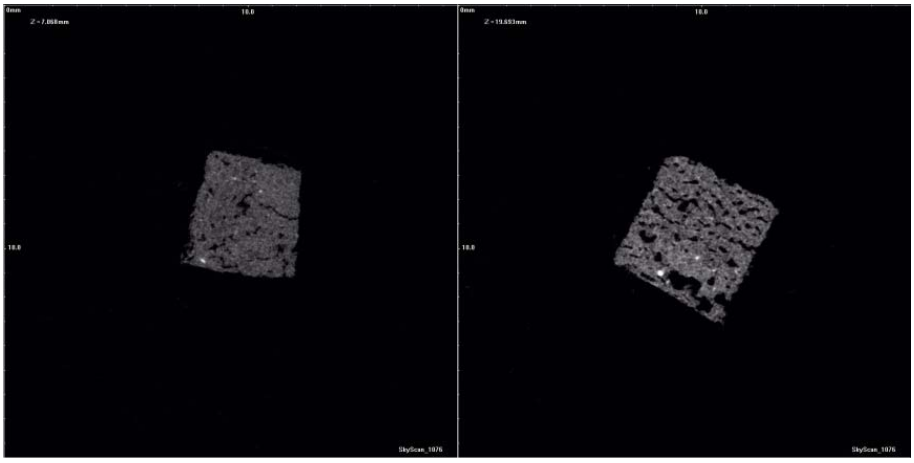

Fig. 3.8. Tomographic investigation of propellant H32E (left) and H32F(right)

Also the size of the oxidizer prills has given rise to problems, because cracks and bubbles were observed by simply visual investigation, making it impossible to do a characterization of the propellant containing the largest ADN particles (H58-272 μm).
For the mixtures containing alane, it is unthinkable to reach 28% of alane with 12 % of GAP for propellants because of decent mechanical properties. It was therefore decided to increase the amount of GAP up to 22%, reducing the amount of ADN touching as less as possible the amount of alane (formulation H54).

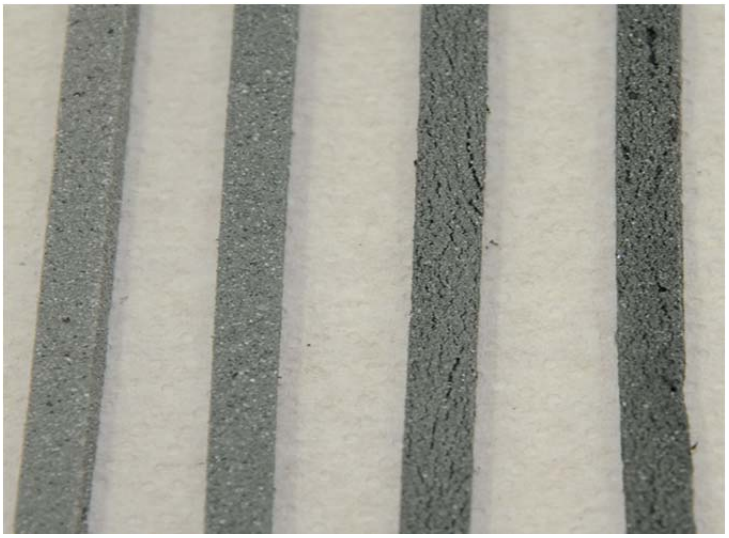

Fig. 3.9. Strands visual analysis, from left to right, H31G, H31D, H31E and H31F

The formulation H53 was tested in order to evaluate the simple substitution of aluminium with alane.

An interesting formulation, also under the point of view of pyrotechnics, is the formulation A5, which contains no oxidizer but only GAP and aluminium.
The last composition (A7) includes a binder which is formed not only by GAP, but also with BAMO and was used to evaluate this new binder formulation with copolymers.
The change of formulation required the execution of further evaluations under the ideal thermodynamic aspect of propellants, which can be easily understood looking at Fig. 3.1 and Fig. 3.2, and summarized in the following tables.
In Tab. 3-3 results are presented for the propellants based on ADN as oxidizer (no thermodynamic code takes into account the dimension particles), and it is easy to understand that the hydrogen of alane plays a decisive role for the grant of specific impulse. It is also very interesting to see the relevance of the condensed products which can represent up to 44 % of the total mass of the products. The calculated ideal specific impulses, for all formulations, are lower with respect to the maxima. But thanks to the wide range of metal content for which high specific impulse can be achieved with ADN/GAP formulations, the difference between the maximum specific impulse and the calculated one is 2 s for ADN/GAP/Al and 3 s for pure ADN/GAP, but much higher for the propellants containing alane (12 s and 10 s). Nevertheless, the ideal specific impulse provided by the alane formulation H54 is 20 s higher than the maximum achieved by AP/HTPB/Al formulation (284 s) if no losses are considered.
The condensed combustion products are mainly composed by liquid alumina for all the formulations.
Mechanical characteristics have been studied, up to the writing of this work, only for the formulation H32 ADN/GAP/Al with bimodal distribution of ADN, for which the characterization is at a more advanced stage. The complete formulation of this propellant, comprehensive of the reaction catalyst (OH terminated) is reported in Tab. 3-4.
The mechanical and physical properties of H32, reported in Tab. 3-5, show a self-ignition temperature which is near the one evaluated for pure ADN reported in Tab. 3-1. It is also remarkable that the propellant shows particular sensitivity both for friction and impact, but lower than usual AP/HTPB/Al propellants [32].
The lower value of the Young's modulus, E, is possibly due to the isocyanate used in the polymer chain.
From the comparison between Tab. 3-3 and Tab. 3-6 it is possible to see the logic that has driven the choice of the AP-based propellants: propellant A1 has quite the same temperature and oxygen balance as the ADN/GAP/Al propellant, the propellant A2 and ADN/GAP/Al have

approximately the same heat of formation; propellant A3 and A4 have been chosen to evaluate the effect of temperature on agglomerations.

Tab. 3-3 Ideal thermodynamic calculation for propellants using ADN (70:1 pressure expansion, adapted nozzle)

Formulations	60% ADN, 24% GAP, 16% Al	60% ADN, 24% GAP, 16% alane	52% ADN, 22% GAP, 26% alane	70% ADN, 30% GAP
Density [kg/m^3]	1735	1590	1564	1616
Oxygen balance [%]	-27.82	-39.18	-54.82	-18.27
T_c [K]	3565	3147.5	3105.6	2903.4
ΔH_f [kJ/kg]	-448.43	-693.61	-773.26	-500.16
I_{sp} (Vac. Frozen) [s]	293.7	297.9	304.7	271.2
I_{sp} (Shifting) [s]	274.6	278.3	286.3	255.3
I_{sp} (Vac. Shifting) [s]	300.2	301.5	312.2	274.5
γ	1.264	1.264	1.288	1.232
Cp [J/(kg K)]	2051.4	2292.4	2475.3	1944.2
C* [m/s]	1593	1638	1642	1574
Products Mean Molar Mass (chamber) [g/mol]	24.803	21.085	19.951	22.738
CO –gas- (chamber) [%]	19.223	19.441	18.528	18.269
N_2 –gas- (chamber) [%]	37.182	37.254	32.755	44.291
H_2O –gas- (chamber) [%]	8.584	10.923	0.398	24.735
CO_2 –gas- (chamber) [%]	1.767	1.426	0.033	11.267
Al_2O_3 –solid- (chamber) [%]	29.968	27.140	40.167	0
Condensed Products Mass Fraction (chamber) [%]	29.968	27.140	40.167	0
Products Mean Molar Mass (nozzle) [g/mol]	27.509	22.573	22.205	22.850
CO –gas- (chamber) [%]	18.662	18.511	18.441	14.354
N_2 –gas- (chamber) [%]	37.274	37.274	32.161	44.335
H_2O –gas- (chamber) [%]	9.003	10.532	0.003	22.623
CO_2 –gas- (chamber) [%]	2.655	2.893	0	17.418
Al_2O_3 –solid- (chamber) [%]	30.231	27.185	42.148	0
Condensed Products Molar Mass Fraction (nozzle) [%]	30.231	27.185	43.777[a]	0

[a] aluminium nitrate is present(1.63%)

The amount of aluminium does not change by moving between the various AP-propellants, but for propellant A6, without aluminium and as used for comparison, the choice has been made to maintain the relative ratio between oxidizer and binder.

Tab. 3-4 Details of the composition H32

Component	Mass Percentage [%]
A1X-81	16.00
ADN 208 µm	42.00
ADN 55 µm	18.00
GAP Diol	19.59
BPS	1.31
Desmodur E305	3.10
DBTDL	0.04
NCO/OH[a]	0.56
BPS/OH[a]	0.80

[a]Catalysts are presumed to be completely reacted in final formulation

The formulation labelled with A7, which includes a different binder formed by the copolymerization of two different energetic monomers (surprisingly creates an additional component in the chain during the reaction [64]), is investigated in order to get better mechanical properties.

Tab. 3-5 Physical and mechanical properties of propellant H32 [courtesy of V. Gettwert]

Property	
Density [g/cm^3]	1.641
Viscosity[a] (328 K) [Pas]	231
Stress σ_{max} [b] [N/mm^2]	0.52
Strain at F_{max} [b] [%]	6.69
Stress σ_{breake} [b] [N/mm^2]	0.48
Strain at ε_{break} [b] [%]	8.7
Young's modulus [b] [N/mm^2]	14.28
Friction sensitivity [N]	144
Impact sensitivity [Nm]	5
Dissociation temperature [c] (DSC) [K]	448
Glass transition temperature [d] [K]	237-345
Self-Ignition temperature [e] [K]	429.5

[a]shear rate 6.28 Hz, [b]at 293 K, [c]heating rate 10 K/min, [d]depend on the method utilized, [e]heating rate 5 K/min

The study of agglomerations on the presented propellants labelled as Ax can be useful to understand how different thermodynamic factors will influence the aggregation/agglomeration behaviour on the combustion surface of propellants.

Tab. 3-6 Ideal thermodynamic calculation for propellants using AP (70:1 pressure expansion, adapted nozzle)

Label	A1	A2	A3	A4	A5	A6	A7
Density [kg/m^3]	1791	1645	1711	1673	1408	1683	1771
Oxygen balance [%]	-25.67	-55.45	-41.48	-49.24	-115.95	-14.05	-29.18
T_c [K]	3574	2537.7	3208.1	2856.5	2446	2981.1	3518.1
ΔH_f [kJ/kg]	-1161.1	-464.2	-794.3	-610.9	966.1	-1380.4	-1245.5
I_{sp} (Vac. Frozen) [s]	283.4	251.9	278.9	266.5	246.2	263.4	283.5
I_{sp} (Shifting) [s]	265.9	250.5	264.1	254.7	238.9	249.3	266
I_{sp} (Vac. Shifting) [s]	291.7	276.5	287.4	279.3	260.6	268.7	291.2
γ	1.262	1.288	1.282	1.288	1.287	1.225	1.264
Cp [J/(kg K)]	1927.6	1888.2	1952.9	1916.4	966.1	1813.8	1945.4
C* [m/s]	1534	1415	1525	1479	1291	1523	1536
Products Mean Molar Mass (chamber) [g/mol]	26.777	22.907	24.362	23.339	16.792	25.041	26.307
CO –g- (chamber) [%]	20.581	35.634	30.204	34.571	5.752	16.546	23.200
N_2 –g- (chamber) [%]	17.864	22.851	20.976	22.434	34.257	21.308	16.129
H_2O –g- (chamber) [%]	8.875	0.021	1.987	0.236	0.004	24.098	8.214
CO_2 –g- (chamber) [%]	2.297	0.006	0.483	0.061	0	15.306	2.167
AlCl –g- (chamber) [%]	1.072	13.529	3.321	8.638	0	0	1.134
HCl –g- (chamber) [%]	15.283	1.873	11.423	5.805	0	20.513	15.460
Al_2O_3 –s- (chamber) [%]	28.886	17.151	26.560	21.234	20.970	0	28.833
Condensed Products Mass Fraction (chamber) [%]	28.886	17.151	26.560	21.234	50.514 [a]	0	28.833
Products Mean Molar Mass (nozzle) [g/mol]	30.032	26.335	26.560	26.153	28.523	25.305	29.343
CO –g- (nozzle) [%]	20.084	27.802	30.446	30.360	5.484	12.497	22.722
N_2 –g- (nozzle) [%]	17.939	23.633	20.988	22.425	33.338	21.372	16.180
H_2O –g- (nozzle) [%]	8.810	0.002	0.290	0.003	0.001	22.178	7.889
CO_2 –g- (nozzle) [%]	3.087	0.001	0.127	0.001	0	21.670	2.927
HCl –g- (nozzle) [%]	17.759	6.675	14.834	7.732	0	21.412	17.848
Al_2O_3 –s- (nozzle) [%]	30.221	26.822	30.203	26.974	22.154	0	30.225
C –s- (nozzle) [%]	0	4.342	0	1.802	28.118	0	0
Condensed Products Mass Fraction (nozzle) [%]	30.221	31.164	30.203	28.776	56.766[b]	0	30.225

[a] Solid carbon is present at 25.21% and Al_4C_3 at 4.334%, [b] AlN at 6.494%

The comparison between the results of the experiments make it possible to understand better the complex mechanism that gives rise to the agglomerations, and its main control parameters.

Chapter 4

Experimental Techniques

4.1 Experimental Setup

All measurements were performed inside the ICT window bomb, allowing a good adjustment of gas pressure (nitrogen) and giving the possibility for non-intrusive measurements and observations.
To investigate the burning behaviour, temperatures and spectra of the presented formulations (Tab. 3-2), a high speed camera and a combined UV/VIS NIR spectrometer were used.
Fig. 4.1 shows the experimental setup.

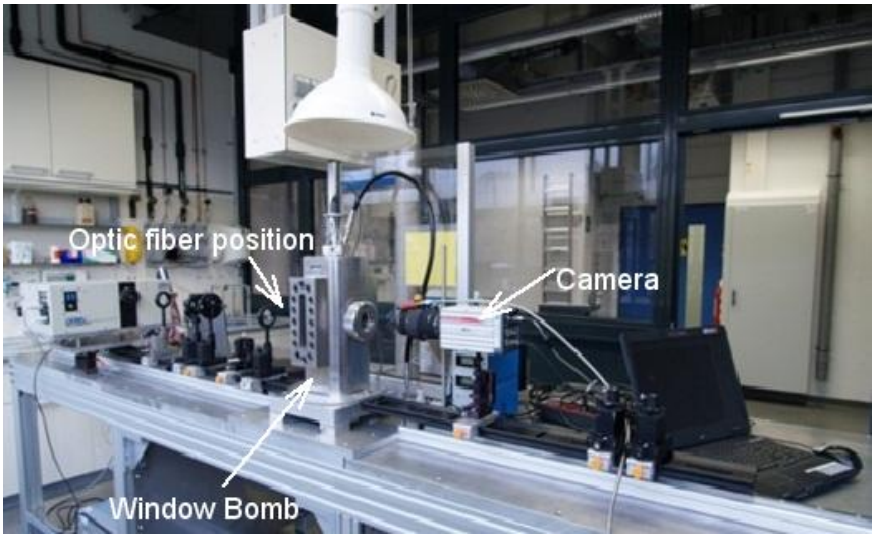

Fig. 4.1. Experimental setup

The ICT window bomb (Fig. 4.2) is a chimney type pressure vessel with a constant gas flow during the combustion process to ensure the removal of smoke allowing an unhindered view on the burning sample. It is also equipped with 4 optical windows, 2 circular, with the possibility to change the type of glass to enable spectroscopic investigation in different wavelength ranges, and 2 rectangular for the visual investigations. The vessel can be used in a pressure range from 0.1 to 15 MPa, even with different gases like air, oxygen, argon and (as it is used here) nitrogen.

Low pressures were achieved by connecting the vessel with a vacuum pump reducing pressure to 0.02 MPa. For each formulation the pressure steps were 0.1, 1, 3, 4 or 5, 7, 10, 13 and 15 MPa.
Ignition was performed using a fuse wire enhanced with about 50 mg of a booster mixture.
To support a linear burning velocity and to prevent rough burning, sometimes an inhibition with Estane^{TM} on the lateral surfaces of the strand was necessary.

Fig. 4.2. ICT window bomb

To observe particle agglomeration and their ignition close to the propellant surface, a long range microscope (Carl Zeiss LRM), with a focus distance of 220 mm and a maximum enlargement scale of 40, was mounted instead of the macro lens of the camera for propellant H31D and H31G. In combination with the camera, an optical resolution of 8 µm per pixel was achieved, but accompanied by the loss of depth of focus, which was reduced to less than 0.5 mm. Due to the low quality of the images obtained with this configuration and due to a better understanding of the aggregation behaviour of aluminium particles inside the entire flame, the classical solution using macro lens was preferred. This combination yields the best compromise between image quality and resolution (13-14 µm per pixel).
In order to collect aluminium particles of the formulation H32 during the burning process, an SEM sample holder was fixed above the strands inside the window bomb, at various distances from the upper surface dependent on the observed flame length. In dependence of pressure the following distances were chosen: 10 mm for 0.1 and 1 MPa, 15 mm for 3 and 5 MPa and at least 5 mm for the other pressure steps. To prevent a possible contamination of the sample holder with the booster mixture, the strands

were ignited only by a fuse wire. The particle collection was carried for all of the investigated pressure levels for the formulation H32.
The collected particles were transferred to a specular sample holder. The second sample holder allows to study the particles that impinge first on the original sample holder.
For the biggest particles it was sufficient to collect them from the bottom of the window bomb after the combustion; however these particles are different from the ones observed on the burning surface, because of their time history and flying path inside the bomb.
To avoid further oxidation of the samples, they were observed soon after the combustion.
The observations were performed using a field emission scanning electron microscope (FE-SEM, Zeiss Supra 55 VP). In addition elemental composition of the particle surface was investigated using energy dispersive element analysis (EDX).
Larger particles were observed with a light microscope RMA 5 (Askania) equipped with a CMOS-Digital-Camera (ABS GmbH).
In order to get spatial-resolved spectra a 2 mm slit diaphragm was fixed in front of the strand, reducing the field of view of the optic fibre. So a better differentiation between surface temperature and the temperature of the gaseous products above the burning surface was possible (Fig. 4.3).

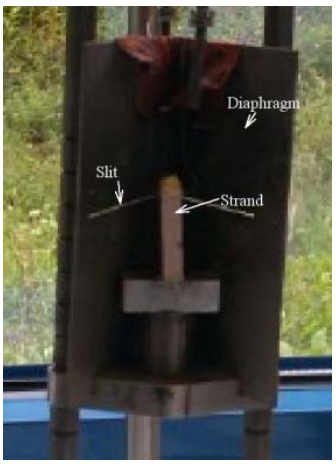

Fig. 4.3. Experimental Set-up (alane strand)

4.1.1 UV/Vis- NIR-Spectrometer

The used spectrometer system is a modular combination of two emission spectrometers working in different spectral ranges. It consists in an NIR spectrometer (MCS 611 NIR 2.2) with a wavelength range from 900 - 2140 nm and a minimum wavelength resolution of 18 nm and an UV/VIS spectrometer (MCS 621 Vis 2) with a wavelength range from 310 – 1100 nm and a wavelength resolution of 10 nm, both from Carl Zeiss AG.

The integration time of the system can be varied from 3 ms to 2 s with a time resolution up to 60 Hz. The detector of the NIR spectrometer consists in an InGaAs diode array and a Si diode array for the UV/Vis spectrometer (both manufactured by Hamamatsu). As optical entrance a 1000 µm glass fibre is used and the spectra were calibrated using a black body radiator.

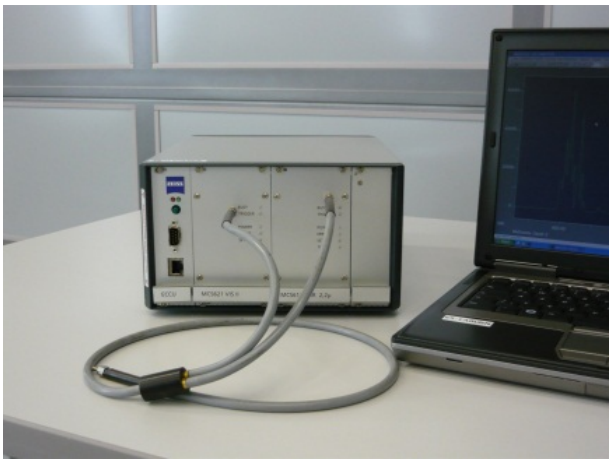

Fig. 4.4. UV-VIS-NIR-spectrograph

Furthermore the different spectral ranges allow different investigations of the flame and the combustion process. In UV/Vis range the spectra of excited Di-atomic molecules (like AlO or OH) and atomic lines of metals (like potassium and aluminium) can be seen. While in NIR range the emission of condensed materials (surface, particles) and water can be observed. In Tab. 4-1 the main features of the spectrometer system are reported.

Tab. 4-1 Spectrometers data

Module	MCS621 Vis2	MCS611 NIR2.2
Spectral range [nm]	310 – 1100	900 – 2140
Detector	Hamamatsu Si diode array, 256 Pixel	Hamamatsu InGaAs diode array, 256 Pixel
Monochromator	Flat field 366 Lines/mm	Plan mesh 300 Lines/mm
Integration time[ms]	3 ms – 5000 ms	0.3 ms – 2000 ms
Reading time[Hz]	Max. 60	Max. 60
Spectral resolution [nm]	10	18

4.1.2 High Speed Camera

To observe the combustion of the propellant, a 24 bit colour high-speed camera (MotionProTM X-3, Redlake) equipped with a 105 mm macro lens or the long range microscope was used. The recording frequency ranges

from 25 fps to 64000 fps. At full resolution (1280 x 1024 pxl) the maximum achievable recording frequency is 2000 fps which can be enhanced up to 64000 fps at the reduced resolution of 1280 x 16 pxl. A typical resolution used for the experiments was 1280 x 160 (horizontal camera) with a frequency of 4000 fps. The exposure time was varied between 250 µs and 50 µs depending on the brightness of the flame.

4.2 Evaluation of the Results

The measurements obtained were mostly treated using self-made software of Fraunhofer-ICT. All the data obtained were then post processed using the software OriginPro 8.5. Some data were not taken into account because of the excessive scatter or for their suspicious value. If it was not possible to give a certain result it was preferred to omit the result or redo the experiment, if possible.

4.2.1 Burning Rate

To get the linear burning rates the movies taken by the high speed camera were analysed with the software AVICORE32 and ABBRAND v2.

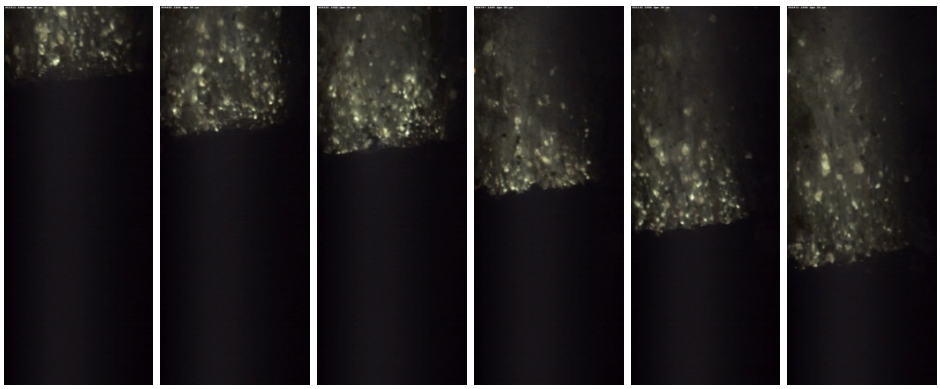

Fig. 4.5. Typical sequence of frames of a burning strand (A1)

First AVICORE32 takes every single frame of the movie (Fig. 4.5), generates an intensity histogram, resulting in an image, which represents the time history of the burning surface (Fig. 4.6).
In Fig. 4.6 are presented the typical regression lines of the investigated propellants. In a second step the pictures obtained from AVICORE32 were evaluated with the software ABBRAND v2 to receive the burning rate. This method is described more detailed by Weiser in [65]. The resulting burning rates were depicted as function of pressure obtaining both the pre-exponential factor and the ballistic exponent using a least-squares fit of Vieille's law.

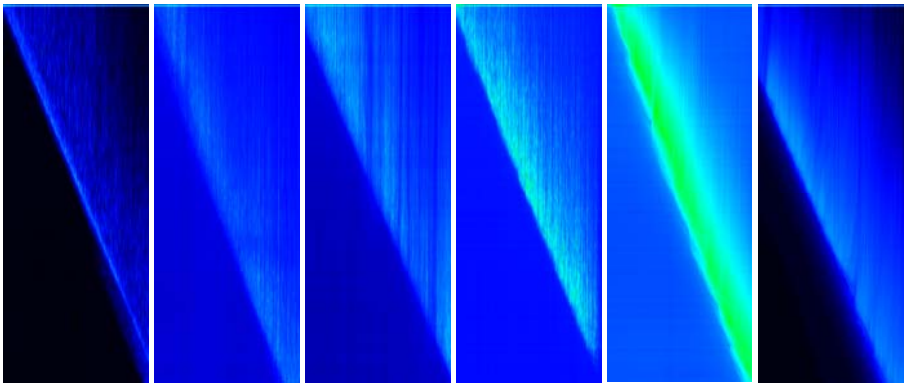

Fig. 4.6. Regression images for the determination of burning rates obtained using the software AVICORE32 (from left to right: H32 at 1 MPA, A3 at 3 MPa, A7 at 5 MPa, A2 at 7 MPa, H59 at 10 MPa and H57 at 13 MPa)

4.2.2 Temperature

The spectral data were calibrated in relative intensity per unit wavelength using a black body radiator. This calibration creates relation between the raw output data of the spectrometer and the input data for the ICT-BaM code which uses theoretical standards of known spectral data.

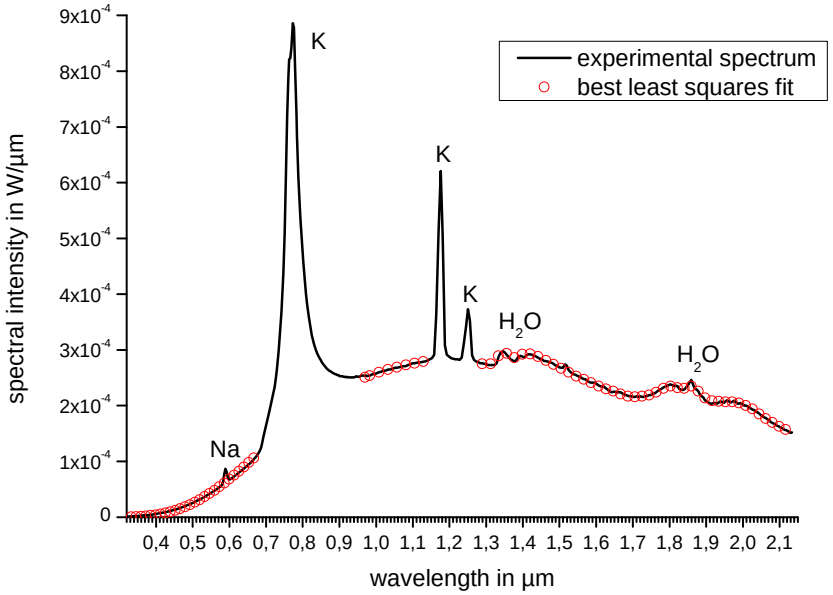

Fig. 4.7. Typical emission spectrum and least-squares fit provided by ICT-BaM code (H32 at 3 MPa)

The purpose of ICT-BaM program is fitting calculated spectra to calibrated spectra measured with different spectrometers in infrared (IR), near infrared (NIR), visible (VIS) and ultraviolet (UV) spectral range. According to the different types of spectra, different models are applied. Continuous radiation is calculated using either the Planck's law of black

body radiation with wavelength-independent emissivity or a model for radiation of soot from [66]. Main bands of water and carbon dioxide can be calculated using the Random Band Model from [66]. This model can be applied to carbon monoxide, nitrogen monoxide and hydrogen chloride using data from [66]. The same model can be used for many metal monoxides with data from [67].
Once the spectra are calculated they have to be fitted to the measured spectra.
Fit parameters are the temperature and the concentration of the expected species. More information can be found in [68].
The Figure 3.7 shows a typical UV/VIS/NIR emission spectrum.
It is possible to see how the potassium impurities act in the spectra giving their typical main maximum at 0.77 µm and secondary maxima at 1.17 and 1.25 µm. Those peaks hide the aluminium peak which should be at 0.689 µm, but fortunately, do not invalidate the temperature measurement.
The temporal resolution of the spectra allow also to estimate the flame length, considered as the time of quite constant intensity after the peak due to the burning surface, multiplied by the burning rate.
The physical principle of work of the emission spectrometer allows an important conclusion concerning the agglomerations study. Since the aluminium particles are supposed to be the brightest particles in the flame it is reasonable to think that the measured spectra are mostly related to these particles. Therefore the measured temperature should be related to the surface temperature of the agglomerations.

4.2.3 Agglomeration

The measuring of the agglomerate size and their behaviour was done analysing the video record and determining the size of all well-defined and detached particles, as shown in [69].
The pressure levels of investigation for the ADN/GAP-based formulations were 0.1, 1, 3, 5 MPa (for mixture H27 only measurements at 1 MPa are available). For AP/GAP/Al formulations it was possible to analyse the agglomeration phenomena up to 13 MPa.
The analysis of the movies was done utilizing video-managing software (VitualDub 1.9.11), in order to achieve better sharpness and better brightness of the obtained movies. Sometime it was also necessary to modify the colour in order to have a better distinction of the agglomerates inside the flame. After this process the obtained movies were imported in ImageJ 1.37v which provides the manual estimation of the diameter of each agglomerates considered valid.
The minimum size of the control sample to get a good population for the statistical analysis was found to be 200. In most cases this requirement could be fulfilled.

The resolution of the video defines the lowest possible measure of the particle. No “one pixel” agglomerate was observed.
The high brightness of the flame again defines another limitation of this technique. Not so bright shining or dark particles can hardly be seen in the movies and are not taken into account.

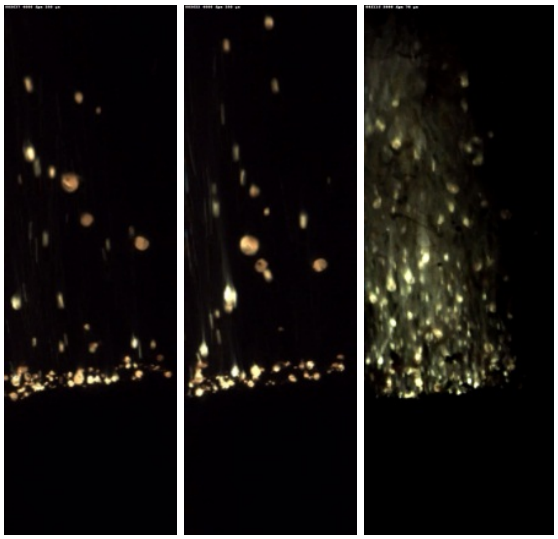

Fig. 4.8. Typical image optimized for the agglomeration study (from left to right, H32 and H53 at 1 MPa and A1 at 3 MPa)

This method also allows the investigation of the aggregation steps on the burning surface of the propellant, the collision between the particles and their movement.
Further investigation of the agglomeration behaviour was made tracking each particle, recording their position from its generation until their leave of the field of view. This makes it possible to study the velocity of the agglomerates.

Chapter 5

Experimental Results

The results obtained will be presented divided into different formulation classes: starting from ADN/GAP formulations (for a better understanding of the behaviour of the pure material as a kind of reference), then ADN/GAP/Al, ADN/GAP/alane and at last the formulations containing AP/GAP/Al.
Since it is the first time that a characterization of this kind of propellants was made in a comprehensive way, it is considered useful to introduce the results starting from what is expected based on the know-how acquired so far.

5.1 Expected Results

The first class of propellants analysed is the one only containing ADN and GAP. Refering to Pak in [27] and Menke in [31] it is expected, that an increase of the particle size of the oxidizer leads to an increase in burning rate with ADN and a decrease using AP assuming an analogue behaviour as it is found in classical AP/HTPB formulation (see Fig. 5.1).
The predicted temperature of the AND/GAP burning surface should be around 900 K (200 K more than the classical AP/HTPB).

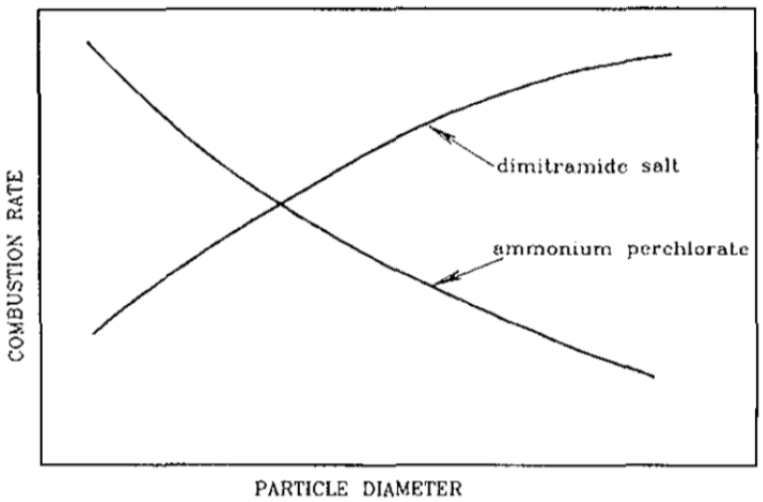

Fig. 5.1. Hypothesized influence of different diameters of the oxidizer particles on the burning rate [27]

The explanation of the opposite burning rate reaction on different sizes of the oxidizer particles based on the assumption of a dominating role of ADN during the combustion.
The addition of micrometre-sized aluminium to ADN/GAP formulation should lead to an aggregation/agglomeration behaviour which provides less but larger agglomerates than the AP/HTPB/Al formulation.
The following factors are assumed to play an important role:

- ADN and GAP both are energetic compounds. They increase the combustion temperature of the burning surface enabling an agglomeration without a structured aggregation;

- The high thermal sensitivity of binder and oxidizer enhance the energetic aspect, so the thermal wave could deeper penetrate the propellant and also the aluminium contained in the condensed phase, forcing the pre-aggregation of the pockets;

- The mechanical properties of the ADN/GAP/Al propellants, can provide higher amounts of aluminium on the burning surface due to the "squeezing" of the strand caused by pressure and temperature;

- A possible molten liquid layer on a burning surface (as in the case of AN) should prevent the detachment of the agglomerates allowing a disproportionate growth.

The high burning rate should mitigate those effects because of the shorter time that the incipient remains on the burning surface. For this reason, increasing pressure should lead to larger number of smaller agglomerates.
The increase of particle size and the bimodal distribution of oxidizer should lead to an increase of agglomerate size, because of the increase of pocket's dimension (Cohen in [41]).
The addition of nano-sized aluminium (activated or not) should lead to a higher number of small agglomerates of the "flake" type (typical of nano-aluminium) on the burning surface [58].
The transition between the coral structure of the aggregate and the spherical agglomerate will be achieved only after detachment.
The addition of alane is presumed to yield lower temperatures compared with the aluminized propellants because of the dissociation of alane and a higher number of smaller sized agglomerates of matrix type (considering the amount of fuel in the formulation is maintained).
The AP based propellants are presumed to generate agglomerates of the same type ("oxide cap") and of the same dimension as ADN/GAP/Al

propellants for the formulation having the same oxygen balance and same adiabatic flame temperature. The formulations with lower adiabatic flame temperature are expected to give rise to smaller agglomerates.
Concerning the formulation A2 (AP/GAP/Al), which has the same heat of formation as the ADN/GAP/Al propellant, it was not taken into account that this thermochemical aspect would affect the aggregation-agglomeration behaviour.

5.2 ADN/GAP

The formulations only composed of ADN and GAP (70:30) were investigated at 5 different pressure levels: 1, 4, 7, 10, and 13 MPa.
The formulation H58 containing oxidizer particles of 272 µm shows problems in manufacturing so it could not be investigated.
The other formulations, H55 (212 µm), H56 (153 µm), H57 (55µm), H59 (55 µm) and H60 (raw crystal) were studied with high speed camera and UV/Vis- NIR-spectrometer.
The irregular combustion of the formulations requires an inhibition (estane) of the side walls of the strands.

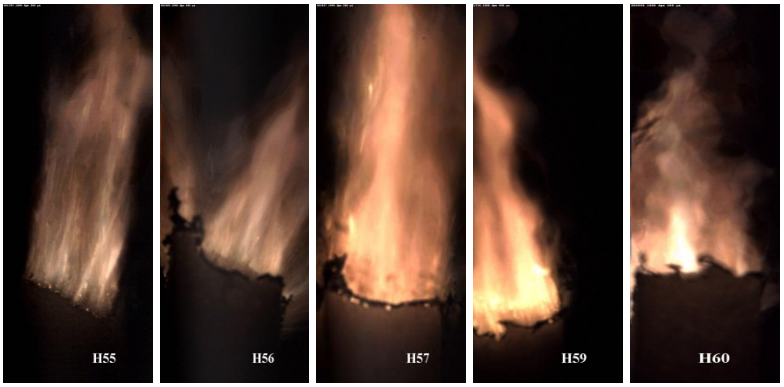

Fig. 5.2. Burning of ADN/GAP propellants at 4 MPa

The inhibition burnt down slower than the strands making it sometimes difficult to have a clear view on the burning surface and to detect radiation emitted by the surface for temperature measurement (see Fig. 5.2).
The flame was regular up to 7 MPa without a dark zone as observed for the double base propellants. The burning surface mostly remains horizontally.
Starting at 10 MPa a combination of smoke and movements of the strands made it difficult to get an unhindered view on the burning strand but the burning rate measurement was not affected. Also the flame shows a less regular behaviour.

The formulation H59 (with 55 µm ADN prills) shows a regular combustion process for the entire pressure range with a stable flame and without a strong generation of smoke.
Flamelets, that appear on the burning surface starting from bright spots, which suddenly disappear, were observed. This was interpreted as the combustion of the carbonic structure left by the first decomposition of GAP (Fig. 5.3). These flamelets are attenuated with increasing pressure, generating a more homogeneous dark orange and magenta flame.

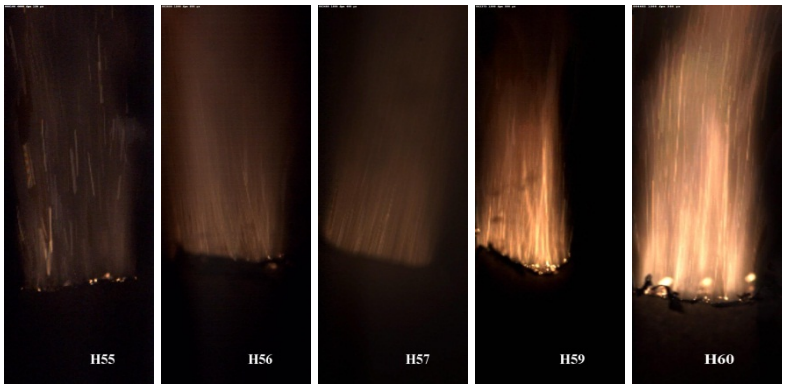

Fig. 5.3. Flames of burning ADN/GAP at 1 MPa with bright spots and flamelets

5.2.1 Burning Rate

The burning rates of the different ADN/GAP formulations do not show significant differences at 1 MPa. The values range from 9 to 10 mm/s. The behaviour changes with increasing pressure where the propellant containing the raw material (ADN in salts) shows the highest burning rates. The burning rates of the propellants containing oxidizer prills of different size are displayed in Fig. 5.4. The propellants containing bigger oxidizer prills show higher pressure dependence (n=0.61-0.66) than the two propellants with fine particles (n=0.47-0.52).

Tab. 5-1 Parameter values of the investigated propellants for Vieille's law

Label	Vieille's Law	Prills dimension	r_b at 7 MPa [mm/s]
H55	$r_b=(9.09 \pm 0.03)P^{(0.61 \pm 0.05)}$	212 µm	29.8 ± 3.0
H56	$r_b=(8.37 \pm 0.05)P^{(0.66 \pm 0.06)}$	153µm	30.3 ± 3.3
H57	$r_b=(10.61 \pm 0.04)P^{(0.47 \pm 0.04)}$	55 µm	26.5 ± 2.2
H59	$r_b=(9.27 \pm 0.03)P^{(0.52 \pm 0.04)}$	40µm	25.5 ± 2.1
H60	$r_b=(9.95 \pm 0.04)P^{(0.79 \pm 0.05)}$	Raw material	46.3 ± 4.7
H58	n.a.	272 µm	n.a.

It should be noted that the propellant H55 (black line), which contains prills more than 60 µm bigger than the prills in the propellant H56 (red line), presents practically the same parameters in Vieille's law as the latter.

For the two propellants H57 and H59 with prill sizes of 55 and 40 µm, respectively, very similar the burning rates are measured except at 1 MPa leading to different parameters in the Vieille's law.
The parameter values of the investigated propellants for the Vieille's laws and the expected burning rate at the classical chamber pressure of 7 MPa are shown in Tab. 5-1.

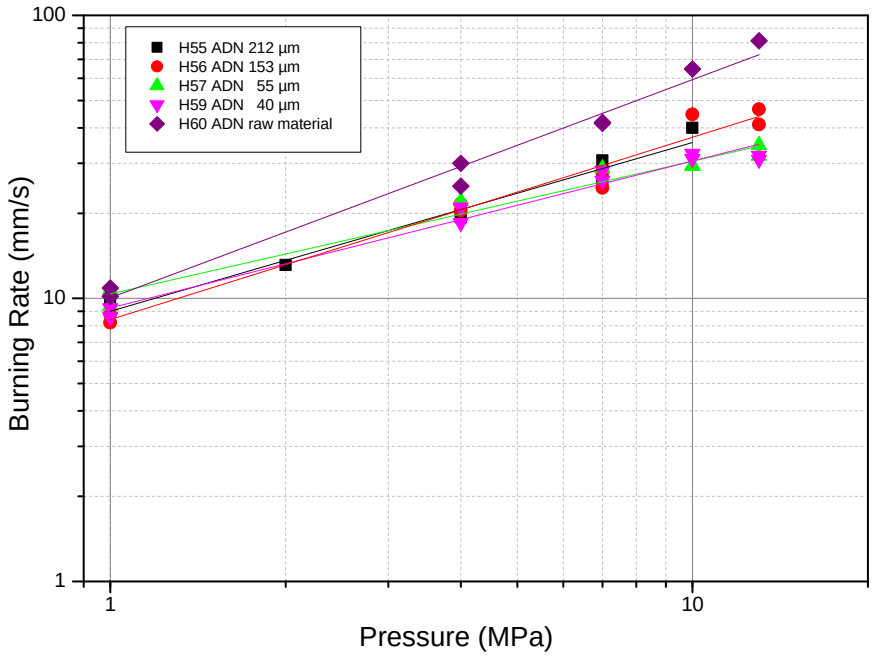

Fig. 5.4. Burning rate versus pressure for different ADN/GAP formulations

Taking into account the uncertainties of measurement it is possible to state that propellants H55 and H56 have quite the same pressure dependence, as well as propellants H57 and H59.
The propellant H57 and H59 shows a pressure exponent comparable with the one of the commercially available propellants.

5.2.2 Temperature

The burning behaviour of all these compositions is characterized by a very dark flame, tending to light magenta and orange.
The colour is mostly due to the presence of potassium an impurity of ADN, which features in a strongly emitting line at 768 nm as shown by Fig. 5.5, and to the burning particles that give the light orange and magenta colours.
The presence of this impurity requires a careful selection of the region of interest when fitting the spectra with the ICT-BaM software to determine temperature.

The presence of intense smoke, probably due to GAP or steam, covers the total emitting flame and makes it difficult to evaluate the temperature from the flame spectra at all investigated pressure levels.
The temperature histories in Fig. 5.6 show similarities with the burning rate evaluation: Up to 7 MPa the propellants with larger oxidizer particles show higher measured temperatures than those with smaller particles. Above 7 MPa all the compositions show a quite common behaviour almost stable around measured flame temperatures of 2250-2350 K in the high pressure range. The compositions with smaller prills, H57 and H59, present a monotonic increase of temperature up to 10 MPa. Unexpectedly with increasing pressure, the composition H55 shows a drop in temperature above 4 MPa.

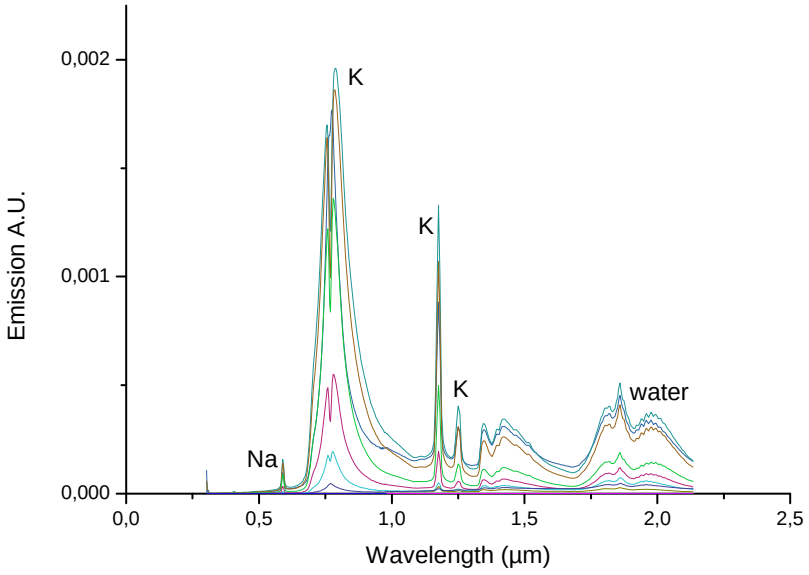

Fig. 5.5. Typical emission spectra (H57 at 7 MPa)

The formulation H60 containing raw ADN shows a quite constant temperature at low pressure (around 2400 K). But the measurements above 4 MPa failed because of a misalignment of the spectrometer's fibre optic resulting in spectra which cannot be used for temperature determination.
At 7 MPa the working pressure, the compositions show a flame temperature between 2250-2450 K.

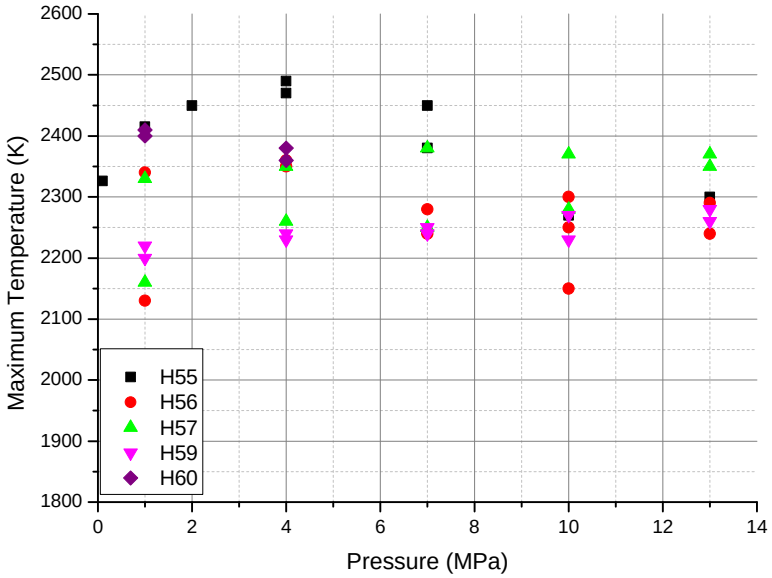

Fig. 5.6. Maximum temperatures measured for the formulations ADN/GAP

5.3 ADN/GAP/Al

The formulations containing ADN, GAP and aluminium can be divided in three main groups:

- H27, a trial formulation to investigate the manufacturing and burning behaviour;
- H31 family with 4 formulations for the study of the effect of different aluminium powder types;
- H32, the “official” formulation with bimodal distribution of oxidizer prills.

The formulation H32 was investigated in more detail.
All the formulations were investigated at different pressure levels from 0.1 MPa to 15 MPa in nitrogen.
The combustion generates intense smoke that could be handled experimentally by regulation of the flow of nitrogen to improve visibility.
All combustion tests were characterized using spectrometer and high speed camera.

The propellant H27 shows mostly a flat burning surface for each level of pressure (1, 2, 4, 7, 10, 13 and 15 MPa).
The flame was very bright without dark zone and changes colour from a light magenta at low pressure to a mostly white/yellow with green corona at high pressure.

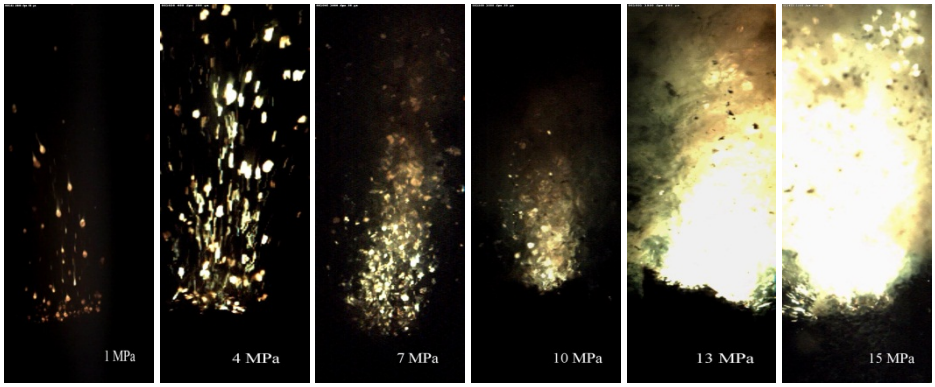

Fig. 5.7. Burning behaviour of propellant H27

The green colour at high pressure may indicate emission of AlO line system at 472, 487 and 513 nm ([73]) that are related to the combustion of aluminium. Unfortunately, the main purpose of the tests performed on this propellant did not include the agglomeration study, but only the study of burning behaviour and burning rate.
The problem of smoke became manifest at 10 MPa and above, but had not affected the measurements.

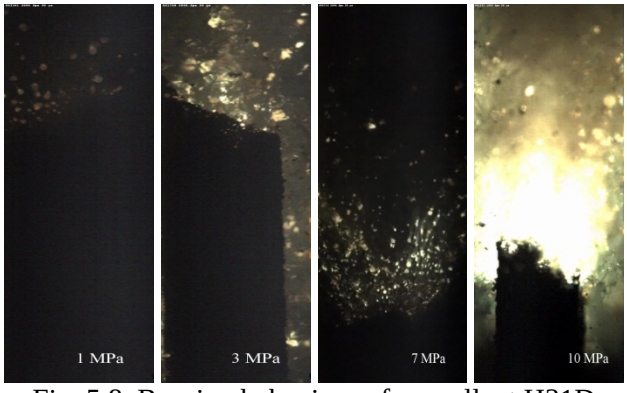

Fig. 5.8. Burning behaviour of propellant H31D

The family H31, charged with different aluminium powders, was investigated at pressure levels of 0.1, 1, 3, 7, 10 MPa. These formulations were produced also to evaluate the aggregation/agglomeration behaviour in ADN/GAP formulations. Therefore, the pressure levels do not include 13 and 15 MPa, and up to 3 MPa the long range microscope was mounted to

the high speed camera. Tests at higher pressure levels were performed with the usual macro lens of 105 mm focal length.
The formulation H31D, containing aluminium with an average size of 5 µm, shows a non-complete combustion of the binder releasing a certain amount of unburned residues. The burning surface was rarely horizontal though the inclination was not so accentuated to invalidate the burning rate measurement.

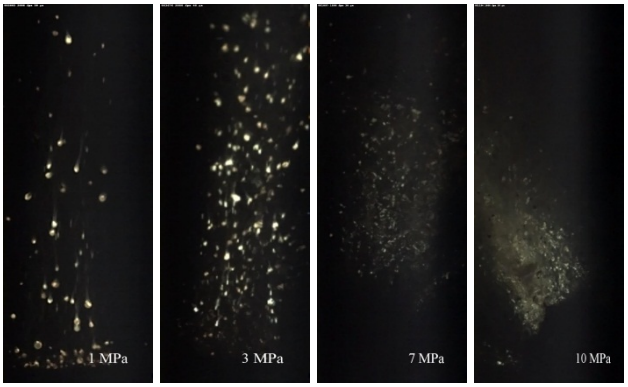

Fig. 5.9. Burning behaviour of propellant H31G

The formulation H31G, containing A1X-81 with an average particle size of 18 µm, shows a stable behaviour with a flat burning surface and rare unburned parts.
For both this micro-aluminized propellants the flame was yellow/white at all pressures under investigation but it became more and more green approaching 10 MPa. Probably at this pressure more aluminium will react in the visible flame creating more intermediate products.


Fig. 5.10. Porous combustion of H31F formulation (3 MPa)

The formulations containing nano-aluminium and nano-aluminium covered with stearic acid present manufacturing problems (Chap. 4.5); for this reason the combustion of propellants H31E and H31F have shown porous

combustion starting from 1 MPa (Fig. 5.10), invalidating the burning rate measurements at higher pressure levels.

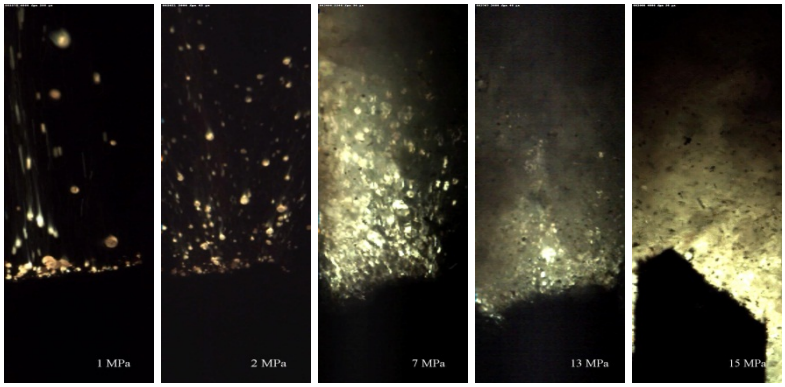

Fig. 5.11. Burning behaviour of propellant H32

The formulation H32, containing oxidizer particles with a bimodal distribution of and aluminium particles of 18 µm, was studied at several pressure levels: 0.1, 0.5, 1, 2, 5, 7, 10, 11, 12, 13, 14, and 15 MPa.
The burning behaviour was similar to the one observed for the compositions H27. The main difference is the presence of non-burning residues observed around the flame. These residues can be associated to the inhibition with estane made to prevent non-linear combustion.
The flame was brighter and more green at high pressure with respect to the other compositions. Starting at 10 MPa the particulates associated to the agglomeration effect were difficult to discern from the overall flame.
The problem of smoke began at 7 MPa requiring a strong modulation of the pressurizing flow to get a clear view on the flame.
Subatmospheric pressure experiments were carried out only for the formulation H32. The resulting pressure deflagration limit (PDL) has been estimated to be lower than 0.02 MPa (minimum achievable for the instrumentation). At this pressure the propellant begins to show the classical PDL behaviour of pulsed/detaching flame.

5.3.1 Burning Rate

For formulation H27 with larger oxidizer particles (Fig. 5.12), the burning rate measurements present high scattering at low and high pressure. But at pressures between 2 and 7 MPa, the measurements reveal nearly the same burning rate at a certain pressure level, which means having a good reproducibility.
Fitting the measured burning rates with Vieille's law, a pressure exponent of about 0.57 has been estimated.
The study conducted on the propellants H31D and H31G has revealed nearly the same burning rate values for both propellants, with the tendency

of lower burning rate for the propellant H31G, which contains aluminium particles of larger size.

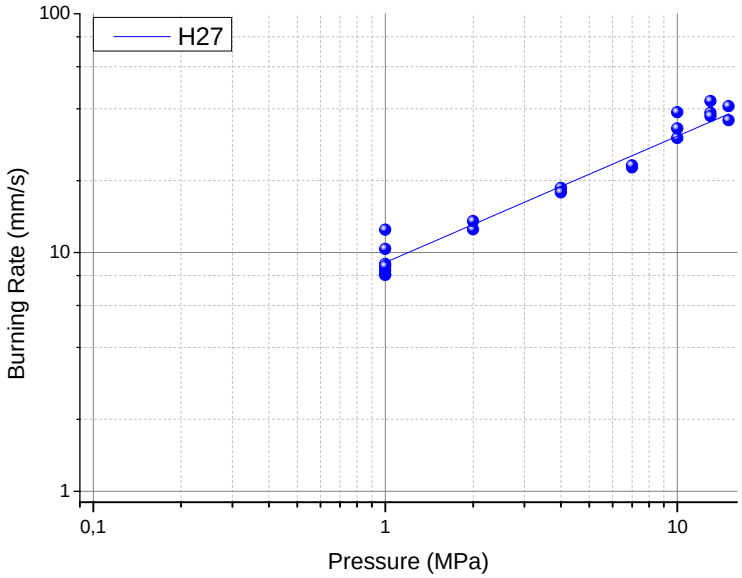

Fig. 5.12. Burning rate versus pressure for propellant H27

Increasing the pressure the burning rates almost overlap (Fig. 5.13).
At a pressure of 0.1 MPa the two compositions present flat burning surfaces and a stable burning behaviour. The disagreement in burning rates, although very small, was traduced in a bad fitting with Vieille's law. Therefore it was decided to start the fitting at a pressure of 1 MPa.
The fitting with Vielle's law (considered quite good since the residual sums of squares were 0.034 for H31G and 0.036 for H31D) exhibits a different pressure dependence for the different aluminium powder sizes. The propellant H31G reveals more sensibility to pressure (n=0.64) compared with the propellant H31D (n=0.52).
The burning rate of propellant H31G overtakes the one of H31D at a pressure of 3 MPa (Fig. 5.13) and the difference between the two pressure exponents is more than 20% but they present quite similar burning rates at working pressure.
To characterize the formulation H32 several burning test were done (between 2 and 6 for each pressure level).
In parallel, additional tests were made to evaluate the inhibitor contribution to burning behaviour.
Fig. 5.14 compares inhibited with non-inhibited strands. The differences in burning rate and in burning behaviour are so small that they fall inside the

uncertainty of measurement. For this reason the subsequent tests were made with estane isolation.

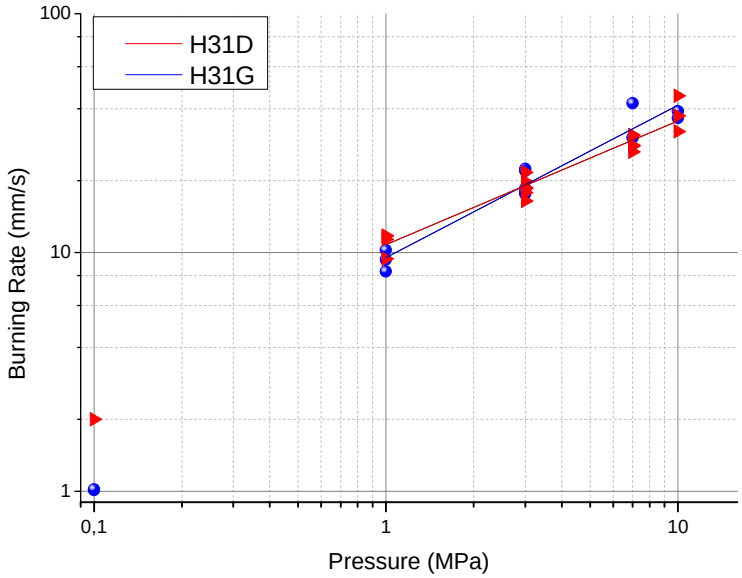

Fig. 5.13. Burning rate versus pressure for different aluminized propellants

The reproducibility was reasonable good and Vieille analysis reveals a pressure dependency of about n=0.58.
At pressure levels higher than 10 MPa both formulations H32 and H27 shows high scattering of burning rates with quite stable mean values between 35 and 40 mm/s.
In Tab. 5-2 the different Vielle parameters are compared. It is noticeable that the formulations H27 and H32 results in quite similar parameters despite the different oxidizer prill technology and prill size distribution.

Tab. 5-2 Parameters for Vieille's law for aluminized formulations

Label	Vieille's Law	Prills size	Al size	r_b at 7 MPa [mm/s]
H27	$r_b=(8.36 \pm 0.01)P^{(0.57 \pm 0.01)}$	228 µm	18 µm	25.3 ± 0.5
H31D	$r_b=(10.79 \pm 0.02)P^{(0.52 \pm 0.03)}$	208 µm	5 µm	29.7 ± 1.8
H31G	$r_b=(9.51 \pm 0.03)P^{(0.64 \pm 0.05)}$	208 µm	18 µm	33.0 ± 3.3
H32	$r_b=(8.58 \pm 0.02)P^{(0.58 \pm 0.02)}$	208 / 55 µm	18 µm	26.7 ± 1.1

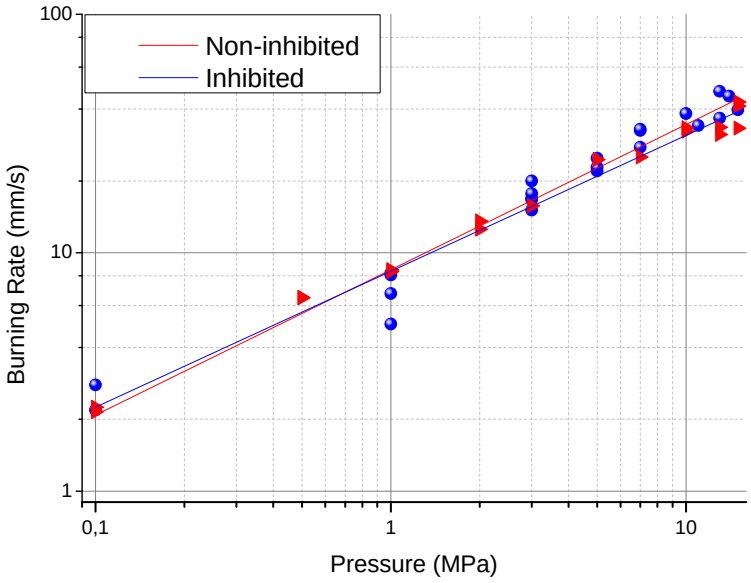

Fig. 5.14. Burning rate versus pressure for the bimodal propellant H32 with comparison between inhibited and non-inhibited strands

5.3.2 Temperature

For all aluminized ADN/GAP propellant compositions, the temperatures show an increasing trend with pressure.

Again it was possible to see a maximum of intensity attributable to the burning surface, probably due to the aluminium lying on the surface during the aggregation/agglomeration phases or other highly emitting particles.

The intensity is gradually reduced in a place considered as the luminous flame or the region of “flight” of detached agglomerates.

As an example, intensity and temperature results from ICT-BaM code analysis are reported in Fig. 5.15 for the propellant H27 at 4 MPa.

Because of the physical principle upon which the temperature evaluation is based, it is allowed to assume that the determined temperatures are an estimation of the surface temperatures of the aluminium particles.

The temperatures of formulation H27 (Fig. 5.16) behaves similar to the formulation H31G (Fig. 5.17). Both the formulations show a maximum temperature around 2750 K at 10 MPa, starting more or less from 2200 K at 1 MPa.

The maximum temperature of formulation H27 seems to maintain a value between 2650 and 2750 K for the pressure range 7-13 MPa (Fig. 5.16).

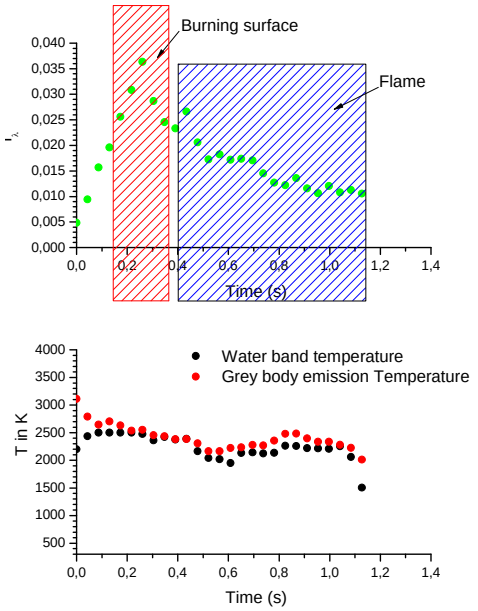

Fig. 5.15. Example for the determination of the position of the burning surface and the flame length in time domain

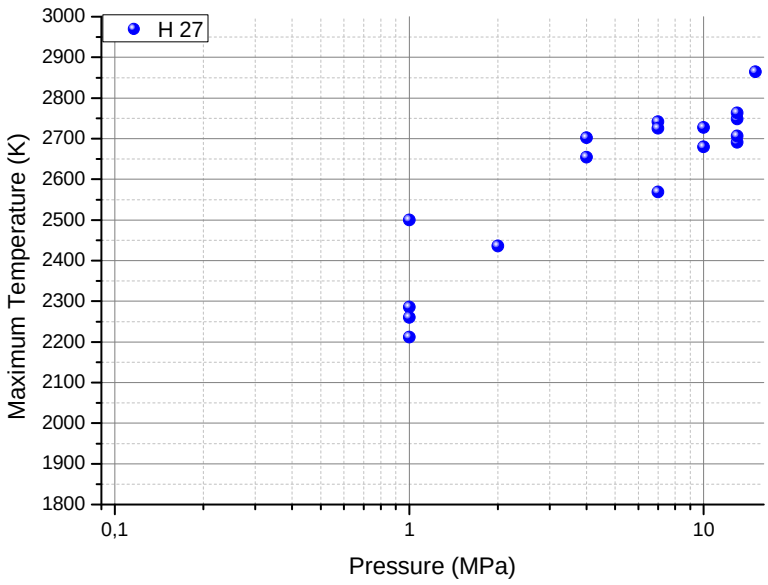

Fig. 5.16. Maximum temperatures versus pressure for formulation H27

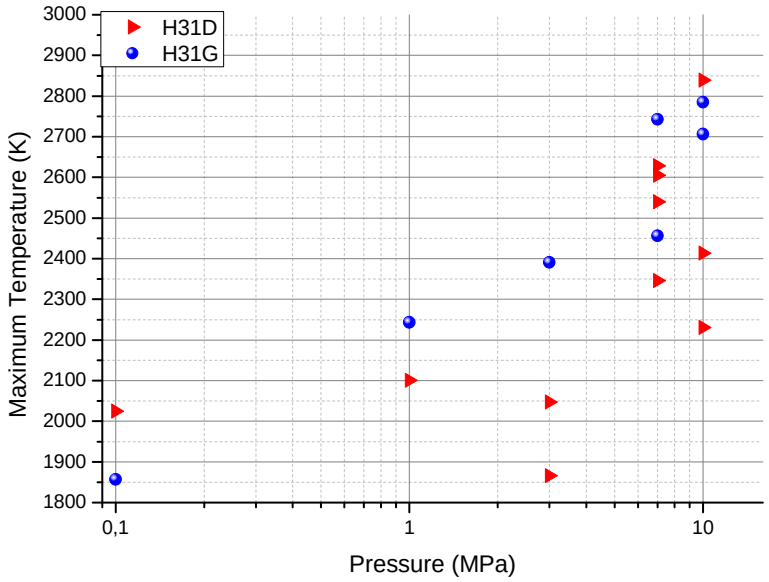

Fig. 5.17. Maximum temperatures versus pressure for formulations H31

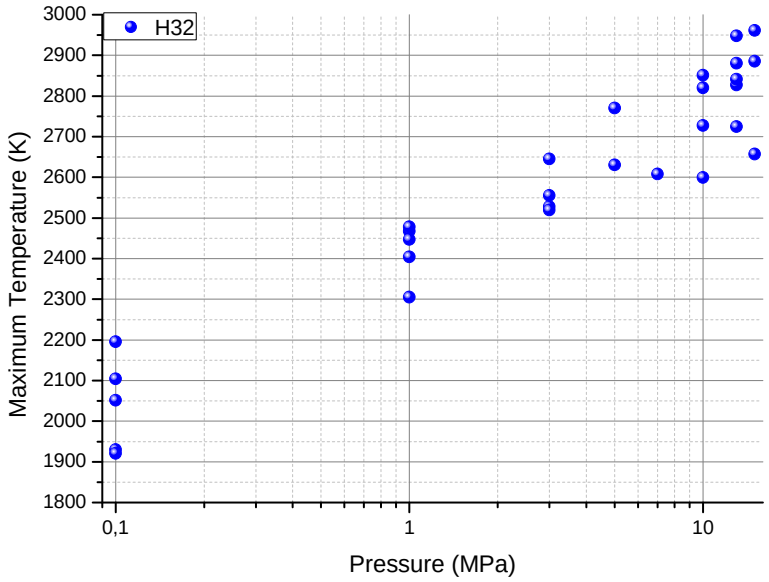

Fig. 5.18. Maximum temperatures versus pressure for formulation H32

The formulation H31D, with the smaller aluminium particles, presents the lowest maximum temperatures, except for atmospheric pressure.
The formulation H32 presents a quite defined increase of temperatures with a range of 250 K for each pressure steps; starting from around 2000 K at atmospheric pressure, up to nearly 3000 K at 15 MPa (Fig. 5.18).
All measured temperatures were higher than the melting point of aluminium, and at 5 MPa and above the measured temperatures are higher than the melting point of alumina at 0.1 MPa (assuming melting temperatures of aluminium and aluminium oxide have low pressure dependencies).
At 10 MPa the temperature was even higher than the boiling point of aluminium at 0.1 MPa for almost all the formulations.

5.3.3 Agglomeration

For all investigated ADN/GAP/Al formulations, the agglomerates do not differ so much from the ones observed in AP/HTPB/Al.
They seem to be mostly round presenting the same cap of oxide (with some minor exceptions) typical for AP/HTPB/Al propellants ([52]).
After lift-off they show the same turning movement passing the flame zone mostly in a straight line.
It had been observed that the aggregation phenomena for the ADN/GAP/Al formulations investigated can be subdivided in the following five steps ([2]):

1) Pre-aggregation inside the condensed phase which result in an increase of the diameter of the emerging aluminium particles (perhaps that the aggregation starts inside the pores left by the pyrolysis of GAP);
2) Emerging of the pre-aggregated particles on the burning surface and possibly first ignition or at least exothermic oxidation;
3) Local aggregation with nearest or underlying particles and completion of the transition between aggregates and agglomerates with formation of the well-known oxide cap;
4) Rolling of the particles on the burning surface which can result in further aggregation with other rolling particles, non-moving particles or possibly fall into a pore of the strand;
5) Possible inflammation and detaching from the burning surface.

The distribution of the particles seems to be affected mostly by the dimension of the oxidizer prills instead of the dimension of the initial

aluminium. Propellant H27, in fact, presents the largest agglomerates and the two propellants H31D and H31G present quite the same results.

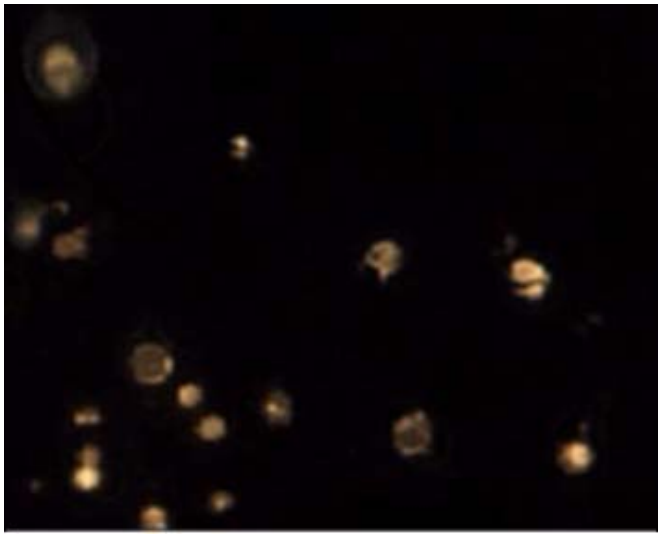

Fig. 5.19. Typical agglomerations for ADN/GAP/Al propellants

Starting at 1 MPa the detachment of agglomerates for propellants H31D, H31G and H32 appears to occur with a relatively narrow distribution of diameters. This narrow range of diameters became smaller and smaller increasing pressure, as it possible to see by the comparison of the histograms presented in Fig. 5.22, Fig. 5.23 and Fig. 5.24 (all the histograms were made on a basis of 400 and 1800 measured agglomerates).

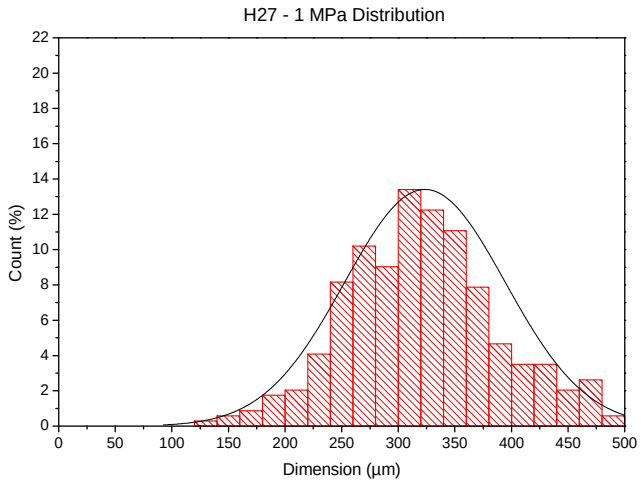

Fig. 5.20. Agglomerate size distribution for H27 propellant (1 MPa)

A study of the emerging particles was conducted for propellant H32.
At the first appearance, all the emerged particles (this means getting visible due to glowing) feature in the same diameters of about 75-80 µm, which is 4 times larger than the particles of the original aluminium powder.
The further increase of diameters due to aggregation/agglomeration effect generates agglomerates for which the dimension grows by a factor of ten or more with respect to the original size of the aluminium, as possible to see looking at Tab. 5-3.

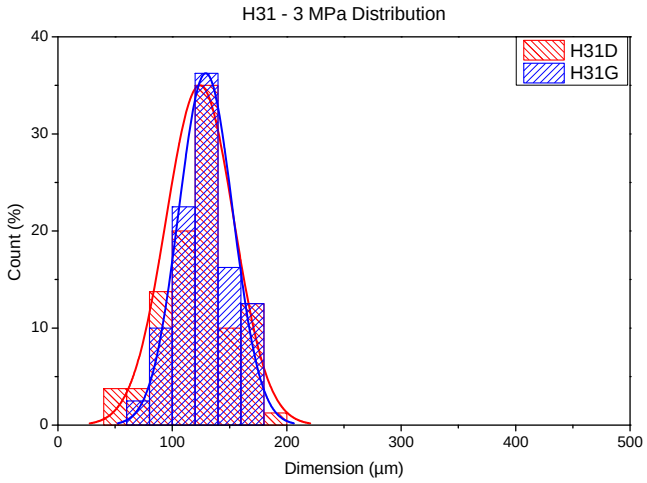

Fig. 5.21. Comparison of distribution and average size for propellants containing different aluminium powders

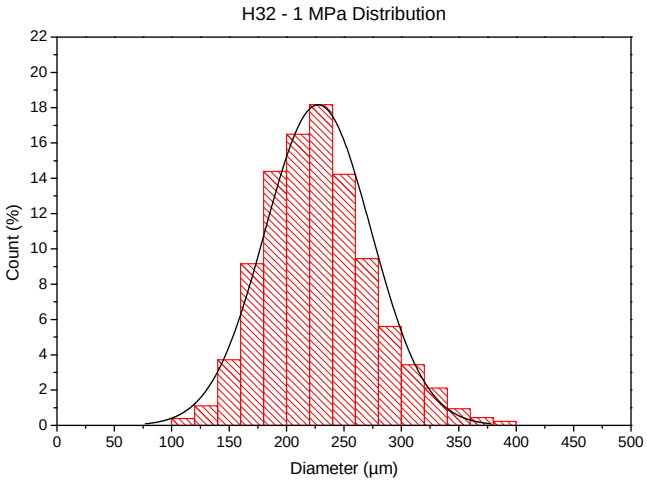

Fig. 5.22. Agglomerate size distribution for H32 propellant at 1 MPa

The behaviour of the particles in the investigated range of pressure, from 0.1 to 5 MPa, seems to be a monotonic decreasing in accordance to what is observed for AP/HTPB/Al propellants in [40] and [58].
From Fig. 5.25 it is clearly visible that an increase of only 20 μm in oxidizer particles size gives rise for an increase of agglomerations size of more than 30% compared with the agglomerations created by the bimodal propellant H32. The lower size agglomerates are created by the propellant with monomodal distribution of oxidizer prills. Again it is possible to see that the changes in aluminium powder size do not change the size of the resultant agglomerates.

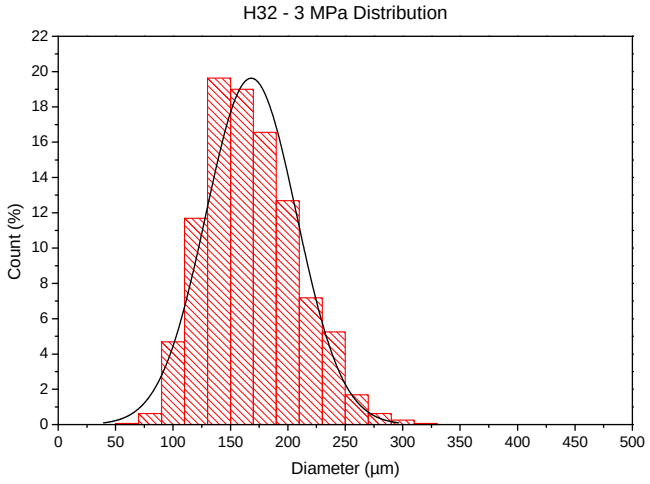

Fig. 5.23. Agglomerate size distribution for H32 propellant at 3 MPa

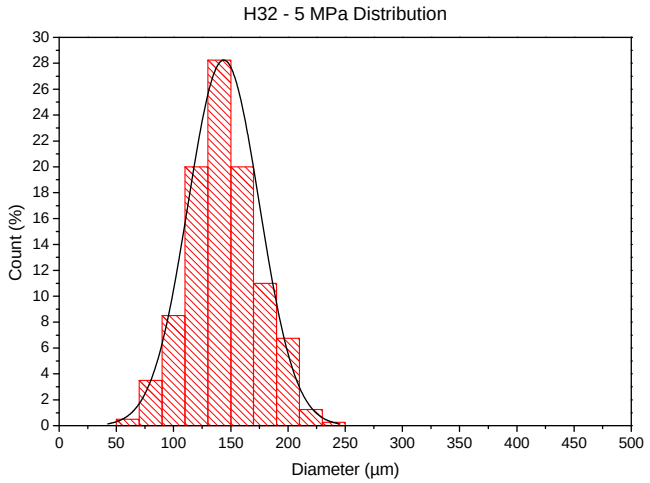

Fig. 5.24. Agglomerate size distribution for H32 propellant at 5 MPa

The high speed video analysis has also shown a phenomenon that has been interpreted as the boiling of the agglomerations. But this behaviour can also be due to minor darker residues of binder or minor oxidized products that collide with the agglomerates, or it is due to the flow field in which the agglomerate is immersed.

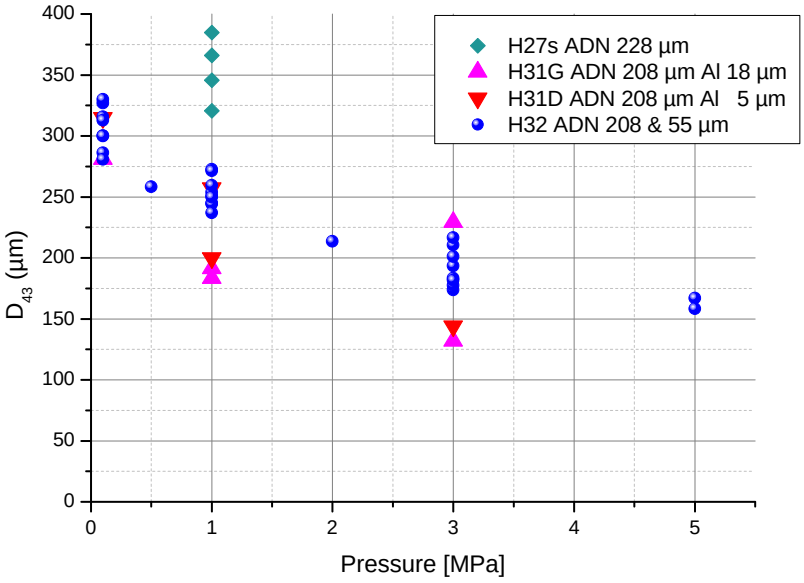

Fig. 5.25. D_{43} of the measured detached agglomerations for the different formulations.

Tab. 5-3 Agglomeration measurements (average on overall observation)

Pressure [MPa]	Label	Average diameters [µm]	D_{43} [µm]	D_{32} [µm]
0.1	H31D	276.8 ± 9.9	315.0	302.5
	H31G	274.0 ± 11.3	323.7	307.6
	H32	264.5 ± 10.1	306.1	292.6
0.5	H32	226.8 ± 8.1	258.3	248.0
1	H27	294.2 ± 11.8	344.0	328.1
	H31D	167.8 ± 7.0	200.1	189.4
	H31G	165.4 ± 5.5	187.4	179.5
	H32	227.5 ± 7.6	255.8	246.3
2	H32	187.1 ± 6.9	213.6	205.2
3	H31D	126.7 ± 4.8	144.0	138.9
	H31G	129.2 ± 3.9	131.9	131.9
	H32	168.1 ± 6.5	195.6	186.6
5	H32	143.9 ± 5.1	163.1	157.0

The boiling of aluminium can explain the hollow particles found in the SEM analysis (Fig. 5.26), and shown in the following pictures, of the residues collection for propellant H32.
The procedure of transferring the particles from the original sample holder to the specular one leads to the possibility to observe the backside of the particles. On this surface holes were observed which probably contained entrapped gas during the hitting against the plate. Another possibility is that the agglomerates were containing aluminium vapour generated after the collision by the flame heating (Fig. 5.27).

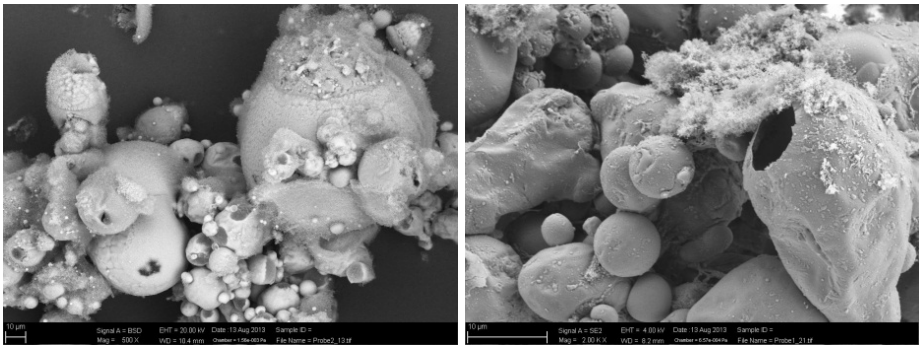

Fig. 5.26. SEM images of hollow collected products (0.1 MPa)

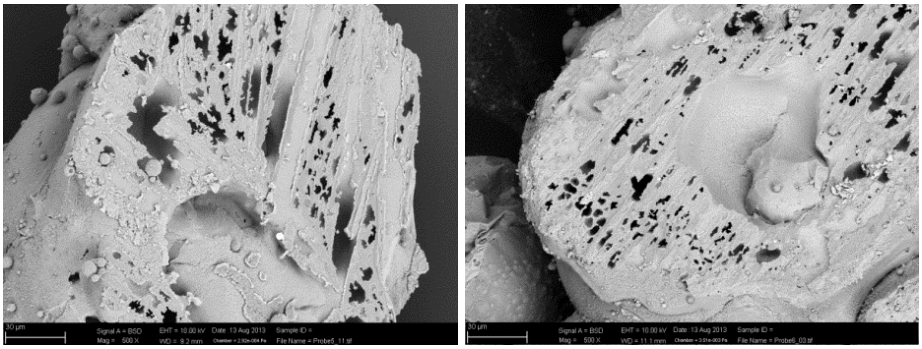

Fig. 5.27. Holes found at the back side of collected samples (3 MPa)

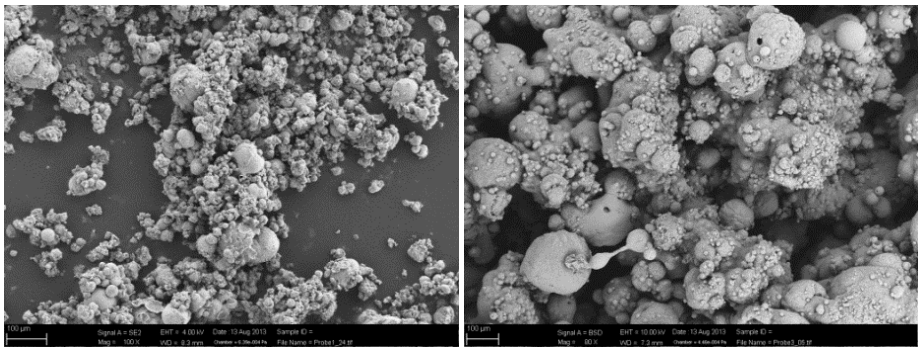

Fig. 5.28. SEM images of particles collected at 0.1 MPa (left) and 1 MPa (right)

At 0.1 MPa many particles with dimensions around 10 µm were found (Fig. 5.28). This is in contrast to the agglomeration analysis presented before, but a possible explanation is that these particles may be small aluminium particles oxidised completely below or at the burning surface at lowers temperatures. The low temperature can be a possible explanation because they are not visible as glowing agglomerates in the movie images. These particles are completely spherical and feature high oxygen content that indicates pure alumina proven by EDX analysis.
At 0.1 MPa also nano-structures of fluffy material could be observed (Fig. 5.29).

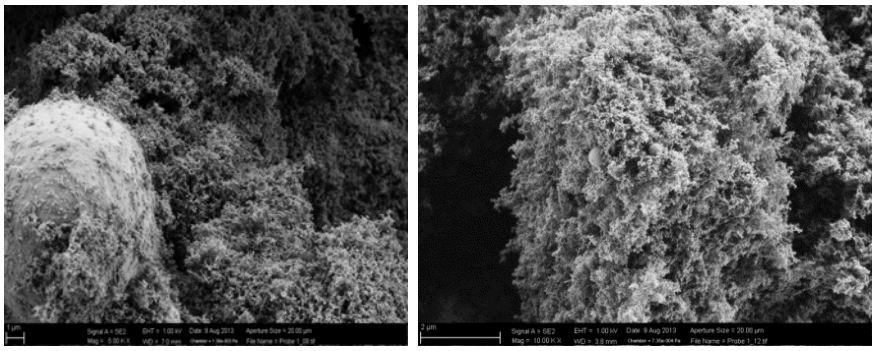

Fig. 5.29. Nano-structures observed at 0.1 MPa

The reason why aluminium creates this kind of surface is up to now not well understood, but in EDX analysis they present a high amount of oxygen which can indicate that they are the result of a re-condensation of burning aluminium.

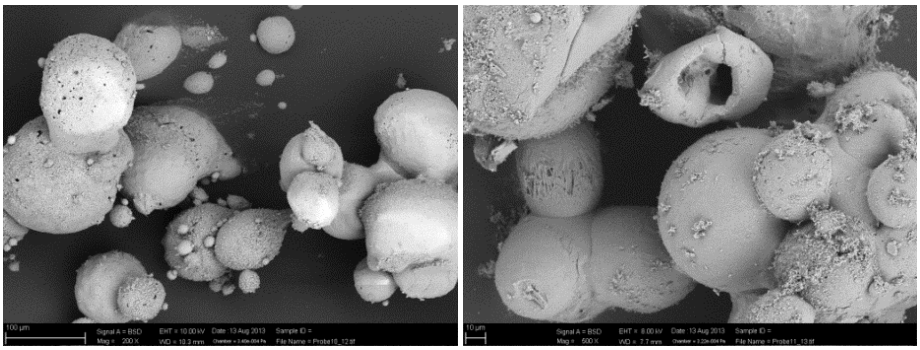

Fig. 5.30. SEM images of particles collected at 13 MPa (left) and 15 MPa (right)

The shape of agglomerates at high pressure seems to change, presenting always the same structures with holes, but closer to porosity (Fig. 5.30 left). At high pressure the re-condensation effect seems to give rise to small spherical particles attached to the agglomerates instead of a nano-structure. Also hollow particles present a more thick shell (Fig. 5.30 right)

At 15 MPa bigger particle appear but of completely different shape, which can be due to a re-condensation behaviour thought the sample holder was only 0.5 mm from the burning surface.
SEM analysis allows confirmation of the well-known behaviour of the "breaking" of the alumina shell, which releases pure liquid aluminium (Fig. 5.31).

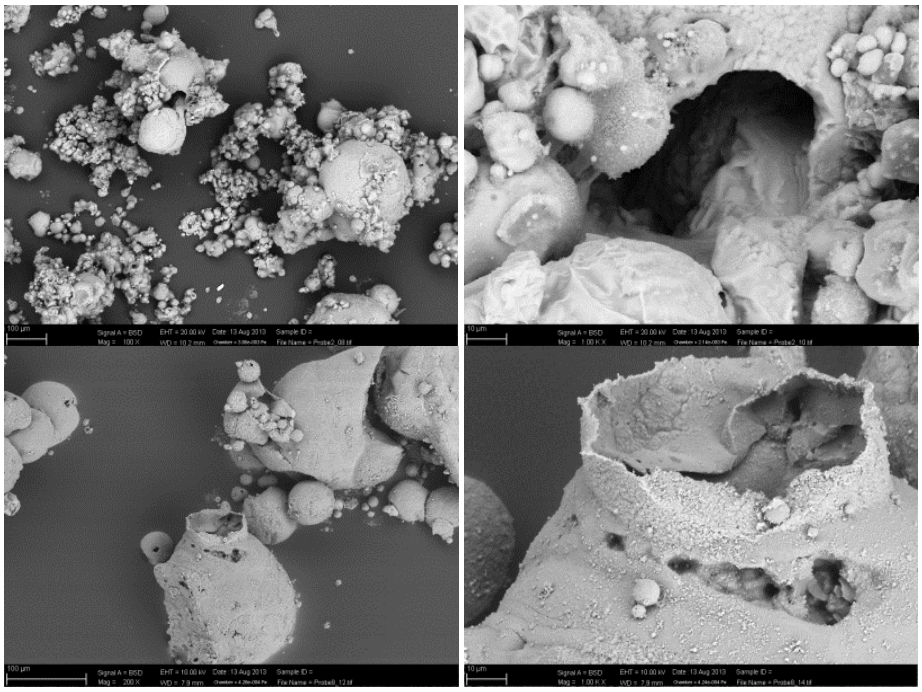

Fig. 5.31. Particles breaking at 0.1 MPa (top) and 7 MPa (bottom)

It was observed that some large particles having still an oxide cap. This indicates an incomplete combustion which is confirmed by EDX analysis with high aluminium to oxygen ratios inside the smaller caps. In general, the ratio of O/Al increases significantly with increasing pressure indicating a more complete oxidation.
Some EDX-analysis, especially taken at 7 MPa and higher, shows an additional content of nitrogen of 10 to 20 mol%. In many cases it is accompanied by carbon in the same order of magnitude. It is not clear if the nitrogen content is caused by the components of the formulation (ADN, GAP) or by the reaction with the pressurizing gas.

5.4 ADN/GAP/Alane

The two formulations containing alane, H53 with 16% and H54 with 26%, show completely different burning behaviours. Both present the

symptomatic colour due to potassium, but the formulation H54 showed an "exotic" burning. H54 creates agglomerations with a size of 1.5-2.5 mm.
For both the formulations burning tests were performed in nitrogen atmosphere inside the window bomb at pressure levels of 0.1, 1, 3, 7, 10, 13 MPa (for H54 also 5 and 15 MPa). Almost three measurements were made at all pressure levels.
The very energetic way to burn of both formulations required the inhibition of the lateral surfaces. Creation of a huge amount of smoke was observed at all pressure steps and sometimes also pieces of unburned strands were observed inside the flame.
The very big agglomerates observed (Fig. 5.32) for formulation H54 were collected from all combustion tests by simply taking the residues from the window bomb once the combustion was finished.
When this propellant was ignited, all the combustion chamber was filled by flames and agglomerates. They had the energy to "jump" through the slit of the diaphragm (high 11 cm) and go around the chamber spreading the flame all around.
This phenomenon was observed almost at low pressure.

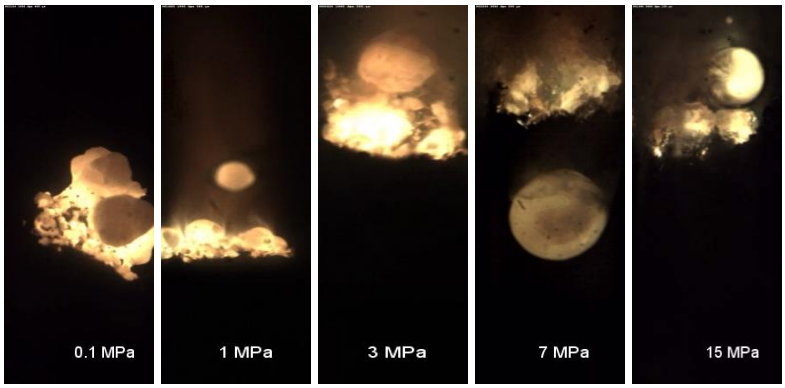

Fig. 5.32. Burning behaviour of propellant H54

The combustion process was not completed until the end of the strand, and in all cases aluminium residues were found in the original position of the strand.
The combustion behaviour of the propellant H53 does not show such large agglomerates, and presents almost a linear burning behaviour independent of pressure. The burning surface was always almost flat, but there have been cases for which the burning start and proceed on the lateral surface despite the inhibition.
Due to the camera settings that had been optimized to visualise the extremely bright aluminium particles on the burning surface, the flame corona was very dark at low pressure.
For both propellants no dark zone near the burning surface was observed.

Fig. 5.33 shows that the agglomerations were quite defined up to 10 MPa, and behave with complete different formation behaviours. According to De Luca [34], they are mostly agglomerates of the first type since transudation, agglomeration and detachment happens mostly at the same position.

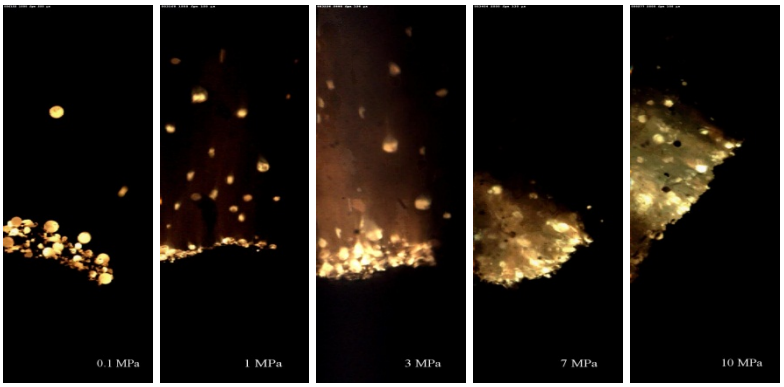

Fig. 5.33. Burning behaviour of propellant H53

For this kind of propellant it was also possible to clearly see what is called a “skeleton layer” of aluminium by Babuk in [52] on the burning surface.

5.4.1 Burning Rate

The measured burning rate data of both alane formulations show a good reproducibility with low scattering (Fig. 5.34).
The biggest scattering is for the formulation creating big agglomerates (H54) at 3 MPa.
This formulation with the “exotic” burning behaviour shows a lower burning rate. The pressure dependences are nearly the same for both the formulations. In fact the determined pressure exponent for formulation H54 is 0.37 and for formulation H53 is 0.35.
The two burning rates differs by about 1 mm/s at 1 MPa up to 5 mm/s at 13 MPa, that should be enough to distinguish one from the other (the difference between the two burning rates is more than two times the estimated error). Despite the drastic change in formulation (from 16% to 26% of alane) it is surprising that the burning rates are close together.
In Tab. 5-4 the fitted burning laws for the two propellants are reported.
The uncertainty in the determination of the pressure exponents is larger than the difference between them. The same cannot be said for the pre-exponential factor. The result is a quite parallel behaviour (Fig. 5.34).
Tab. 5-4 shows that the burning rates are again too high for space application at classical working pressure.

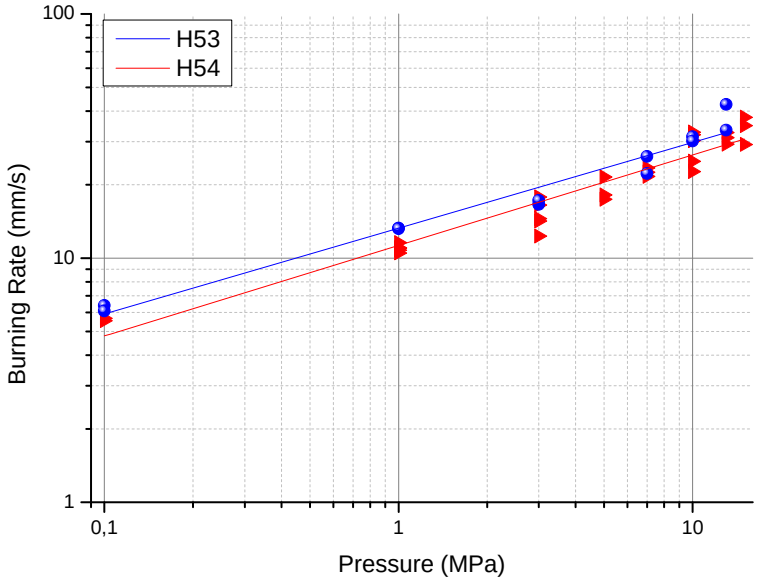

Fig. 5.34. Burning rate of formulations H53 and H54

Tab. 5-4 Vieille parametersfor formulations containing alane

Label	Vieille's Law	Alane content	r_b at 7 MPa [mm/s]
H53	$r_b=(13.48 \pm 0.02)P^{(0.35 \pm 0.03)}$	16%	26.2 ± 1.6
H54	$r_b=(11.47 \pm 0.02)P^{(0.37 \pm 0.02)}$	26%	23.6 ± 1.0

5.4.2 Temperature

The temperature measurements show mostly an increasing trend with pressure for both propellants up to 10 MPa. For higher pressures the behaviour apparently changes what can be interpreted as a stabilization of maximum temperature.

The accuracy of this temperature measurement method is estimated around ±200 K so it is possible to state that at 0.1 MPa the measured temperatures for the particles are between 1950 and 2350 K for both propellants.

With increasing pressure it seems that the propellant with the lower amount of alane had a much higher temperature up to 10 MPa.

For pressures above 7 MPa H54 shows the highest temperatures. At a pressure of 7 MPa both propellants show a temperature between 2700 and 2850 K (in average).

The spectra analysis showed the absence of a distinct water band for both propellants. So the fitting of that band was difficult or sometimes impossible.

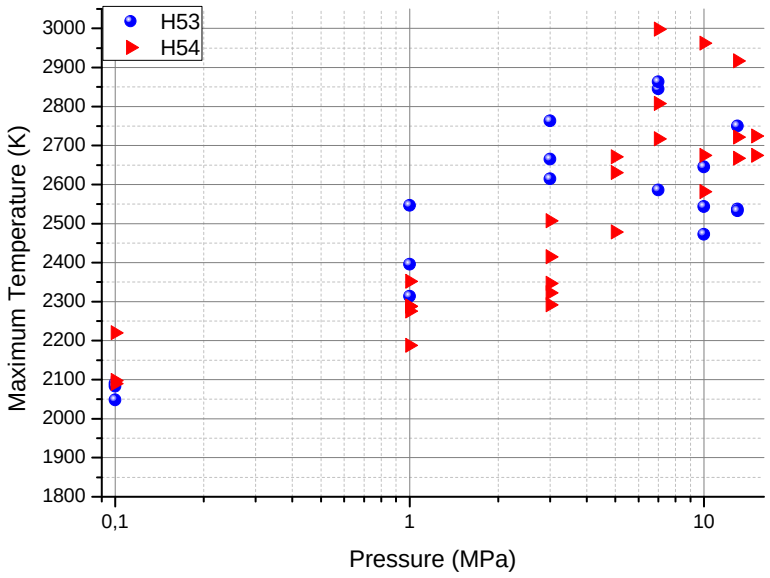

Fig. 5.35. Maximum measured temperature for propellants with alane.

One possible explanation is that the water around the flame (at lower temperature) absorbs the energy released from the water inside the flame. This phenomenon is known as “water self-absorption”. Another explanation is that all the water acts as oxidizer.
For both formulations the usual potassium peak can clearly be seen. The sodium peak was larger than for the other propellants.

5.4.3 Agglomeration

The propellant H54 presents agglomerations of the matrix type, with a visible oxidation of the aluminium part.
The type of agglomerates and a rough estimation of their dimensions are possible from Fig. 5.36.
It is not clear if this abnormal growth of agglomeration is due to a liquid layer created by the melting of ADN or must be attributed to a retention force of the skeleton layer. But maybe a complete new mechanism should be considered in future.
A liquid layer can be observed, looking at Fig. 5.37, but looking to its colours and to its way to form agglomerates, it may consist of aluminium or aluminium oxide.
Some tests performed with a lateral burning of the strands at 0.1 and 1 MPa have clearly shown the skeleton layer of aluminium.

This can be a further confirmation that the liquid layer should not be attributed to the ADN, but to aluminium.

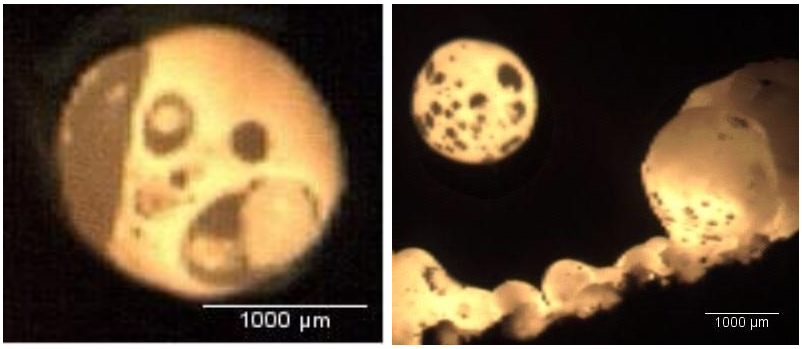

Fig. 5.36. Agglomerations formed during the burning of propellant H54

In Fig. 5.38 the skeleton layers observed for the formulations containing alane are shown. Both formulations show the same behaviour, but H53 give rise to smaller agglomerates.
The composition containing less alane creates agglomerates of the matrix type (Fig. 5.39) up to 3 MPa. At 5 MPa it also forms agglomerates with oxide cap. Then, only oxide cap agglomerations were observed for pressures higher than 7 MPa.

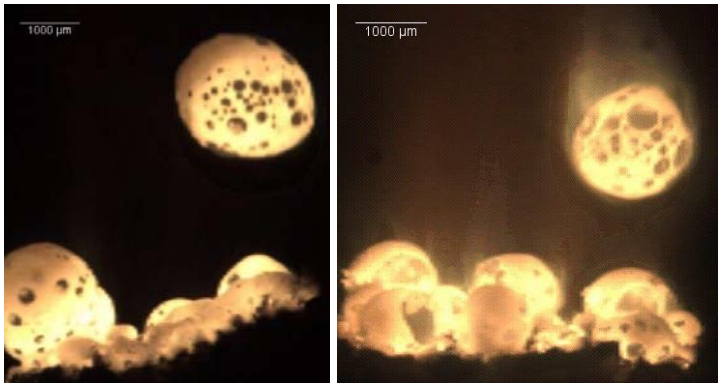

Fig. 5.37. Burning surface and detaching agglomerates for propellant H54 (0.1 and 1 MPa)

Common observations for both propellants are the “eruptions” of the agglomerates: the agglomerates tend to increase an area of their surface and then develop a kind of bubble which disappears suddenly.
This can be due to hydrogen or to gaseous intermediates (like AlH or AlO) which should be created and entrapped into agglomerates during the aggregation process.
The aggregations remain for a long time on the emerging point of the aluminium and tend to “absorb” the bridge around their position.

Agglomerates have been observed starting from a flat area of aluminium and then suddenly became a sphere and detach.

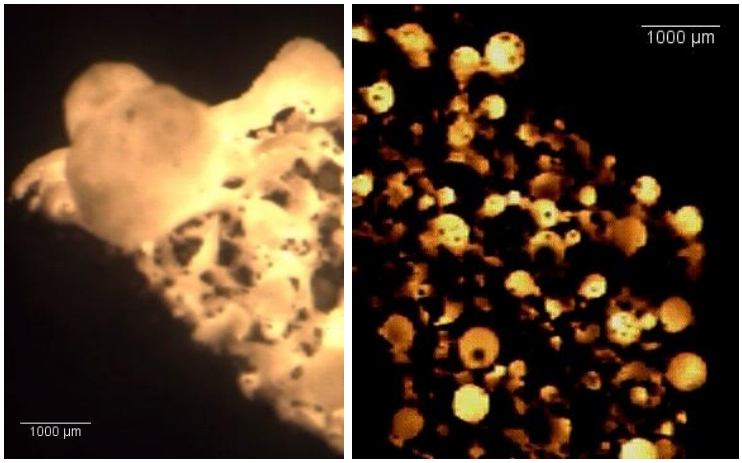

Fig. 5.38. Skeleton layer observed for propellant H54 (left) and H53 (right) at 0.1 MPa.

Fig. 5.39. Burning surface and detaching agglomerates for propellant H53 (0.1 and 1 MPa)

Despite this way to aggregate, the observation has not revealed parts of unburned propellant attached to the agglomerates. The analyses of the residues confirm this observation.
The dimension of agglomerates is bigger than the ones observed in the aluminized formulations (Fig. 5.39). This is an opposite result with respect to what is obtained for AP/HTPB/alane propellants.
The formulation H53 showed the usual decreasing trend in agglomerates dimension with pressure, as shown in Fig. 5.40.
The measured dimension of agglomerates released by H53 at 10 MPa is close to the dimension obtained for the propellant H32 at 3 MPa.
At a pressure of 7 MPa the agglomerates are very big reaching an average diameter of 157 µm.

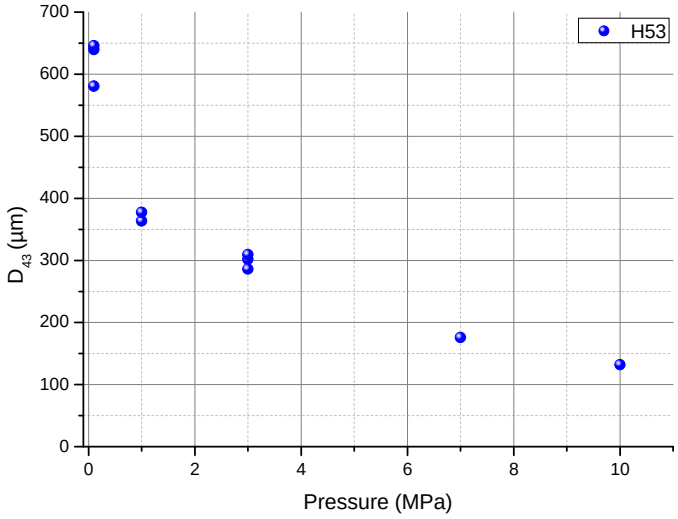

Fig. 5.40. D_{43} of the measured detached agglomerations of propellant H53

For this propellant the distribution of diameters of the agglomerations is always monomodal, but narrow only at pressures higher than 3 MPa.

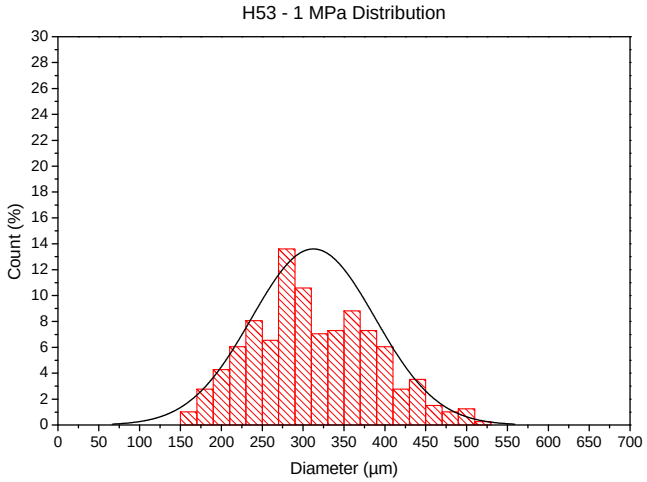

Fig. 5.41. Agglomerate size distribution for H53 propellant at 1 MPa

Tab. 5-5 Agglomeration measurements for propellants containing alane (average on overall observation)

Label	Pressure [MPa]	Average diameters [µm]	D_{43} [µm]	D_{32} [µm]
H53	0.1	495.5 ± 24.0	616.4	578.9
	1	312.6 ± 12.5	364.3	348.2
	3	273.2 ± 8.4	301.5	292.2
	7	156.8 ± 5.2	175.6	169.5
	10	116.5 ± 4.3	131.8	127.3
H54	0.1	1406.0 ± 69.1	1720.4	1634.0
	1	1336.1 ± 62.3	1617.1	1533.0
	3	1499.2 ± 59.6	1788.8	1680.7
	5	2051.6 ± 89.5	2397.0	2300.0
	7	2464.3 ± 137.4	3196.0	2964.2
	10	1667.4 ± 132.3	2707.0	2388.3
	13	2091.3 ± 132.3	2873.0	2638.4
	15	1909.0 ± 153.1	2489.3	2422.3

Looking at the histogram of Fig. 5.41, and comparing it with the histogram of Fig. 5.42, it is clear how the pressure contribute to the generation of agglomerates for which the diameters is included in a range from 100 to 200 µm. The range seems to be doubled at 1 MPa.

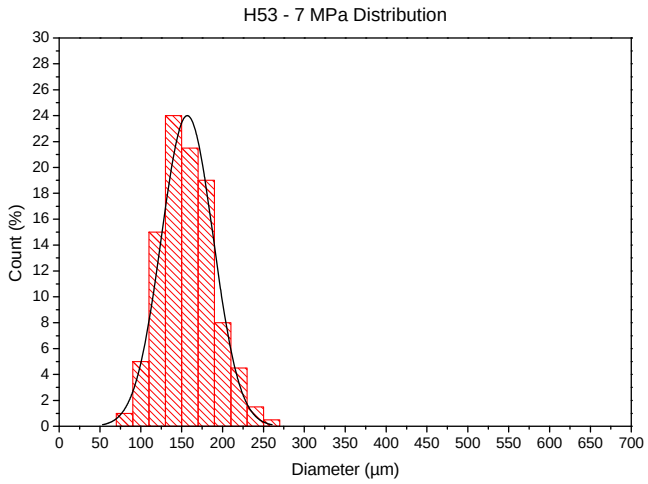

Fig. 5.42. Agglomerate size distribution for H53 propellant at 7 MPa

Since the agglomerates that can be measured for formulation H54 are no more than 20 for each pressure step a statistical approach was not possible to do.
However it is considered to be important to report the results obtained from the measured particles, which is shown in Fig. 5.43.

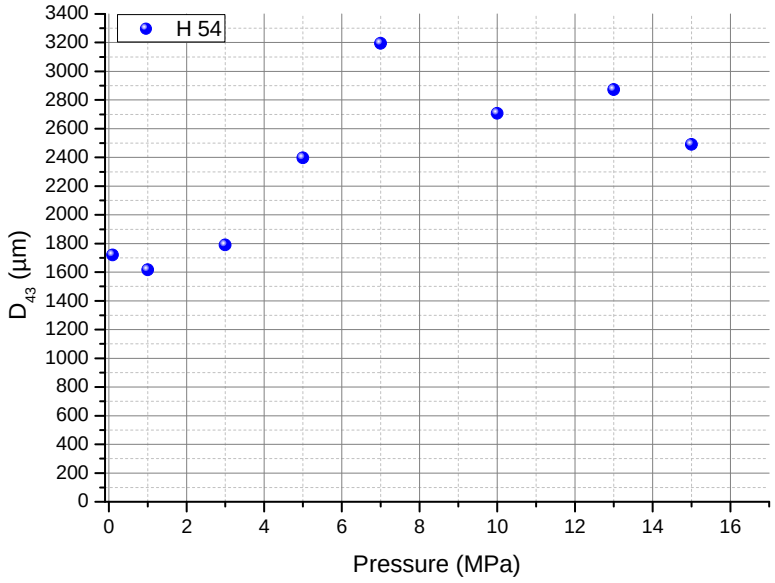

Fig. 5.43. D_{43} of the measured detached agglomerations of propellant H54

The agglomerates are always larger than 1.3 mm reaching a maximum of 2.5 mm at 7 MPa. This is completely unacceptable under the point of view of two phase loss. However, it allows the collection of agglomerates without the use of sample holders.
These collected agglomerates were big enough to be studied under optical microscope.

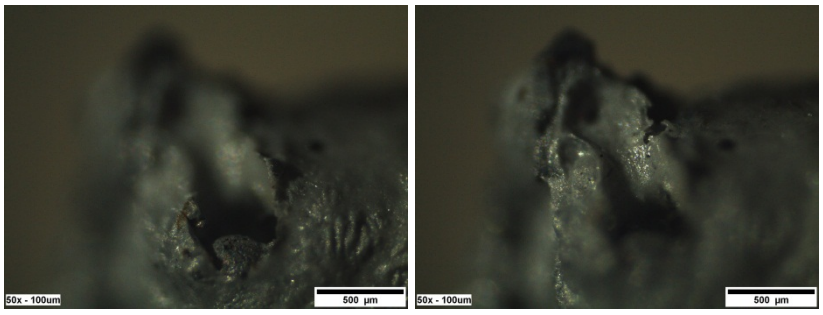

Fig. 5.44. Brocken shell (13 MPa)

The analysis showed almost the same type of particles found for the H32 propellant, with the same broken oxide shells (comparison between Fig. 5.44 and Fig. 5.31) or the same kind of holes (Fig. 5.45 and Fig. 5.27).
Most of the samples present a quite perfect round shape (Fig. 5.46).

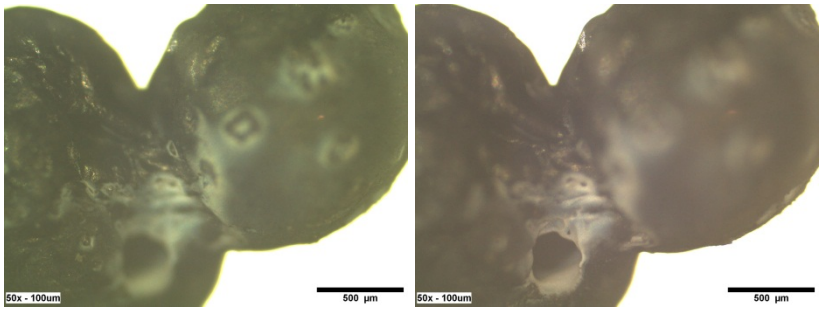

Fig. 5.45. Holes and white alumina (1 MPa).

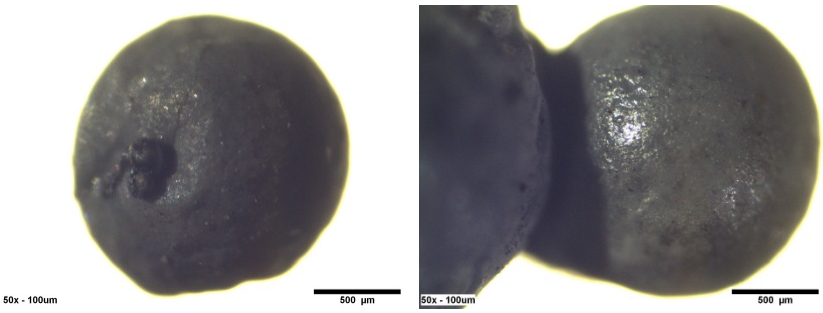

Fig. 5.46. Spherical agglomerate at 5 MPa (left) and 15 MPa (right)

Also alumina shells split in half were observed (Fig. 5.47). Both the halves present the same type of porosity observed for the high pressure agglomerates collected for propellant H32.
The presence of porosity also inside shells gives a further confirmation on the hypothesis of gases retained inside the agglomerates. What is surprising is the presence of these gases not only inside the agglomerates, but also inside the aluminium oxide shells which seems to be a sort of protection of the entire system formed by aluminium plus gases.

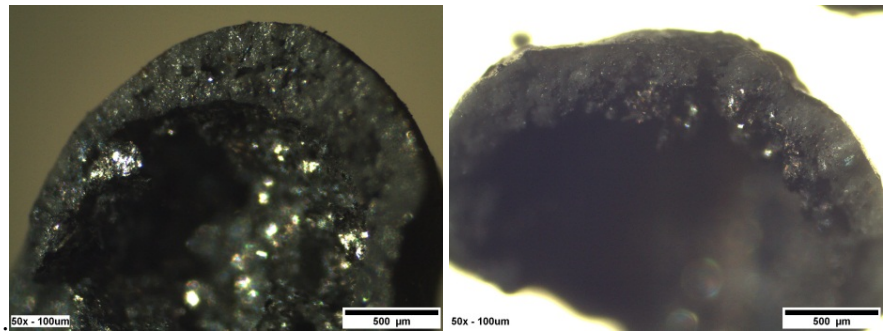

Fig. 5.47. Broken alumina shells at 3 MPa (left) and 5 MPa (right).

5.5 AP/GAP/Al

The formulations containing AP demonstrated combustion with the presence of some unburned residues in all cases.
The burning surface was mostly flat and regular, but to ensure that an inhibition with estane was provided for all compositions.

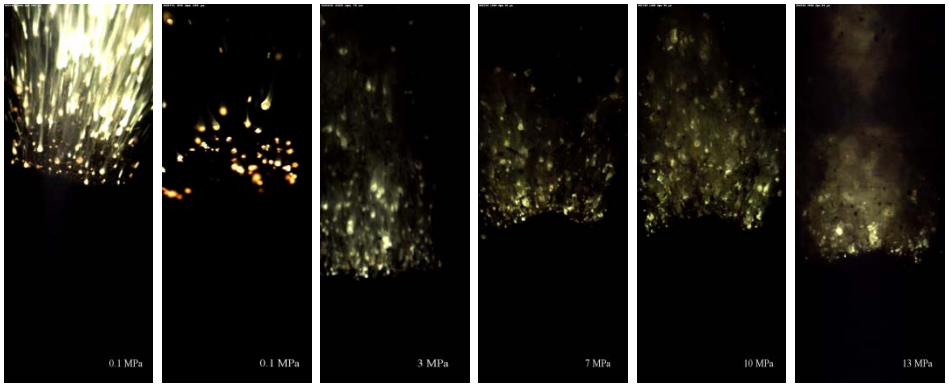

Fig. 5.48. Burning behaviour of propellant A1

The flame was mostly a divergent flame for which the colour was yellow for pressures up to 3 MPa and then more green at increasing pressures for the formulations containing aluminium.
For the formulation A6, without aluminium, the flame was little and dark without the presence of a dark zone.
For all compositions a strong formation of smoke was observed, probably due to GAP pyrolysis. The composition A5, containing only GAP and aluminium, creates so much smoke that the strand was hidden, and therefore could not be analyse in the following.

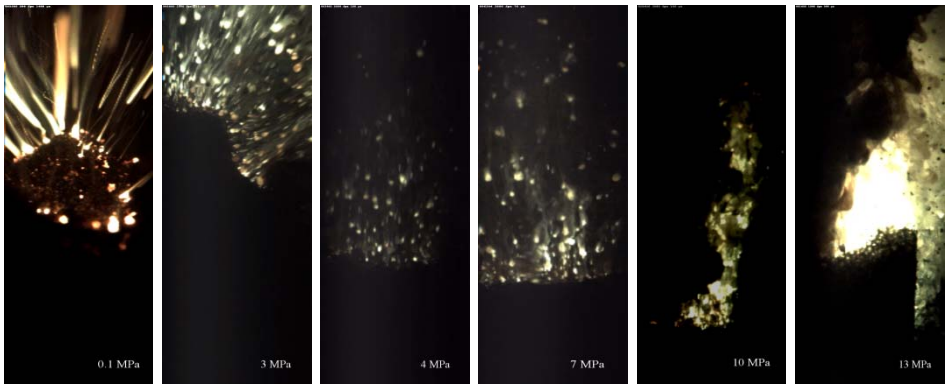

Fig. 5.49. Propellant A2 burning behaviour's

In Fig. 5.48 the burning behaviour of the propellant A1 is shown, which is supposed to have the same oxygen balance and adiabatic flame temperature as the bimodal propellant H32. It can be seen that it provides well defined agglomerations up to 13 MPa. From the first picture to the left, it is possible to see that the burning surface is mostly made of hemispherical particles which should be interpreted as oxidizer prills. It could be that the surface was not porous and not in molten state for this formulation.
The same thing cannot be said for the formulation A2, which is supposed to have the same heat of formation as the H32 propellant. This formulation shows pores at high pressure (Fig. 5.49) and a good combustion with a flat burning surface was very difficult to observe.

Fig. 5.50. Residues from formulation A2

From the combustion of A2 it was possible to collect residues of unburned strand material. From video analysis it seems that the entire strand burns, but using high contrast and high luminosity video it was possible to observe a strange behaviour, like a “banana peeling” of the strand for which the skin gives the residues.
The residues are shown in Fig. 5.50 and seem mostly made of carbon that can indicate an incomplete combustion of GAP. Burning tests without inhibition did not change this behaviour.
The huge amount of GAP (45%) could be the main reason for the incomplete burning.
Fig. 5.49 also shows the massive amount of smoke created by this formulation.
Propellants A3 and A4, with adiabatic flame temperatures calculated around 3200 and 2850 K, respectively, show an incomplete transition between aggregates and agglomerates at 0.1 MPa. Also no ignition of the detached agglomerates level was observed at this pressure.

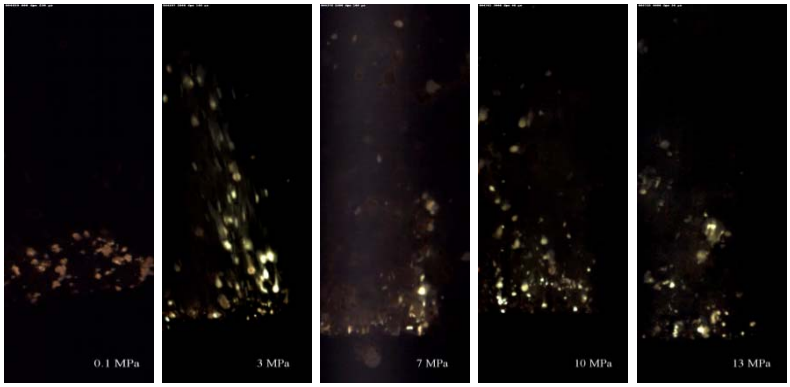

Fig. 5.51. Burning behaviour of propellant A3

Both formations produce less smoke than propellant A2.
Formulation A4 seems to be the one with the better burning behaviour because of the less amount of smoke, the more dense flame and relatively low amount of unburned residues.
The measurement of the agglomerations was possible up to 13 MPa for all the AP-formulations, since agglomerations were extremely defined for the whole pressure range.

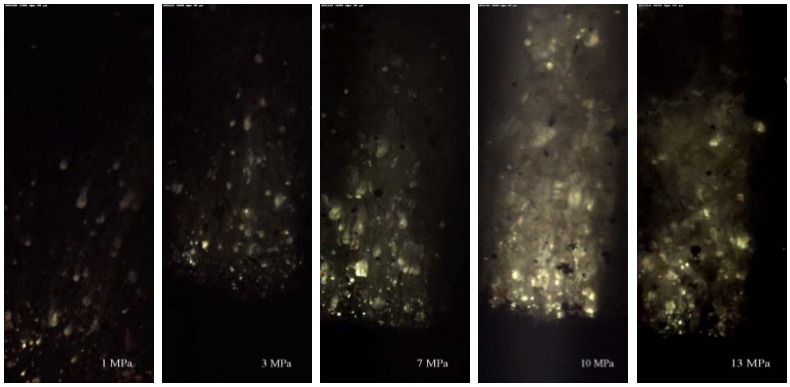

Fig. 5.52. Burning behaviour of propellant A4

From the burning tests of formulation A5 it was possible to collect some residues that can be attributed to an incomplete burning of GAP.
These residues consist of carbonized structures and are extremely porous (Fig. 5.53). They remain due to the low oxygen balance of this formulation ([52]).
The formulation without metals, the A6 propellant, shows an extremely dark and little flame for pressures lower than 3 MPa.
On Fig. 5.54 flamelets can be seen that probably results from the combustion of a carbon layer on the burning surface (like ADN/GAP). The flame became smaller with increasing pressure. This creates strong

difficulties to analyse the spectrometric results also because of the low brightness of the flame.

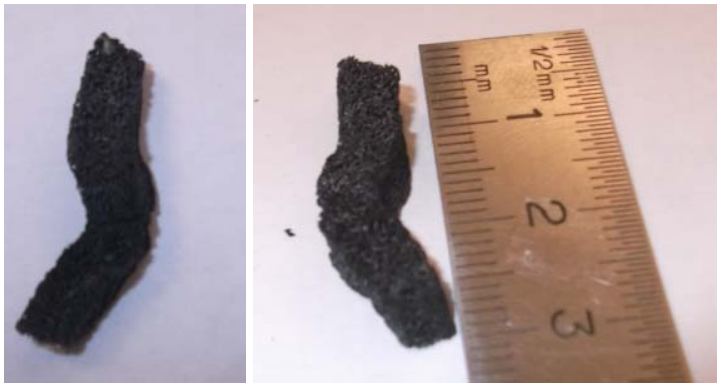

Fig. 5.53. Residues from formulation A5

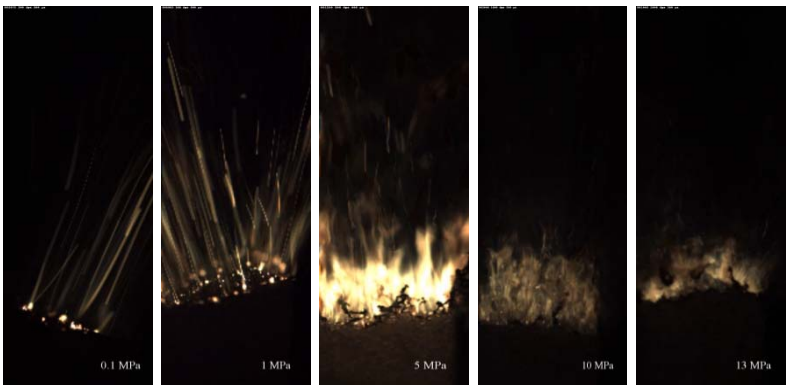

Fig. 5.54. Burning behaviour of propellant A6

For formulation A7 no significant changes in burning behaviour were observed with respect to formulation A1. It presents the same colours and the same intensity of brightness.

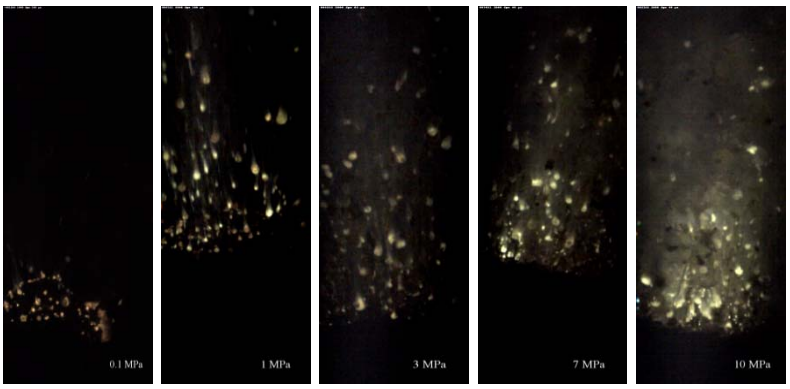

Fig. 5.55. Propellant A7 burning behaviour's

5.5.1 Burning Rate

For all formulations under investigation a study on the influence of the estane inhibition on the burning behaviour has been carried out. Looking at the previous figures it is possible to see that in some cases estane burns slower than the strands, creating some residues and eventually influencing the burning rate.

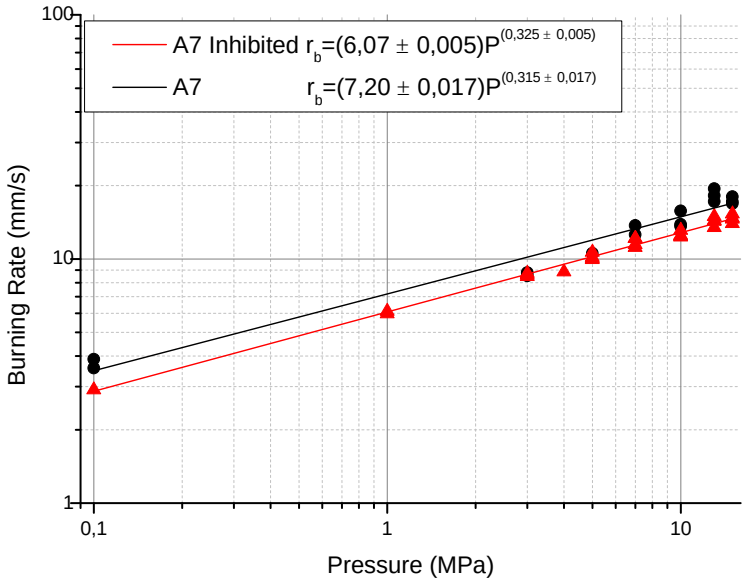

Fig. 5.56. Effect of inhibition on the burning rate

For all formulations a difference of about 1 mm s^{-1} MPa^{-n} has been found in the pre-exponential factor of the Vieille's law. A typical case is presented in Fig. 5.56. For this reason the pre-exponential factors of Vieille's law have to be increased. No other differences have been found.
The burning rate measurements, made at pressure steps of 0.1, 1, 3, 4, 5, 7, 10, 13 and 15 MPa, showed a common burning rate at 0.1 MPa of 2 to 3 mm/s for all formulations except for propellants A4 andA6.
Formulation A6 starts from 1.4 mm/s at 0.1 MPa and reaches 21.3 mm/s at 15 MPa, demonstrating its relatively high pressure dependence (almost in contrast to the other AP formulations). The calculated ballistic exponent is n=0.51. For the AP-formulations under investigation, this is the highest pressure dependence.
All the others formulations present ballistic exponents between 0.3 and 0.4, as reported in Tab. 5-6, and pre-exponential factors between 5.4 and 6.8 mm s^{-1} MPa^{-n}.

The formulations A3 and A4, for which the Vieille's law is somewhat different, show practically the same burning rate at 7 MPa.
This common burning rate is clearly visible looking to Fig. 5.57, which shows also an extremely common behaviour for the propellants A4 and A2.

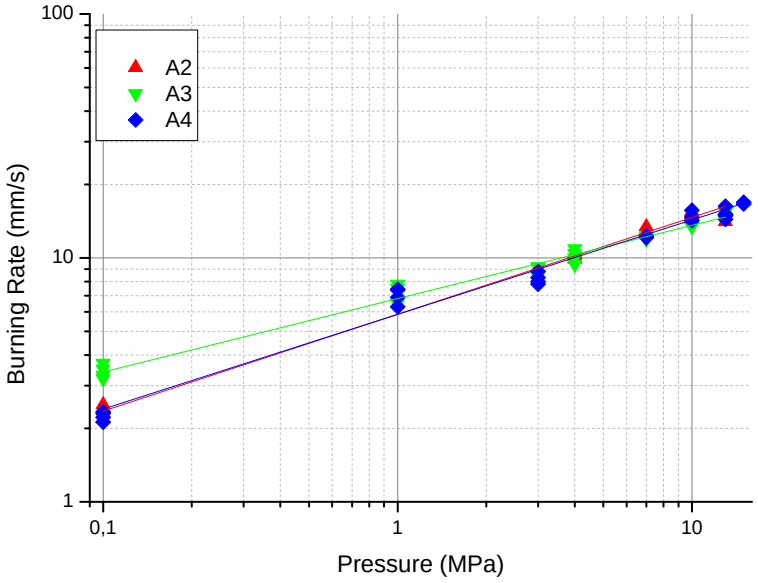

Fig. 5.57. Burning rate and fitting of Vieille's law for A2, A3 and A4

This is surprising since the formulation A4 was the best performer in terms of combustion and A2 was the worst one. This concordance can be expected looking at the amount of GAP contained in the formulations: A2 and A4 differ by only 4 per cent in content, but this do not completely explain the different burning behaviour.

Tab. 5-6 Parameters of Vieille's law fitting for the AP-based formulations

Label	Vieille's Law	r_b at 7 MPa [mm/s]
A1	$r_b=(6.34 \pm 0.01)P^{(0.38 \pm 0.01)}$	13.3 ± 0.3
A2	$r_b=(5.87 \pm 0.01)P^{(0.40 \pm 0.01)}$	12.8 ± 0.3
A3	$r_b=(6.81 \pm 0.01)P^{(0.30 \pm 0.01)}$	12.2 ± 0.3
A4	$r_b=(5.86 \pm 0.01)P^{(0.39 \pm 0.01)}$	12.5 ± 0.3
A6	$r_b=(5.36 \pm 0.02)P^{(0.51 \pm 0.02)}$	14.5 ± 0.6
A7	$r_b=(6.07 \pm 0.01)P^{(0.32 \pm 0.01)}$	11.3 ± 0.2

In Fig. 5.58 it is also possible to see that the small change in binder content can relax the pressure dependence from 0.38 to 0.32 with relatively small

change in the pre-exponential factor (comparison between A1 and A7) and without change in the burning behaviour.
The change in ballistic exponent is traduced in a variation of about 2 mm/s (Tab. 5-6) at working pressure that grows up to 8 mm/s at 13 MPa (from 13 mm/s for A7 to 21 mm/s for A1).

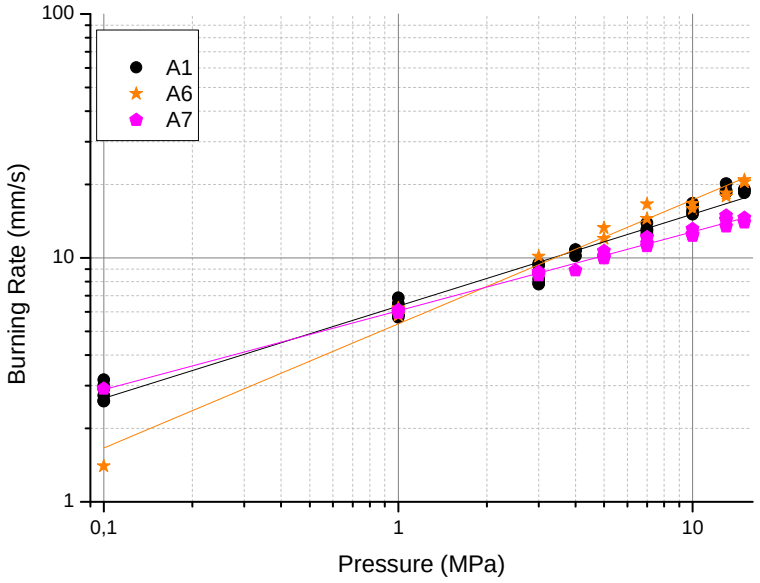

Fig. 5.58. Burning rate and Vieille's law for A1, A6 and A7

5.5.2 Temperature

The common burning behaviour of propellants A1 and A7, and in particular the common brightness of the flame, is reflected in the temperature measurements. Fig. 5.59 shows the quite equal maximum temperatures reached by the brighter particles of both propellants.
Starting from about 2050 K at 0.1 MPa the two propellants stabilize their maximum temperatures between 2550 and 2650 K for a pressure range between 4 and 15 MPa.
Looking at Fig. 5.60 formulation A4 presents a trend similar to A1 and A7, but 200 K lower.
The formulation A2 seems to move more in accordance with formulation A3. From 7 MPa the formulation A3 seems to stabilize around 2150 K instead formulation A2 continue to grow until it reaches the temperature of the propellant A4, between 2350 and 2450 K.
The low value measured at high pressure for formulation A3 is considered to be suspicious and should not been taken into account. Maybe the

produced smoke covered the hot flame and the spectrograph only detected the emission of the cold smoke.

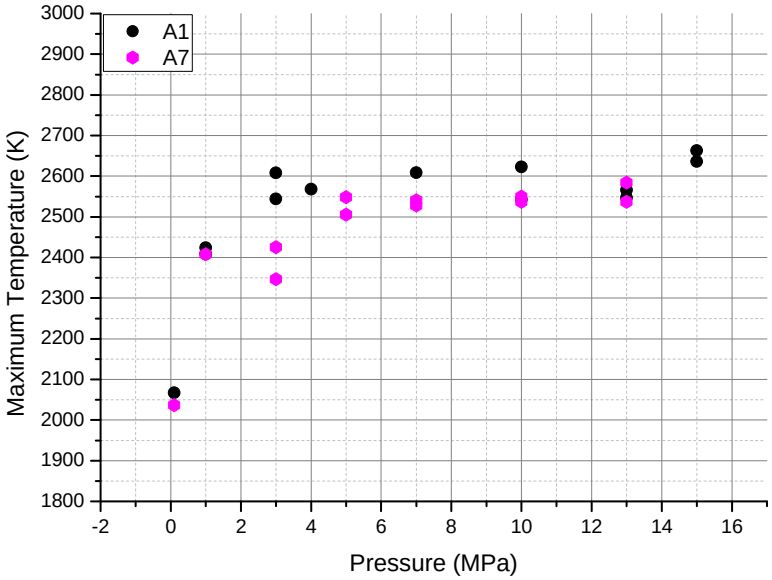

Fig. 5.59. Maximum Temperature of formulations A1 and A7

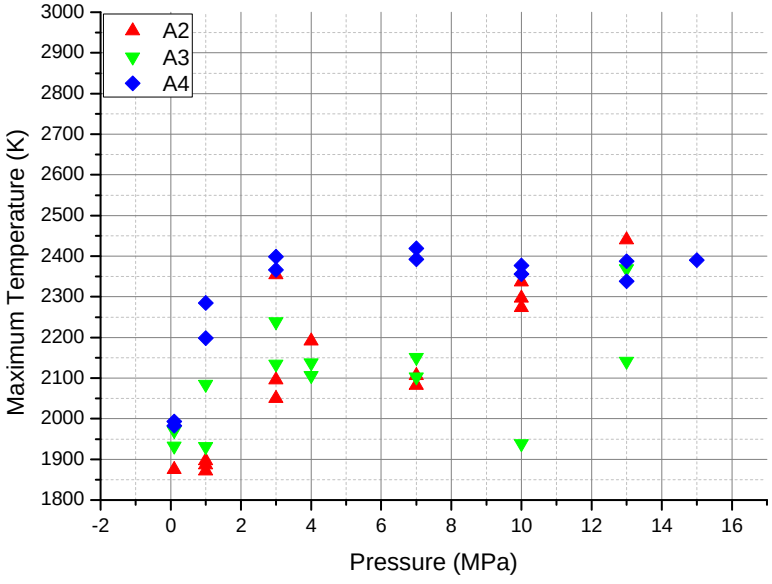

Fig. 5.60. Maximum Temperature of formulations A2, A3 and A4

5.5.3 Agglomeration

All the investigated AP formulations present the same oxide-cap type of agglomerates for pressures higher than 1 MPa. For the formulations A3 and A4, the possibility was observed (below 3 MPa) that aggregates do not do a complete transition from aggregate to agglomerate. Therefore, the detached particles were aggregates with a "coral" structure.

The aggregation is mostly performed where the transuded aluminium appears first. This aggregation behaviour was common for all the formulations at all the pressures investigated.

The measurements of the agglomeration size show a decreasing trend of size with pressure. This trend is less marked than the one observed for the formulations containing ADN/GAP.

The difference, from 1 to 13 MPa, for all the AP-based formulations is lower than 140 µm.

The trend is shown in Fig. 5.61 and Fig. 5.62.

The measured diameters of the aggregates for the AP-formulations are always lower than the one measured for formulations containing ADN/GAP/Al (Fig. 5.25).

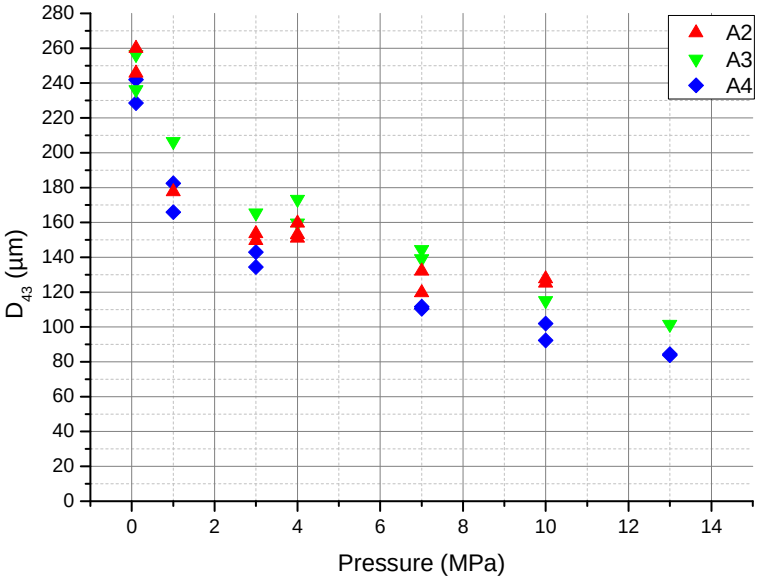

Fig. 5.61. Agglomeration measurements for formulations A2, A3 and A4.

The bigger aggregates/agglomerates are released by formulation A2 at 0.1 MPa. At 1 MPa the size is reduced drastically reaching the value of formulation A4. For A2 the increasing pressure does not decrease the diameter of the aggregates too much (Fig. 5.61).

At working pressure the measured agglomerates are included in a dimension range of 40 µm, with the larger dimension for propellant A3, followed by A2, A1, A4 and A7, as it is possible to see looking at Fig. 5.61 and Fig. 5.62.
In Fig. 5.62 it is possible to see that a minor change in binder content give rise to a faster decreasing in agglomerates dimension. This is surprising since the pressure dependency of formulation A7 is lower than that of A1. The agglomerates released by A7 are 10 to 30 µm smaller at working pressure than the agglomerates observed for A1.

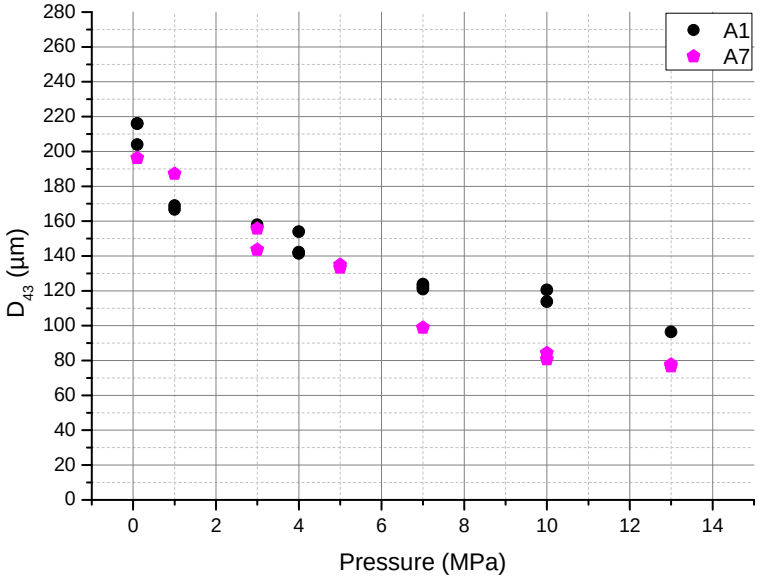

Fig. 5.62. Agglomeration measurements for formulations A1 and A7.

The distribution of the agglomerates follows the usual trends of distribution: from a wide range of size at low pressure to a narrow distribution at 13 MPa. This was observed for all the formulations under investigation.
Figure 5.63 and Fig. 5.64 are two typical examples of particle distributions at different pressure levels.
The distribution width has a maximum of about 300 µm at 0.1 MPa, and then it reduces to 150 µm at 5 MPa, 100 µm at 7 MPa to reach the smallest width of only 75 µm at 13 MPa.
The results of the statistical analysis (400 to 600 measured agglomerates for each pressure) are reported in Tab. 5-7. The formulation A1, with the same adiabatic flame temperature and nearly the same oxygen balance as

formulation H32, shows agglomerates dimension always lower than the latter.

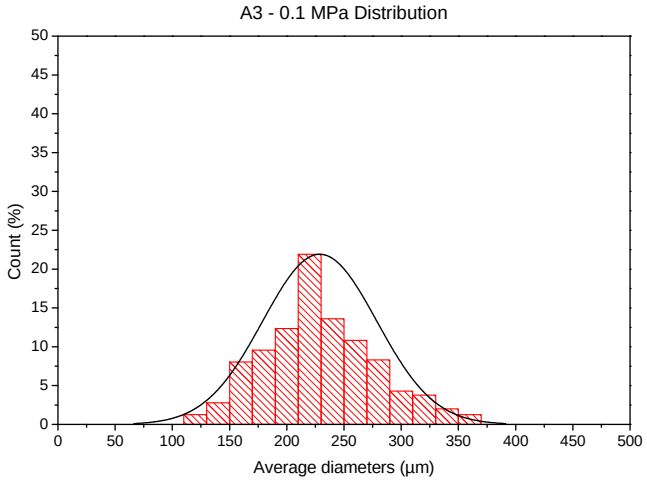

Fig. 5.63. Agglomerate size distribution for formulation A3 at 0.1 MPa

But formulations A4 and A7 have the smallest agglomerates for all pressures investigated.

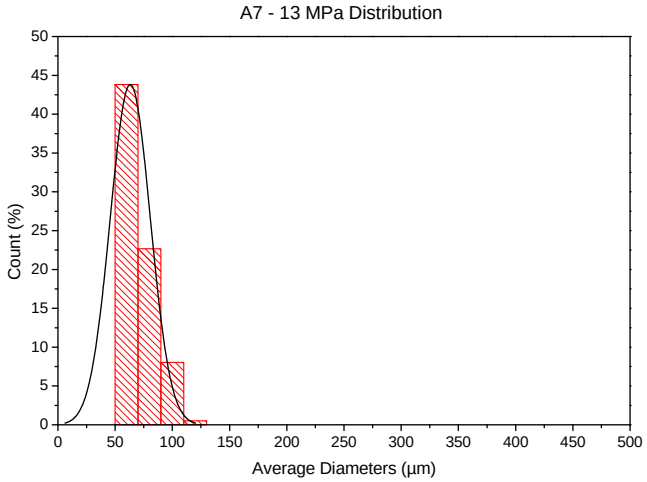

Fig. 5.64. Agglomerate size distribution for formulation A7 at 13 MPa

Tab. 5-7 Agglomerations measurements for AP-Based formulations (average on overall observation)

Label	Pressure [MPa]	Average diameters [µm]	D_{43} [µm]	D_{32} [µm]
A1	0.1	193.3 ± 5.9	212.8	206.5
	1	152.4 ± 4.6	167.9	162.8
	3	140.6 ± 4.8	157.9	152.5
	4	129.3 ± 4.4	145.7	140.3
	7	108.7 ± 3.8	122.5	118.3
	10	98.5 ± 4.1	116.7	110.9
	13	83.5 ± 3.3	96.4	92.6
A2	0.1	221.3 ± 8.2	252.0	242.7
	1	157.4 ± 5.2	177.7	170.5
	3	136.6 ± 4.4	151.8	146.9
	4	129.8 ± 4.5	146.4	141.1
	7	110.9 ± 4.2	127.2	122.1
	10	109.9 ± 4.3	126.7	121.7
A3	0.1	228.8 ± 8.2	260.3	250.2
	1	175.0 ± 7.0	206.5	195.9
	3	147.1 ± 5.1	165.3	159.7
	4	142.7 ± 5.7	166.1	158.9
	7	122.5 ± 4.7	142.0	135.7
	10	94.8 ± 4.4	115.1	108.9
	13	86.8 ± 3.6	101.5	97.0
A4	0.1	201.3 ± 8.1	236.2	224.8
	1	147.8 ± 6.4	175.9	167.5
	3	114.1 ± 5.2	139.4	131.3
	7	91.0 ± 4.2	111.2	105.0
	10	82.6 ± 3.5	98.2	93.3
	13	67.1 ± 3.3	83.8	78.7
A7	0.1	170.9 ± 6.5	196.3	188.5
	1	161.2 ± 6.3	187.2	178.8
	3	124.5 ± 5.3	149.2	141.1
	5	107.3 ± 5.4	134.2	126.2
	7	76.4 ± 4.0	98.8	91.7
	10	67.7 ± 3.0	81.3	77.2
	13	63.3 ± 2.9	76.9	72.7

Chapter 6

Discussion of the Results

The results presented in the last chapter have trust at some hypothesis and ideas. These interpretations have to be taken with care since the development of ADN/GAP-based propellants is still under development. The following suppositions, based only on a preliminary study, have to been confirmed or confuted. However, some ideas have found confirmation and some important considerations could be done in the scope of future work and possible utilization of this kind of propellants.

6.1 ADN/GAP

The obtained results completely confirm what is supposed by Pak in [27] and Menke in [31]. The increase of the size of the oxidizer prills is reflected in a higher pressure dependence of the burning rate, at least at high pressure, since at low pressure the measured value are quite the same (Appendix 1).
This could be due to the important role that ADN plays in the combustion. It is not possible to state that the combustion is completely dominated by ADN because of the absence of its usual plateau in the pressure range from 5 to 10 MPa. However, it is clear that its participation in the combustion process is the very important, in particular observing the flamelets released from the burning surface. These flamelets start from bright spherical particles (probably the combustion of the carbonised structure leaved by the pyrolysed GAP.
The comparison between the results of ADN/GAP and pure ADN as monopropellant (Fig. 2.3) shows a reduction of burning rate due to the binder.
This is a surprising result since Fujisato, in [70], did a similar study considering nearly the same formulation but with HTPB as binder (PB/ADN blue line in Fig. 6.1). This formulation shows a liquid layer on the burning surface and a pressure exponent about twice as high as what results from the ADN/GAP experimental campaign presented in Chap. 5 (1.1 against 0.50-0.65). So the binder must have a strong effect in the combustion. The interaction between the decomposition of pure ADN-particles ([3]) and the carbon structure of pyrolysed GAP could define a “preliminary reaction” in the condensed phase.

The change of binder will change this reaction and influence burning rate and pressure dependence.
However, other investigations using other azide polymers are necessary to confirm this explanation.

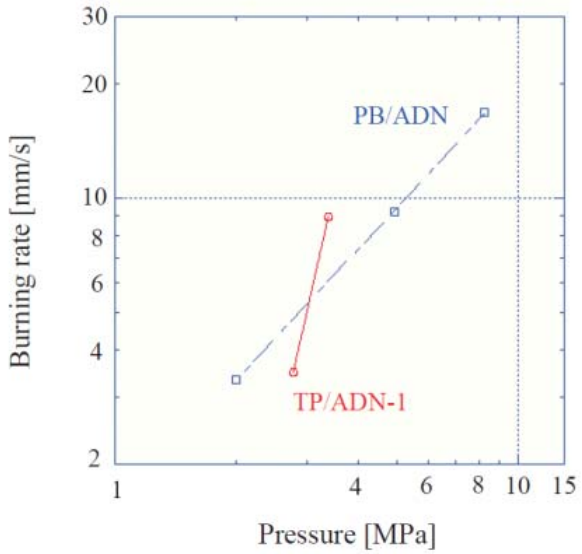

Fig. 6.1. ADN/HTPB burning rate vs. pressure (PB/ADN blue line) [70]

In Fig. 6.2 the burning rates of ADN/GAP propellants are fitted with Vieille's law.
The two propellants H57 and H59 show practically the same burning rate law, with a difference in prill dimensions of 15 µm. The same result is obtained for the formulations H55 and H56, but the difference in prill size was about 60 µm.
It seems to be possible that there is a dimension of prills for which any further increase does not affect the pressure dependences.
This conclusion must be proved by other measurements with different prill sizes.
Wingborg has conducted experimental tests on a propellant with prill dimensions similar to H57 in [71], but with different prilling technology. He found a similar pressure exponent of 0.49. So, it could be stated that the method of prilling does not influence the burning law.
The behaviour of the propellant can be well described by Vieille's law (Fig. 6.2). In addition all the ADN formulations have much higher burning rates compared with a commercially available AP/HTPB/Al propellant, of which the data are used as a reference.

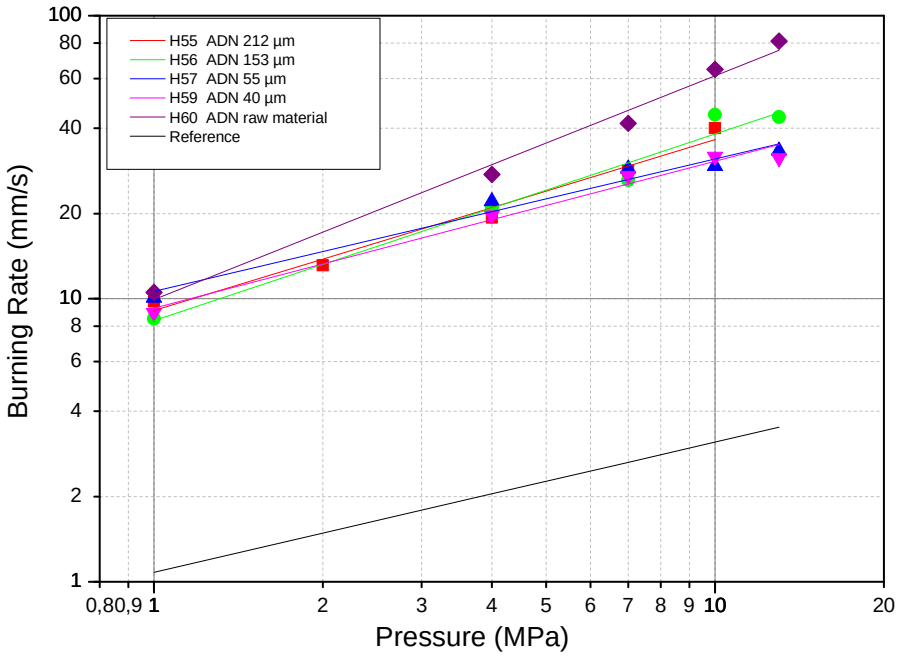

Fig. 6.2. Mean of the measured values for each pressure level for different ADN/GAP formulations fitted with Vieille's law (Chap. 5)

The Figure 6.3 displays the mean values of the maximum temperatures for each pressure level together with the calculated adiabatic temperature (black line). The temperature peak of the formulations H55 and H56 at 4 MPa is noticeable. For higher pressure levels these formulations show the tendency to realign their behaviour with the other formulations.
The temperature difference is higher than the accuracy of the measurement, but the reason of this effect is not understood.
From 7 MPa to 13 MPa almost all the formulations have shown the same flame temperature, between 2250 and 2400 K. The formulations with smaller prills present almost the same increasing behaviour of temperature.
All the measured temperatures are around 70% to 80% of the adiabatic flame temperature increasing with pressure.
Inside the window bomb a real flame never reaches the adiabatic flame temperature due to cooling effects by the purge gas and radiative heat loss. Also non-equilibrium and not complete reactions may be responsible for lower temperatures.
However the measured temperatures are extremely close to the adiabatic one with respect to the conditions inside the window bomb. So, it is possible that the adiabatic flame temperature can be nearly reached inside the thermally isolated combustion chamber of a rocket motor. This would

be traduced in a specific impulse of 274.5 s (shifting equilibrium and adapted nozzle in vacuum).

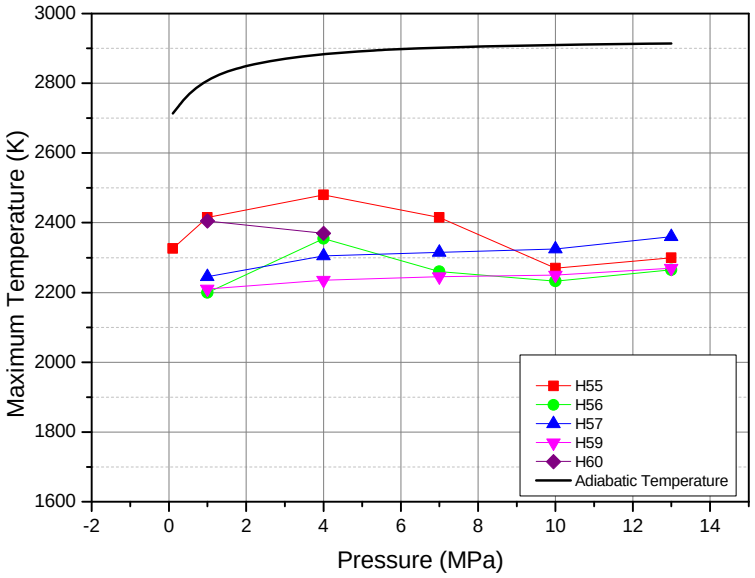

Fig. 6.3. Mean of measured maximum temperatures for different ADN/GAP formulations compared with the calculated adiabatic flame temperature

This impulse is only 15 s less than the calculated specific impulse of the commercial AP/HTPB/Al propellant (289.6 s under the same conditions for AP/HTPB/Al 68/14/18). It has to be pointed that the pure ADN/GAP propellants do not suffer in 2P flow loss. The estimation of this loss is about 21 s for the reference formulation [56][72]. This means that the pure ADN/GAP composition have potentially 6 s more in specific impulse than the commercial propellant.
Unfortunately, it has to admit that the burning rate of ADN/GAP formulations is extremely high for civil purposes. Some ballistic modifiers must be added to reduce the burning rate at 7 MPa from 25-30 mm/s to 7-18 mm/s.

6.2 ADN/GAP/Al

The better combustion provided by formulation H32 makes it an optimum choice from the point of view of combustion residual.
Since the formulation containing ADN prilled by FOI (H27) with a monomodal size distribution and the composition H32 with a bimodal distribution practically shows the same pressure dependence (Fig. 6.4).

Perhaps that is the dimension of the coarse particles of the oxidizer that controls this parameter [41].
The only difference between these two compositions is the dimension of agglomerates.
The pressure exponent obtained by Vieille's law fitting was not so far from the one obtained for the composition H55 (with almost the same dimension of prills).
Another confirmation of this statement is the pressure exponent obtained for the composition H31G, which is also almost equal.
In all cases the pressure exponent is around 0.58.
Looking at both parameters of Vieille's law (in particular to the pre-exponential factor) and at Fig. 6.4, it is possible to see that the H31G shows a higher burning rate than the other two compositions.

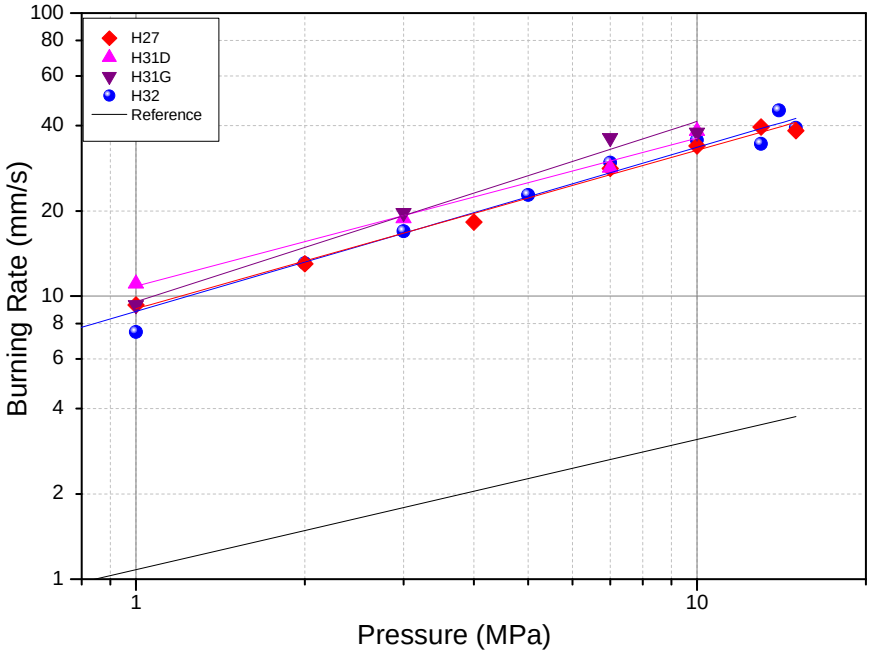

Fig. 6.4. Mean of the measured burning rate values for each pressure level for different ADN/GAP/Al formulations fitted with Vieille's law (Chap. 5)

An explanation of that could be found in the consideration make so far for the pure ADN/GAP propellants: probably the fine part of the bimodal distribution is lowering the burning rate acting on the pre-exponential factor. But it does not explain why the formulation H27 overlaps with the formulation H32.
The motivation of this trend could be found in the origin of the oxidizer prills used for the manufacture of formulation H27. Since they are prilled by FOI it is possible that during the transport ADN manifests its

hygroscopicity absorbing water. The absorbed water may slow down the burning rate of H27 towards the same level of H32.
The formulation H31D shows a lower pressure dependence if compared to the other formulations. This behaviour could be better analysed looking to Fig. 6.5.
The higher temperatures measured could be according to better combustion. So, seems that the bigger aluminium particles participate better in the combustion process than the small aluminium contained in H31D. This lower participation in combustion is reflected on the burning rate through lower heat feedback from the flame.

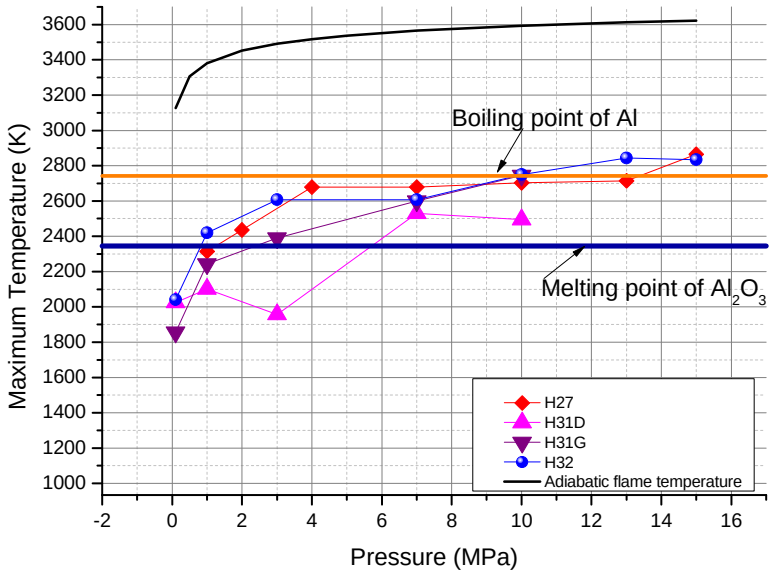

Fig. 6.5. Average temperatures for ADN/GAP/Al formulations (boiling point of Al 2743 K and melting point of alumina 2345 K at 0.1 MPa)

Looking at Fig. 6.5 it is possible to see that in this range of pressure both formulations exceed the boiling temperature of aluminium of 2743 K at 0.1 MPa.
The temperature measured for these formulations in the pressure range from 4 to 10 MPa seems to be very stable and could indicate that a part of heat feedback is used for the aluminium boiling (Fig. 6.5).
Figure 6.5 also shows that starting from 3 MPa almost all the formulation's temperatures are higher than the melting point of alumina. This is also an important result since the eruptions observed from the agglomerates must be motivated by a liquid state of the alumina shell and production of gaseous species inside the agglomerates (probably AlO).

From the same figure it is also possible to note that the temperatures of the compositions H27 and H32 follow the same trend as the adiabatic flame temperature.
The adiabatic flame temperature has an interesting peculiarity: it is always higher than the alumina boiling point. This means that if inside the combustion chamber of a rocket the adiabatic conditions are completely reached, and if the elongation of the rocket is enough to guarantee a complete reaction, no solid particles will reach the throat.
Multiplying the time scale of spectrometric measurements with the burning rate measurements it was possible to convert time scale to height above burning surface.

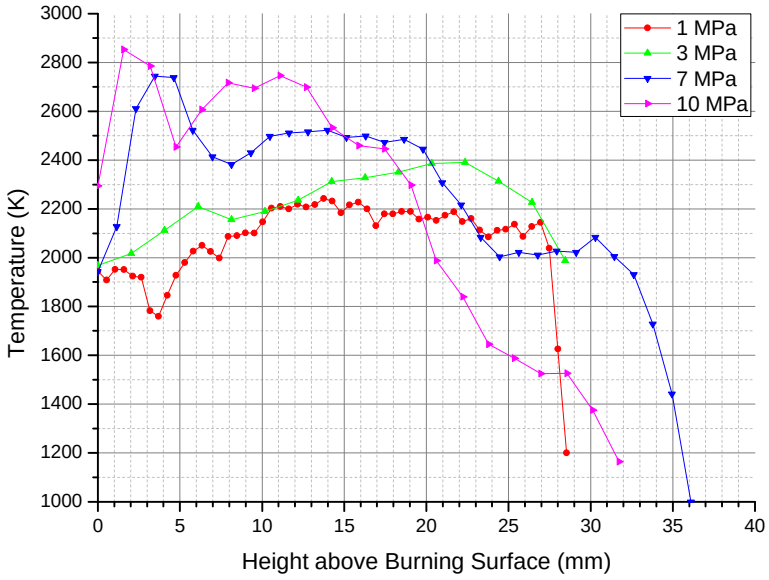

Fig. 6.6. Temperatures in dependence of the height above burning surface for H31G

Figure 6.6 allows making some considerations about the behaviour of formulation H31G. The temperature maximum at high pressure is probably associated to the burning surface. The following decrease and then increase again should be the beginning of the brightest flame zone. At high pressure the maximum in temperature is reached near the combustion surface. Instead At low pressure the maximum is reached in the flame zone.
It is also interesting to note the reduction in length of the bright flame with increasing pressure, from about 27 mm at 1 MPa to 14 mm at 10 MPa.
Similar results were obtained for propellant H31D.

Another discussion can be made on formulation H32 for which the length of the flame seems to be quite stable around 14 mm for all the pressure levels investigated (Fig. 6.7).
This formulation shows a less defined peak at the burning surface but a stronger decrease of temperature with distance (at high pressure). This could lead to a re-condensation effect of aluminium at a certain distance from the burning surface.
The quite constant length of the flame could be an effect of the thermal conditions, for which the temperature is always (except at 0.1 MPa) higher than the melting point of alumina and close to the boiling point of aluminium. It could be possible that this thermal condition is maintained for all pressure levels generating the same flame length.

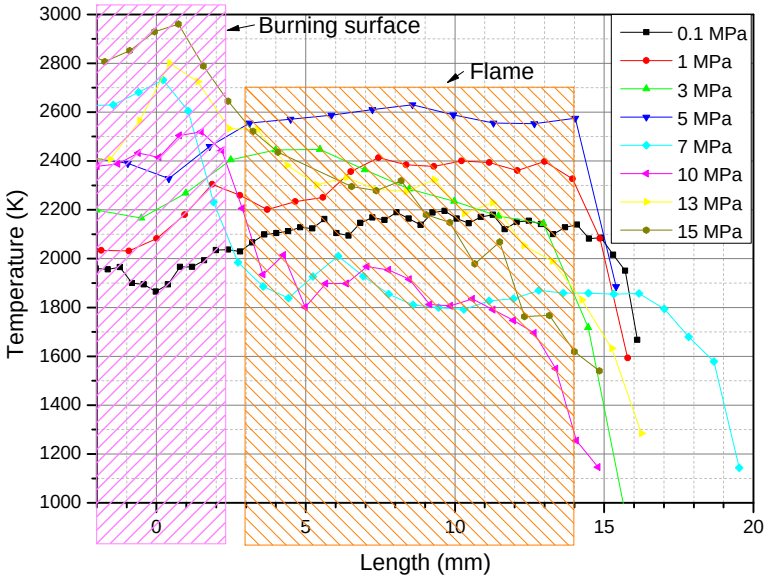

Fig. 6.7. Flame length for formulation H32

6.2.1 Agglomeration

The observed agglomeration behaviour has been studied in more detail and related with the observed situation on the burning surface. The high temperatures confirm the collection of hollow/porous particles, and in particular confirm that the aluminium (still be present inside the liquid oxide shell) evaporated together with gaseous intermediate combustion products. This could be the factor that allows the agglomerated particles to detach, since the physical experience teaches that smaller particles are easier carried by a gas flow than larger ones [75]. The detachment of bigger particles can only be explained by the assumption of a decreasing

density during the agglomeration process. Since the density of aluminium (2.7 g/cm^3) is lower than alumina's density (3.94 g/cm^3) an additional factor must be considered. An enclosure of gas that decreases the total density of the agglomerate during the oxidation process could explain all the observations.
The presence of gaseous intermediate combustion products of aluminium, most probably AlO, inside the agglomerations can be motivated by the way of oxidation of aluminium: it proceeds by diffusion through the oxide layer.
Remember that for all the formulations, emerged particles of the same size (around 77 μm) were observed. On the base of Beckstead, in [38], it is possible to estimate the burning time of these particles using Eq. 6.1.

$$t_b = \frac{\alpha D^{\eta}}{X_{eff} P^{0.1} T^{0.2}} \tag{6.1}$$

With

$$X_{eff} = C_{O_2} + 0.6\, C_{H_2O} + 0.22\, C_{CO_2} \tag{6.2}$$

Where t_b is the burning time of the particle, α=0.00735, η=1.8, D is the diameter of the agglomerated particles at first appearance, P is the pressure, T is the temperature and C_x is the concentration of species x.
The assumption is that they were only made of aluminium at first appearance.
The results are reported in Fig. 6.8.
It was observed that the particles stay on the burning surface for 0.12-0.20 s at a pressure of 0.1 MPa to about 0.05-0.1 s at a pressure of 5 MPa. At higher pressures the particles should stay for about 2.5-4 ms. This means that the particles can completely burn, generating oxide, before detaching.
Also the velocity of the particles has been studied, following their moving through the flame.
A common minimum speed of 0.4 m/s was found. In temporal domain one particle needs almost 0.035 s to pass through the entire flame for formulation H32.
Starting from these considerations it seems logical to collect only oxide particles on the sample holder, but EDX measurements do not confirm this expectation.
The observation of pure aluminium on the sample holders requires also a minimum of gaseous aluminium inside the flame for the entire pressure domain.

The considerations made up to now only consider particles made of aluminium at the first appearance, but most of the agglomerated particles emerge with an oxide shell that slow down the complete combustion. The oxidized part of the particles, usually not a simple shell, should have enough time to melt. For a combined effect of gravity and heat drawback from the flame, the oxide became a cap on the lower part of the agglomerate (the "oxide cap") like described in [38] for AP/HTPB/Al-propellants.

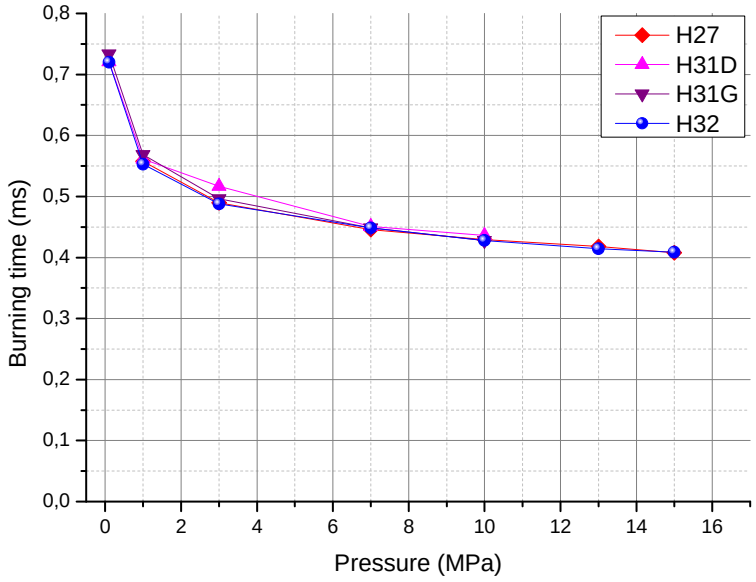

Fig. 6.8. Burning time of the agglomerated particles [38]

The dimension of these agglomerates is the one that should be considered, almost at this stage of characterization, for the 2P loss.
The size of the oxidizer prills is one of the key factors influencing the size of the agglomerations. The formulation H27 give rise to agglomerates more than 60 μm larger than the other formulations at 1 MPa.
The formulation H32 shows agglomerates which have dimensions between the formulations H27 and H31 (Fig. 6.9).
A possible explanation could be the theory of pockets expressed by Cohen in [41]: a bimodal distribution leads to an enlargement of pocket size encouraging the aggregation of more metal powder, creating larger agglomerations.
Following the procedure proposed in [41], it was possible to estimate the size of the aggregations inside a pocket: the result was not so far from the

measured dimensions of particles at their first appearance (by calculation 82 µm and by measurement 77 µm).

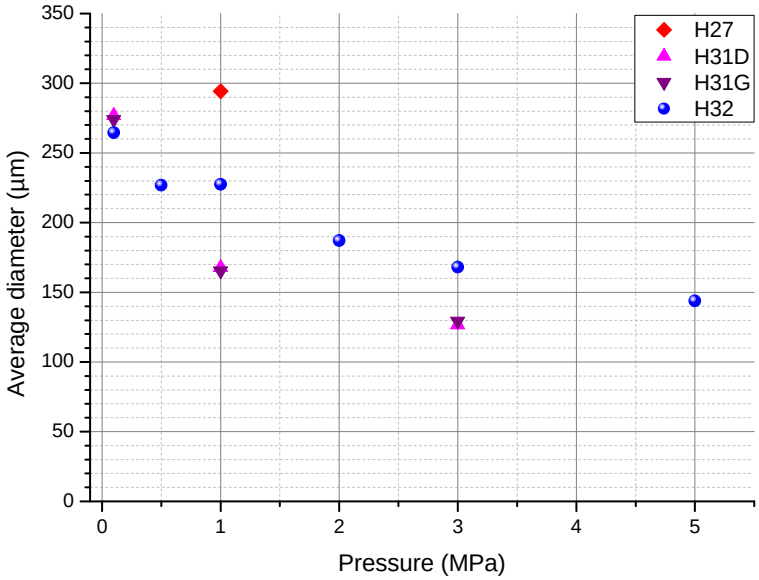

Fig. 6.9. Average size of agglomerations for the formulations ADN/GAP/Al

The agglomerates measured for ADN/GAP/Al propellants were always larger than the ones created by the commercial formulation of AP/HTPB/Al.
The used AP/HTPB/Al give rise to agglomerations with an average diameter between 120 and 160 µm at 1 MPa and between 130 and 80 µm at 2.5 MPa ([72]).
On the combustion surface a liquid layer was not observed so it is improbable that this is the main cause for this increment of size.
This increment could be due to the higher temperatures reached by the ADN/GAP/Al propellant, because higher temperatures will increase the oxidation of Al (e.g. Arrhenius law).
The same results obtained for the two formulations H31D and H31G, with fuel powder of different dimensions, lead to an important conclusion: the initial dimension of the aluminium powder does not affect the dimension of the agglomerates (Fig. 6.9).
There is a possibility that the disappearing inside the pores leaves the particles the time necessary to aggregate further making the original dimensions of the particles irrelevant. It is considered that the time spend by the agglomerates on the burning surface is pertinent in order to create

enough enclosed gas to let they reach the requested density for the detachment.

6.3 ADN/GAP/Alane

The combustion process of the formulations containing alane is quite interesting. The alane content do not influence the pressure dependence, but only the pre-exponential factor of the Vieille's law.
From the video analysis it seems that the combustion of ADN/GAP is faster than the aggregation process of aluminium. The skeleton layer of aluminium contained in the condensed phase is observable even when the condensed phase no longer exists.

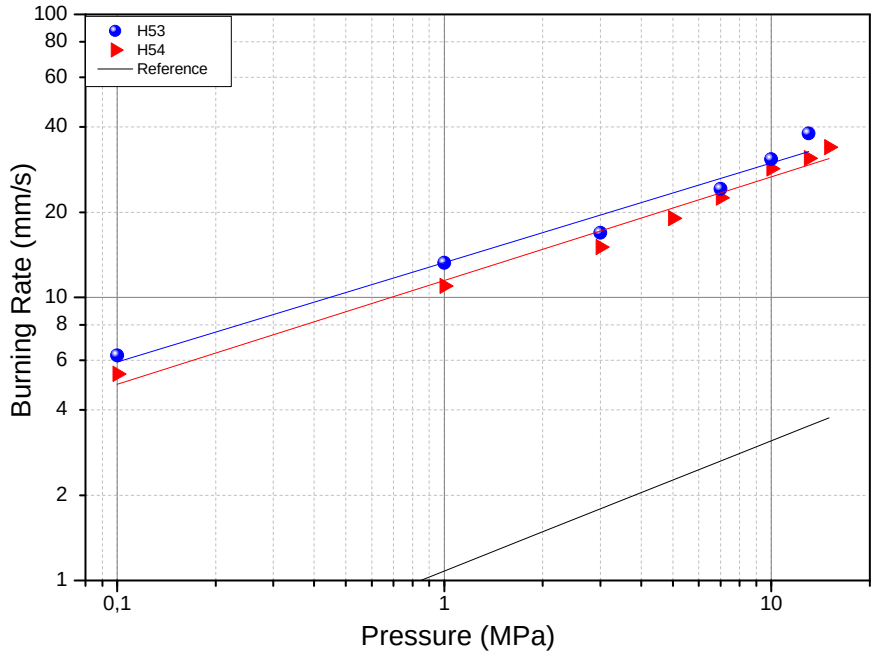

Fig. 6.10. Mean of the measured burning rate values for each pressure level for ADN/GAP/alane formulations fitted with Vieille's law

Analysing the colour of the skeleton layer it is realized that it mainly consists of oxidized aluminium. The low amount of water and CO_2 obtained by the ideal thermochemical calculations for formulation H54 (Tab. 3-3) make it possible to state that aluminium has reacted with all the oxidizing agents near the burning surface.
Fig. 6.10 shows that the Vieille's law do not approximate well the burning behaviour of formulation H53.

The possibility of a liquid layer of aluminium and aluminium oxide is confirmed by the temperature measurements, shown in Fig. 6.11. In most cases, both formulations have temperatures higher than the melting point of alumina, and often higher than the boiling point of aluminium.
At 7 MPa it seems that the formulation H54 approaches its adiabatic flame temperature. This means a mostly complete reaction of all the compounds of the formulation.

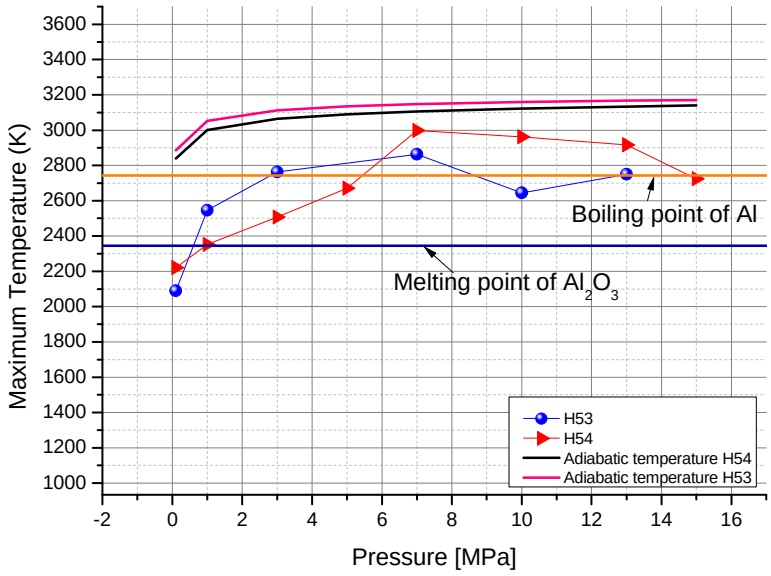

Fig. 6.11. Average of maximum temperatures for each pressure level for two different ADN/GAP/alane formulations

6.3.1 Agglomeration

The matrix shape of the agglomerations found its explanation looking at Fig. 6.11: the huge amount of oxidizer available on the burning surface allows the molten skeleton layer building a liquid surface, protecting the processes below this layer. In this way, the evaporated aluminium (because of boiling, oxidizer diffusion, or reaction with hydrogen) is allowed creating “bubbles” with a shell made of the alumina that was lying on the burning surface, and with a core made of these gaseous products. The liquid state of alumina also allows these gases to move, reaching the surface of the agglomerate and creating the matrix shape. Further confirmation of gas inside agglomerates can be found in the collected products often made of simple shells, white (typical colour of alumina) hollow spheres or broken agglomerates.

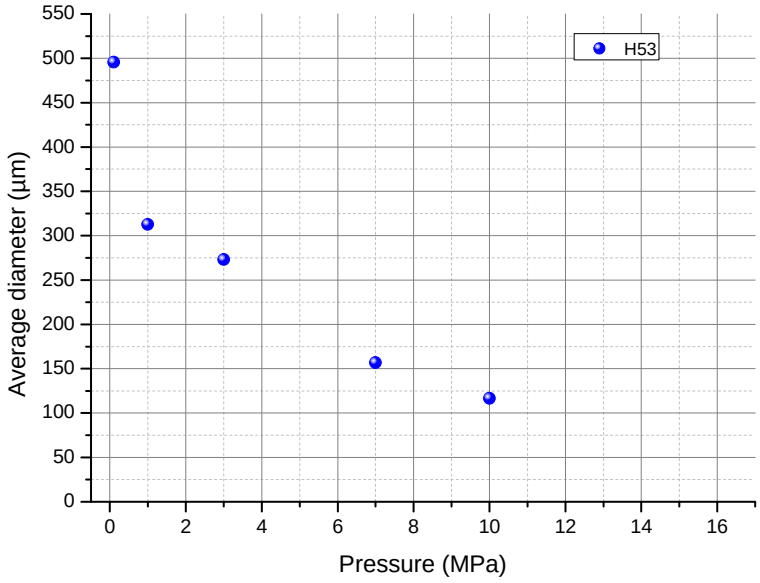

Fig. 6.12. Average diameter of agglomerates vs. pressure for formulation H53

The absence of matrix agglomerates and the presence of the "oxide caps" at pressures higher than 7 MPa for formulation H53 can be explained by the amount of aluminium available at the surface. Perhaps there is not enough aluminium to behave as described before. The thermal conditions (Fig. 6.11), the reaction products (Tab. 3-3) and the burning rates (comparison between Tab. 5-2 and Tab. 5-4) are quite similar to the one observed for formulations H32 and H27 at these levels of pressure. So it seems natural that the shape of agglomerates is quite the same.
It was not necessary to find a prediction formula for these formulations since the agglomerations were big and defined enough to be measured up to 10 MPa.
At working pressure the measured agglomerations have dimension of 157 µm against the 109 µm for the formulation H32 and the estimated 59 µm for the AP/HTPB/Al propellant.
The burning rate measured at working pressure for formulation H53 is about 26 mm/s, which is 11 mm/s higher than the optimal value, so ballistic modifiers must be used. The adiabatic temperatures are lower than the ones of the ADN/GAP/Al propellants and not so much higher than the AP/HTPB/Al reference.

6.4 AP/GAP/Al

The combustion experiments carried out for the formulations containing AP show an intensive development of smoke and a tendency to incomplete burning. Increasing the amount of oxidizer is considered not to be useful to maintain good mechanical properties. However the Vieille's law interpolation was quite good, (see Fig. 6.13).
These formulations tend to have a lower burning rate if compared with ADN/GAP.

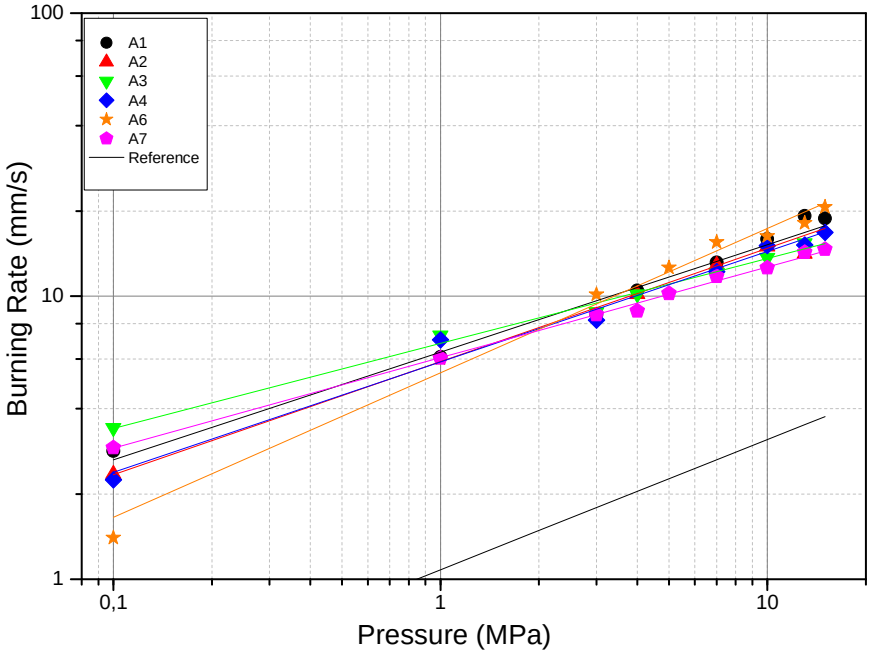

Fig. 6.13. Mean of the measured burning rate values for each pressure level for AP-formulations fitted with Vieille's law (Chap. 5)

The burning rate at working pressure is about 12.5 mm/s. The Vielle's law fits show also lower pressure dependencies. These peculiarities make AP-formulations relatively interesting for application. The burning rate seems to be lower than the optimal one but tend to align if the formulation without aluminium is considered (A6 14.46 mm/s); the weak point of A6 is the extremely low specific impulse (268.7 s).
Looking at the temperatures presented in Fig. 6.14 and Fig. 6.15 it is notable that the two formulations A2 and A3 lying mostly under the temperature of the melting point of alumina. The remaining formulations, instead, show about the same temperature level as the formulations containing ADN/GAP.

The temperatures measured for formulation A2 are very interesting because despite the "peeling effect" and the incomplete combustion they are closest to the corresponding adiabatic flame temperature.

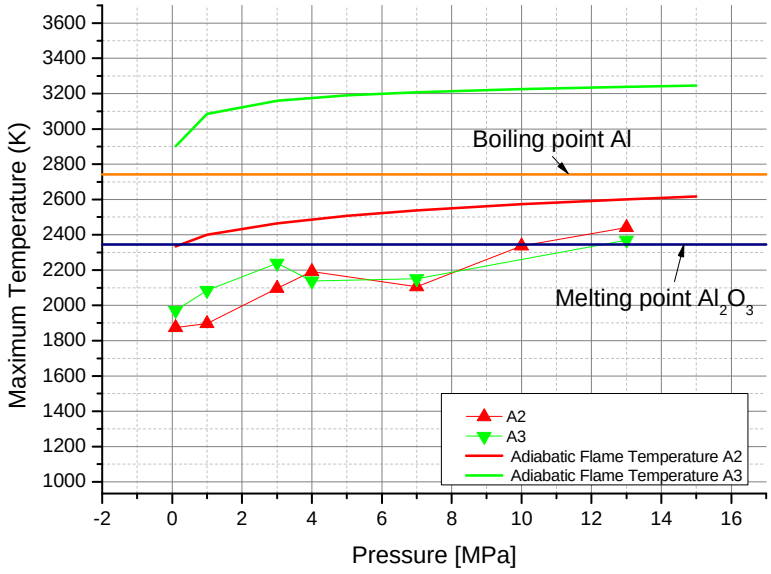

Fig. 6.14. Average maximum temperatures for A2 and A3

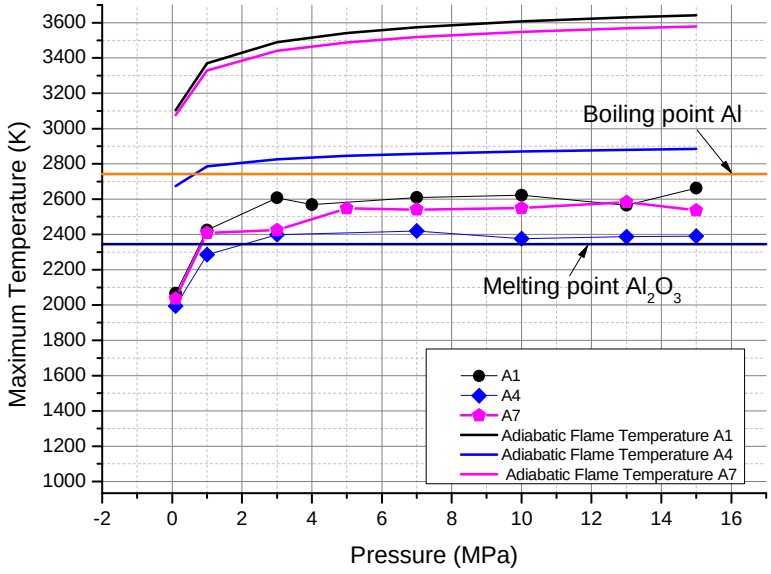

Fig. 6.15. Average maximum temperatures for A1, A4 and A7

This could be explained looking at the combustion products in Tab. 4-6, which indicate a deficit of oxidizer. The same can be stated for formulation A4, which is also “close” to adiabatic flame temperature, but not presents a similar huge amount of residues.
The simple increase of 4% in oxidizer amount of formulation A4 leads to an increase of maximum temperature of about 100 K, stabilizing it around the melting point of alumina.

6.4.1 Agglomeration

The agglomeration analysis of the formulations containing AP does not show any defined dependences on the thermodynamic data. There was no correlation between oxygen balance or adiabatic flame temperature and size of agglomerates.
The factor that seems to control the size of agglomerates is the maximum temperature reached: comparing the dimensions illustrated in Fig. 6.16 and Fig. 6.17 with the temperatures of Fig. 6.14 and Fig. 6.15 it is possible to state that the formulations that show higher temperatures give rise to bigger agglomerates.

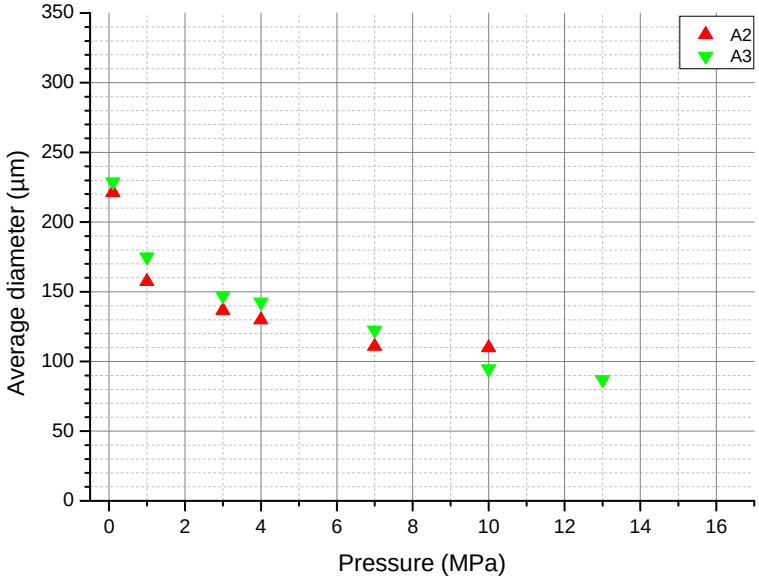

Fig. 6.16. Average diameter of agglomerations measured vs. pressure for formulations A2 and A3

The formulations A2 and A3 show about the same temperatures and also the same size of agglomerations although their difference in formulation is

9% of oxidizer, more than 600 K in ideal adiabatic flame temperature and 14% in oxygen balance.
Also the binder seems to play an important role in the agglomeration dimensions. Comparing formulations A1 and A7, these two formulations are practically equal under the thermodynamic point of view, and also the temperatures measured are quite the same, but the difference in agglomerates size is more than 40 μm at working pressure.
The study of the formulations containing AP was performed in order to see if common thermodynamic parameters for different kinds of formulations can lead to equal agglomeration results. Unfortunately ideal thermodynamic seems to be irrelevant for agglomerates prediction. Probably because aggregation/agglomeration phenomena are kinetically controlled and chemical thermodynamics assumes infinitive reaction rates without kinetic considerations. The agglomerations would be inside a chemical environment completely different to the one assumed for ideal thermochemistry, making the correlation with different thermodynamic parameters unfeasible.

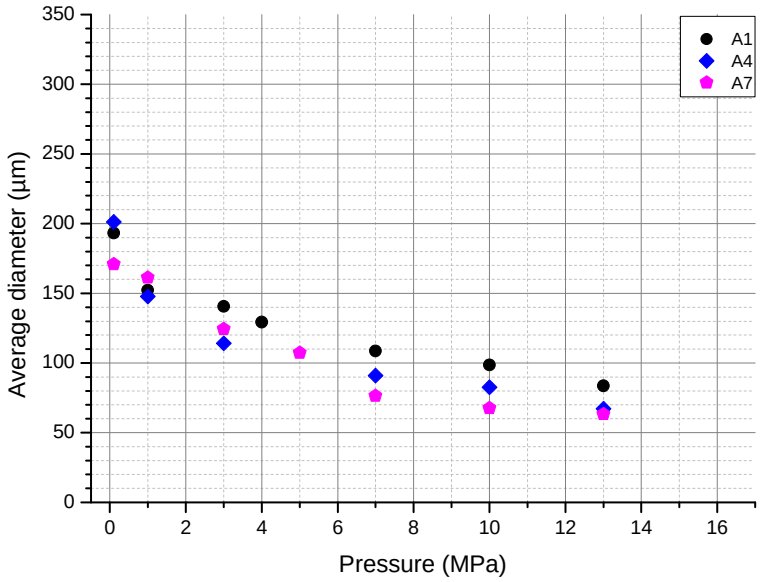

Fig. 6.17. Average diameter of agglomerations measured vs. pressure for formulations A1, A4 and A7

The formulation A1 gives rise to agglomerations smaller than the ADN/GAP/Al formulations, despite the similar oxygen balance, adiabatic flame temperature and oxidizer to binder ratio.
Formulation A2 forms agglomerations of about the same size as formulation H31G. This is very interesting because the common parameter

between the two formulations is the enthalpy of formation. Anyway the common points are only two (at 1 and 3 MPa).
No correlation between enthalpy of formation and dimension of agglomerates has been found.
These formulations were not studied for possible applications, and the presented problems in combustion do not encourage their use.

Chapter 7

Agglomeration Detachment Model

Starting from the dynamics of a single particle immersed in a viscous flow, for which only weight and aerodynamic drag are considered as active forces, as reported in [34], it is possible to cast a simple analytical model which allows clarifying the physical dependencies of agglomeration detachment.
For a matter of simplicity, the full equations of motion are not considered and the reported results only concern the detachment size of particles from the burning surface.

7.1 General Equation

The equilibrium considered is between the body forces and the aerodynamic drag provided by the hot gases flowing around the particle

$$Body\ Forces - Drag = 0 \tag{7.1}$$

By simple substitutions and assuming a zero-dimensional particle model

$$ma_{cc} = \frac{1}{2}\,\rho_g\,S\,C_d\,(V-u)^2 - mg_0 \tag{7.2}$$

where ρ_g is the density of the gas phase, S is the exposed particle surface, C_d is the drag coefficient, V is the gas velocity from the propellant gasification, u is the velocity of the particle, m is the mass of the particle, and a_{cc} is acceleration of the particle defined as

$$a_{cc} = \frac{du}{dt} \tag{7.3}$$

Using the mass balance equation at the propellant interface, it is possible to state

$$\rho_c r_b = \rho_g V \tag{7.4}$$

where ρ_c is the propellant density and r_b is the burning rate.

Substituting Eq. 7.4 in Eq. 7.2, with ρ_p particle density, one obtains

$$\frac{4}{3} r_p \, \rho_p \, a_{cc} = \frac{1}{2}\left(\frac{{\rho_c}^2}{\rho_g} r_b + \rho_g u^2 - 2 \, \rho_c r_b u\right) C_d \tag{7.5}$$

The main stream gas density around particles is estimated using the state equation of perfect gases, being the temperature under consideration in the range 1000–3000 K

$$\rho_g = \frac{PM}{RT_s} \tag{7.6}$$

where P is the pressure, M is the mean molecular mass of the combustion products, R is the perfect gas constant and T_s is the temperature over the burning surface of the strands (generally higher than 2000 K if just agglomerates are considered).
For the propellant burning rate the Vieille's law is commonly accepted

$$r_b = aP^n \tag{7.7}$$

Substituting Eqns. 7.6 and 7.7 in the previous Eq. 7.5, it is possible to obtain the following force balance

$$\frac{4}{3} r_p \, \rho_p \, a_{cc} = \frac{1}{2}\left(\frac{RT_s}{MP} \, {\rho_c}^2 a^2 P^{(2n)} + \frac{PM}{RT_s} u^2 - 2 \, \rho_c a P^n u\right) C_d \tag{7.8}$$

in which the drag coefficient (C_d) and particle density (ρ_p) are unknown.

7.1.1 Stokes's Drag Coefficient

For inert particles immersed in a viscous flow Stokes proposed an estimate of the drag coefficient, for very low values of the Reynolds number, as

$$\begin{cases} Re < 0.1 \\ C_d = \frac{24}{Re} \end{cases} \tag{7.9}$$

The definition of Reynolds number has to account for the relative velocity $V - u$ between gas and particle

$$Re = \frac{2 r_p \, \rho_g (V-u)}{\mu} \tag{7.10}$$

where μ is the viscosity of the gas phase around particles and r_p is the radius of the particle.

Substituting the Stokes drag coefficient and the definition of Reynolds number in Eq. 7.8, one finds

$$\frac{4}{3}\pi {r_p}^3 \rho_p a_{cc} = \pi r_p \frac{6RT_s}{MP} \rho_c \mu a P^n - \pi {r_p}^2 \frac{6}{r_p} \mu u$$

Assuming now that the particle is exactly at the moment of first detaching, and the only force acting on it is its weight, one can further state

$$\begin{cases} \frac{du}{dt} = 0 \\ u = 0 \end{cases} \tag{7.11}$$

which provides a convenient simplification

$$\frac{4}{3}\pi {r_p}^3 \rho_p g_0 = \pi {r_p}^2 \frac{6RT_s}{r_p MP} \rho_c a P^n \mu \tag{7.12}$$

Most of the parameters of Eq. 7.12 can be obtained using ideal thermodynamic calculation (see Tab. 3-3) and the standard Vieille's law.
Using Sutherland's formula, it is possible to calculate the viscosity of the main reaction products of combustion

$$\mu_x = \mu_0 \frac{T_0 + C}{Ts + C} \left(\frac{T}{T_0}\right)^{\frac{3}{2}} \tag{7.13}$$

where μ_x is the viscosity of species x.
Looking at the ideal thermodynamic calculations reported in Tab. 3-3, it is possible to note that the main combustion products for ADN/GAP/Al formulations are carbon monoxide and nitrogen, for which the coefficients of the Eq. 7.13 are shown in Tab. 7-1.

Tab. 7-1 Sutherland's parameters

Species	C	T_o [K]	μ_0[Pa.s]
N_2	111	300.55	$18.27 \cdot 10^{-6}$
CO	118	288.15	$17.2 \cdot 10^{-6}$

Using then the concentration of these species as evaluated in the combustion chamber section (since the experimental results were obtained inside a window bomb), it is possible to obtain a weighted viscosity of the gas phase as

$$\mu = C_x \mu_x + C_y \mu_y$$

Considering now a burning surface temperature for ADN/GAP/Al formulations of 900-1000 K (see Chap. 2) and using Eq. 7.12, it is possible to estimate the particle size for which a detachment from the burning surface is expected.

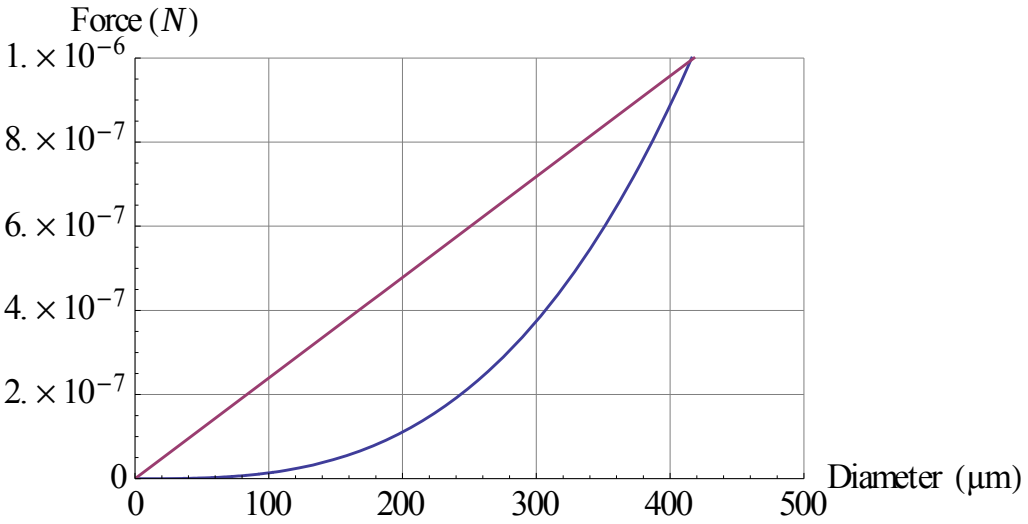

Fig. 7.1. Expected detachment size for aluminium at 0.1 MPa

In Fig. 7.1 the weight of the particle (blue line) and the aerodynamic drag due to the flow (purple line) are shown in function of particle size. These values result, respectively, from the first and the second member of Eq. 7.12.

The above figure describes the size of particles for which detachment is allowed: these are all the particles whose size falls in the area where the purple line is over the blue one. This means that the aerodynamic forces are higher than the particle weight, making thus possible detachment.

Figure 7.1 was obtained considering particles formed of only aluminium (density 2700 kg/m^3); it is possible to see that the equilibrium point, where the hypothesis of stationarity (Eq. 7.11) is valid, occurs at about 410 μm for the pressure level of 0.1 MPa. A different result is obtained if particles of only Al_2O_3 (3900 kg/ m^3) are considered, as shown in Fig. 7.2: the equilibrium point now occurs at about 350 μm for the same pressure level of 0.1 MPa.

On the other hand, bear in mind that this simple model does not take into consideration the retainment forces acting on the particle.

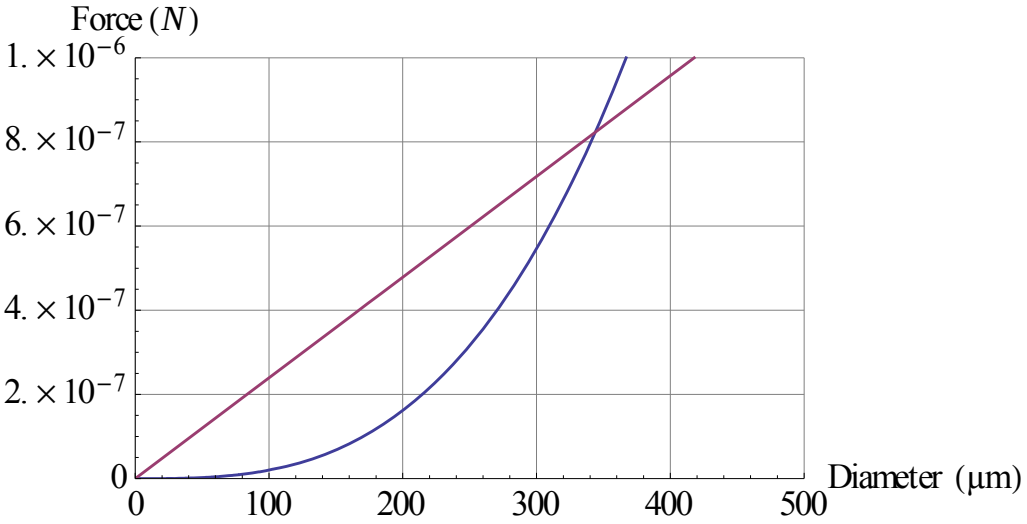

Fig. 7.2. Expected detachment size for alumina at 0.1 MPa

Comparing Fig. 7.1 and Fig. 7.2, it is possible to appreciate how the difference in density acts on the detachment of the particles: aluminium, which is less dense than alumina, forms particles bigger than the ones made of only oxide.

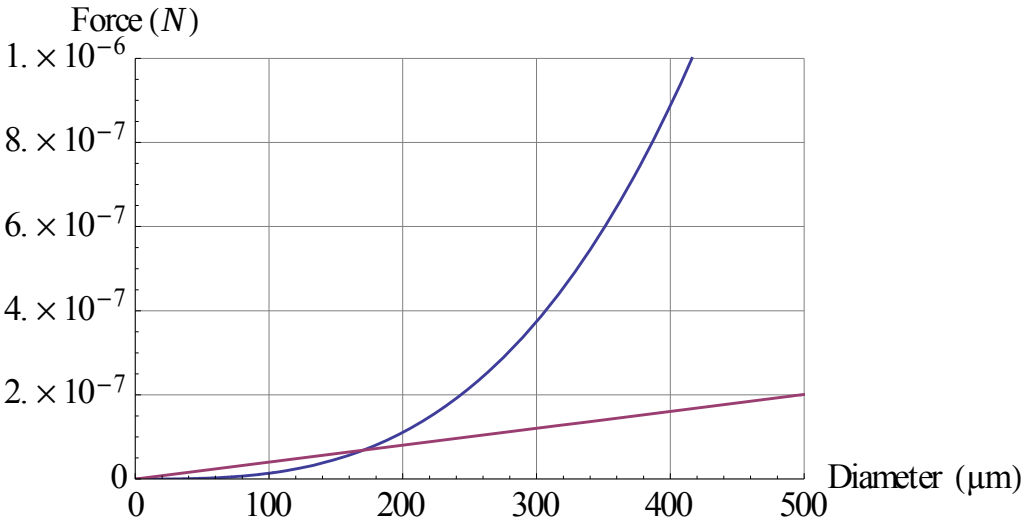

Fig. 7.3. Expected detachment sizes for aluminium at 7 MPa

Figure 7.3 allows also to evaluate the effect of pressure on the detachment of particles. Pressure affects the slope of the aerodynamic force line drastically, with a strong reduction of the diameters for which the detachment occurs. The detachment diameter decreases from a maximum of 410 μm for aluminium at 0.1 MPa to 180 μm at 7 MPa.

The influence of different physical parameters on the variation of the agglomerate size can be investigated starting always from the Eq. 7.12

$$r_p = \sqrt{\left(\frac{9\,\rho_c R T_s a P^n}{2\,\rho_p\,a_{cc} M P} - \frac{\rho_c u}{2\,\rho_p\,a_{cc}}\right)\mu}$$

and considering again the hypothesis in Eq. 7.11

$$r_p = \sqrt{\left(\frac{9\,\rho_c R T_s a P^n}{2\,\rho_p g_0 M P}\right)\mu} \tag{7.14}$$

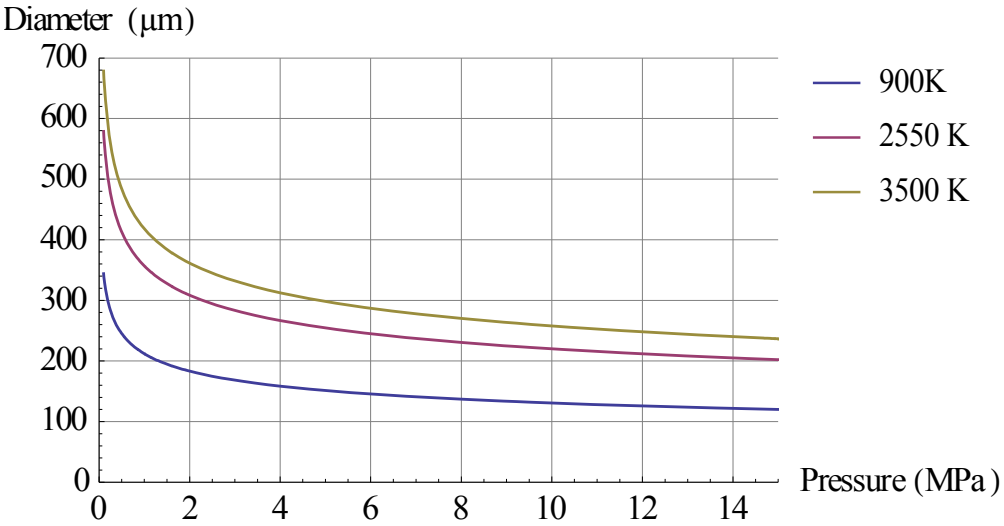

Fig. 7.4. Size of particles vs. pressure at various temperatures

The dependency from pressure, shown in Fig. 7.4, is very interesting since its shape is practically the same of the one experimentally observed for ADN/GAP/Al formulations. In accordance to that, it seems that the sizes of particles monotonically decrease with increasing pressure.
Increasing the temperature from the 900 K of the burning surface to the 2550 K of the flame or 3500 K of the particle wake, the pressure dependency better reflects the experimental results.

7.1.2 Oseen's Drag Coefficient

For a higher Reynolds range, the approximation proposed by Oseen (1910) is considered valid

$$\begin{cases} 0.1 < Re < 1 \\ C_d = \frac{24}{Re}\left(1 + \frac{3}{16} Re\right) \end{cases} \tag{7.15}$$

Substituting the Oseen's model for drag coefficient into Eq. 7.8 gives

$$\frac{4}{3} r_p \, \rho_p \, a_{cc} = \frac{9 \, {\rho_c}^2 a^2 P^{(2n-1)} R T_s}{4M} + \frac{9 \, PM}{4RT} u^2 - \frac{9}{2} \, \rho_c a P^n u + \\ + \left(\frac{6 R T_s \, \rho_c a P^{(n-1)}}{M} - 6u \right) \frac{\mu}{r_p}$$

And applying now the hypotheses of Eq. 7.11, it is possible to get an equation with dimension of forces

$$\frac{4}{3} \pi {r_p}^3 \, \rho_p \, g_0 = \pi {r_p}^2 \left[\frac{9 \, {\rho_c}^2 a^2 P^{(2n)} R T_S}{4MP} + \left(\frac{6 R T_S \, \rho_c a P^n}{MP} \right) \frac{\mu}{r_p} \right] \qquad (7.16)$$

Using Eq. 7.16 is possible to repeat the same considerations made for Eq. 7.12.
The main difference is the order of magnitude of the results, since they increase by a factor of about 20 with respect to the ones obtained using the Stokes assumption.

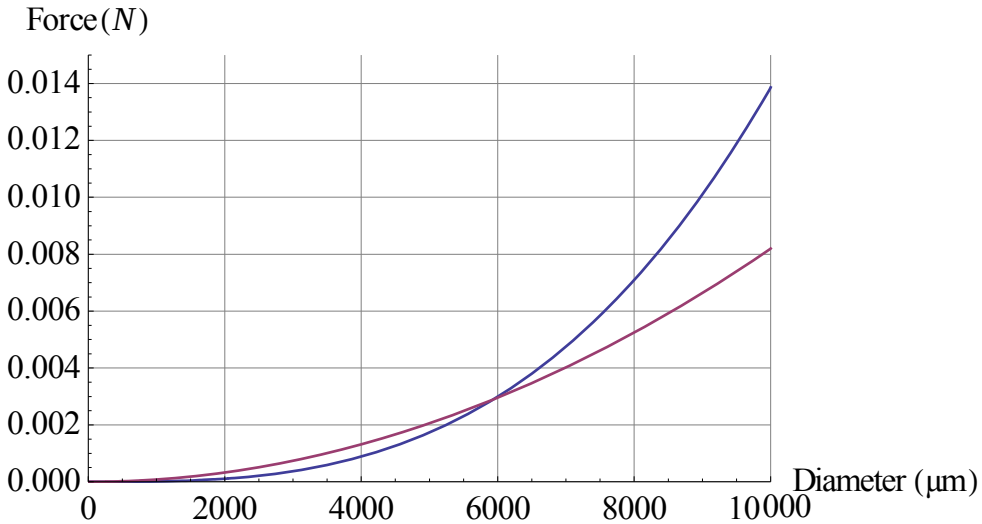

Fig. 7.5. Drag and weight forces (Oseen) for aluminium at 0.1 MPa

From Fig. 7.5 it is possible to evaluate how the introduction of a constant factor inside the drag coefficient leads to an exaggerated increase of the particle size that can detach from the surface.
The behaviour of the drag is in opposition to what is observed with the Stokes assumptions, since an increase of pressure reflects now an increase of detachment particle dimension.

Manipulating Eq 7.16 it is possible to obtain a second order equation for which the unknown is the particle radius

$$\frac{8}{3}\rho_p\, a_{cc}\, {r_p}^2 + \left(9\,\rho_c a P^n u - \frac{9\,PM}{2RT}u^2 - \frac{9\,{\rho_c}^2 a^2 P^{(2n-1)} RT_s}{2M}\right) r_p + \\ + \left(12u - \frac{12\,\rho_c RT_s a P^{(n-1)}}{M}\right)\mu = 0$$

which have solution,

$$r_p = \frac{3}{16\,\rho_p\, a_{cc}}\left[-\left(9\,\rho_c a P^n u - \frac{9\,PM}{2RT}u^2 - \frac{9\,{\rho_c}^2 a^2 P^{(2n-1)} RT_s}{2M}\right) \pm \right. \qquad (7.17)$$
$$\left. \pm\sqrt{\left(9\,\rho_c a P^n u - \frac{9\,PM}{2RT}u^2 - \frac{9\,{\rho_c}^2 a^2 P^{(2n-1)} RT_s}{2M}\right)^2 - 128\,\rho_p\, a_{cc}\left(u - \frac{\rho_c RT_s a P^{(n-1)}}{M}\right)\mu}\right]$$

and applying the hypothesis in Eq. 7.11,

$$r_p = \frac{3}{16\,\rho_p\, g_0}\left[\left(\frac{9\,{\rho_c}^2 a^2 P^{(2n-1)} RT_s}{2M}\right) \pm \right.$$
$$\left. \pm\sqrt{\left(-\frac{9\,{\rho_c}^2 a^2 P^{(2n-1)} RT_s}{2M}\right)^2 + 128\,\rho_p\, g_0\left(\frac{\rho_c RT_s a P^{(n-1)}}{M}\right)\mu}\right] \qquad (7.18)$$

Obviously, only the positive solution has physical relevance.
The confirmation to the tendencies of the enlargement of the particles with pressure is clearly shown in Fig. 7.6.

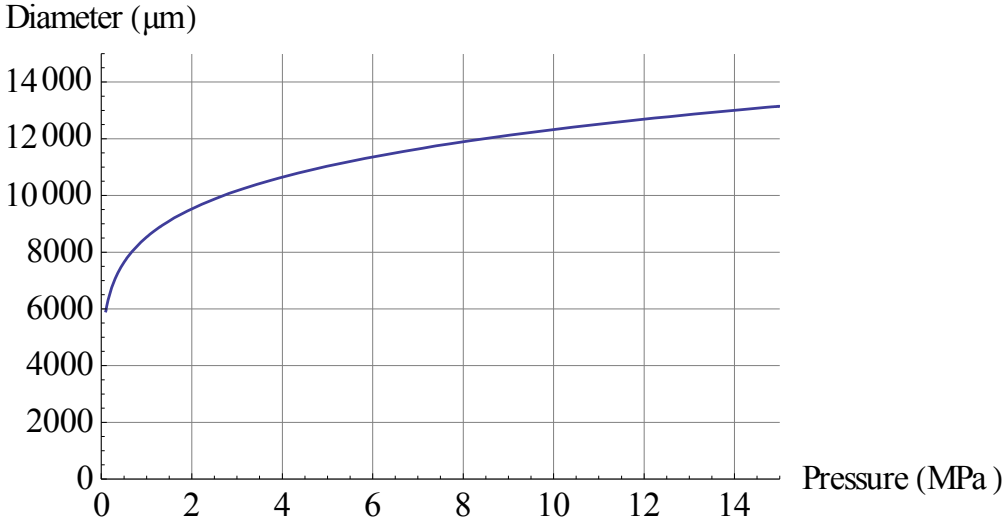

Fig. 7.6. Size vs. pressure (Oseen)

A common trend between the two drag coefficient models (Stokes and Oseen) is the decreasing of detachment size with increasing particle density.

7.1.3 Fourth order approximation

A further increase of Reynolds number leads to consider the drag coefficient used by Veyssiere [75] and Kuhl [76] for the modelling of aluminium particle combustion in an explosive regime,

$$C_d = \frac{24}{Re} + \frac{4.4}{\sqrt{Re}} + 0.42 \tag{7.19}$$

The substitution of Eq 7.19 inside the Eq. 7.8 gives rise to a quadratic term in the right side and considering also the forces acting on the particle, one finds

$$\frac{4}{3}\pi r_p^3\, \rho_p\, g_0 = \pi r_p \left[\frac{6\mu\, \rho_c R T_s a P^n}{MP} + 1.1 \sqrt{\frac{2 r_p\, {\rho_c}^3 (aP^n)^3\, \mu R^2 {T_s}^2}{M^2 P^2}} + \right.$$
$$\left. + \frac{0.12\, r_p\, {\rho_c}^2 (aP^n)^2 R T_s}{MP} \right] \tag{7.20}$$

The analysis of the forces gives results similar to the ones obtained considering the Oseen's assumption, but with a reduced scale factor of about 10.

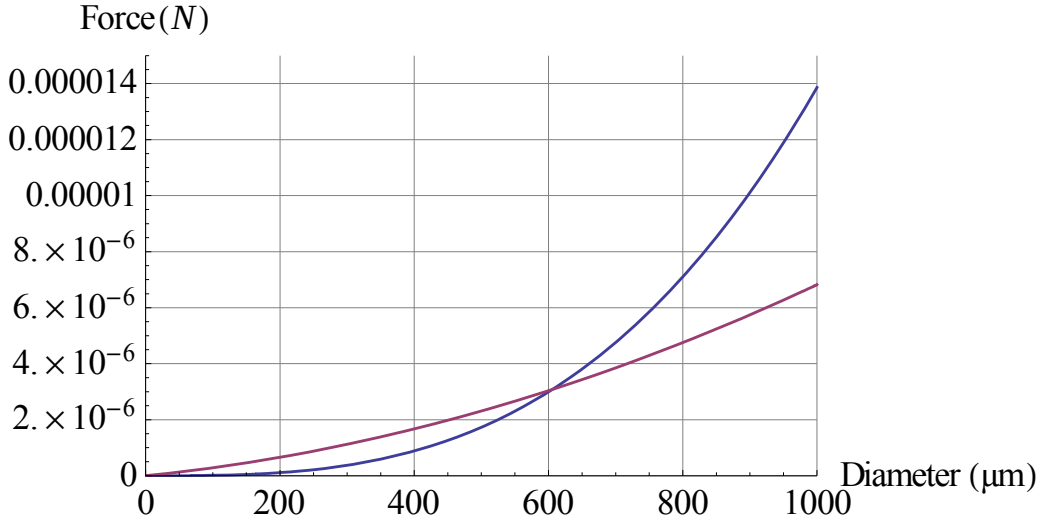

Fig. 7.7. Drag and weight forces (4th order approx.) for aluminium at 0.1 MPa

It is noticeable that the behaviour of drag force has the same shape of the one in the Oseen's case. But the size increment is less marked than that obtained using Oseen's model, as it is possible to see from Fig. 7.7.
Also for the Fourth Order Approximation the increase of density gives rise to agglomeration of lower dimension.
After some minor passages, and applying the hypotheses of Eq. 7.11, it is possible to rewrite Eq. 7.20 in the following form

$$r_p^2 \frac{16}{3} \rho_p g_0 - r_p \left(0.84 \frac{{\rho_c}^2 R T_s}{MP} (aP^n)^2\right) - \\ -\sqrt{r_p}\, 4.4 \sqrt{2\mu \frac{{\rho_c}^3 R^2 {T_s}^2}{M^2 P^2} (aP^n)^3 - 24\mu \frac{\rho_c R T_s}{MP} aP^n} = 0 \qquad (7.21)$$

By substituting the unknown r_p with the variable δ,

$$\delta = \sqrt{r_p}$$

it is clear that Eq. 7.21 is a fourth order equation of the type

$$a\delta^4 + b\delta^2 + c\delta + d = 0$$

which can be solved with the Ferrari`s method.
The four solutions are not reported here for a manner of space, but the study of the pressure influence on the particle size leads to results that do not differ from the ones obtained with the Oseen's drag coefficient, with a similar increment of dimension with the increment of size (see Fig. 7.8).

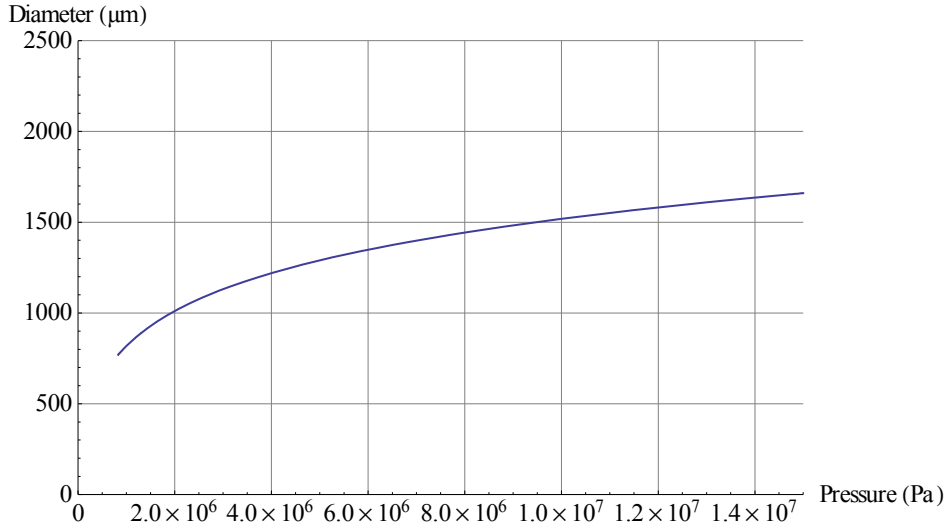

Fig. 7.8. Size vs. pressure (4th order approx.)

7.1.4 2P Flow Drag Coefficient

In the case of two phase (2P) flow, like the one under consideration here for agglomerate production, it is convenient to introduce the volumetric solid fraction Z of the 2P mixture (gas+particles). By definition, $Z \equiv V_p/V$ being V_p the particle volume with respect to the total volume $V=V_g+V_p$. Under these circumstances, the classical Stokes expression is replaced (see Pai [77]) by

$$\begin{cases} Re < 0.1 \\ Z > 0.1 \\ C_d = \frac{200}{Re} \frac{Z}{(1-Z)^2} \end{cases} \tag{7.22}$$

Starting from Eq. 7.8 and applying the stationarity condition in concomitance with the Eqns. 7.4, 7.6 and 7.7, the force balance obtained is not so different from Eq 7.12, and also the radius equation is similar to Eq 7.14, in fact

$$\frac{4}{3}\pi {r_p}^3 \rho_p g_0 = 50\pi {r_p}^2 \frac{6RT_s}{r_p MP} \rho_c a P^n \mu \frac{Z}{(1-Z)^2} \tag{7.23}$$

$$r_p = \sqrt{\left(\frac{75\,\rho_c RT_s a P^n}{2\rho_p g_0 MP} \frac{Z}{(1-Z)^2}\right)\mu} \tag{7.24}$$

However, the explicit introduction of the volumetric solid fraction Z leads to predicted results much closer to the experimental observations, as shown in Fig. 7.9 and Fig. 7.10.

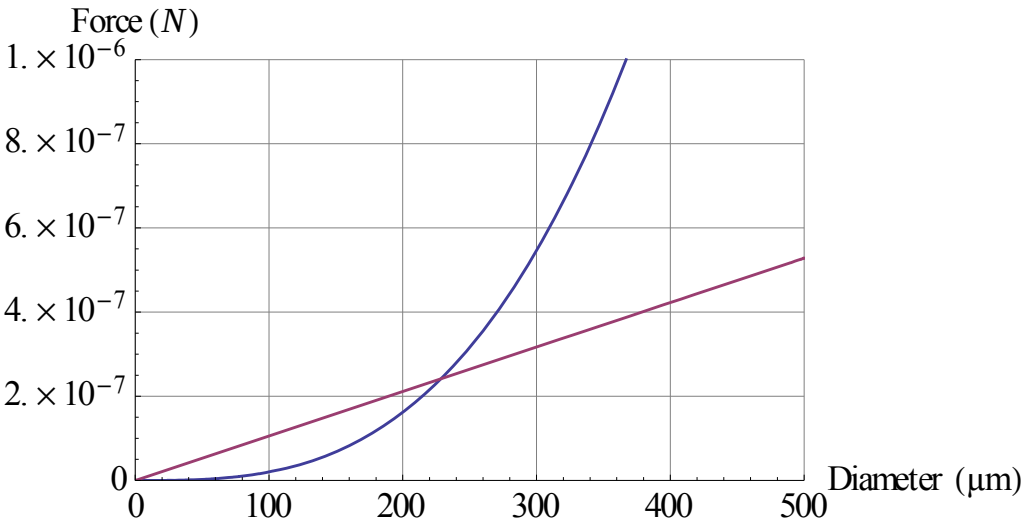

Fig. 7.9. Drag and weight forces (Modified Stokes) for alumina at 0.1 MPa

The volumetric solid fraction Z offering the best fit of the experimental results is 0.048 if a temperature between 900 and 2550 K is considered (Fig. 7.10). The volumetric solid fraction Z is related to the mass solid fraction Y by means of the following simple expression $Y = Z\,\rho_p / \rho$ being ρ the 2P mixture density. Thus Z=0.048 corresponds to Y= 0.30 that is the volumetric solid fraction calculated for the ADN/GAP/Al formulations at 7 MPa.

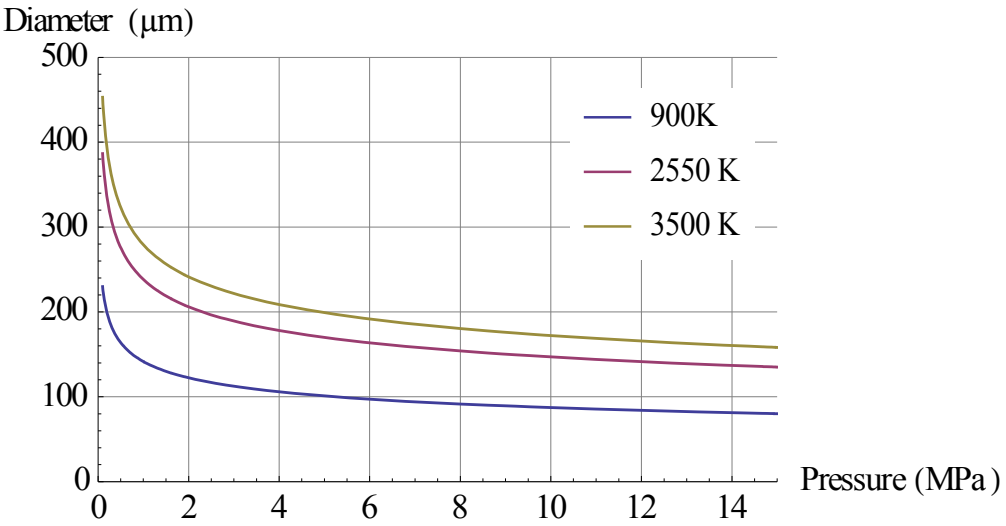

Fig. 7.10. Size vs. pressure (Modified Stokes)

7.2 Reynolds Number Estimation and Discussion

The various considerations made until now can be applied in particular to the agglomeration results presented in Chap. 5.

7.2.1 Reynolds Number Estimation

However, the temperature around the agglomerate might be appreciably different from those measured for the basic propellant matrix (2550 K for ADN/GAP/Al formulation).

Starting from the definition of Reynolds number (Eq. 7.10) and applying the Eqns. 7.4 and 7.6, it is possible to get an analytical equation for Reynolds number as

$$Re = \frac{1}{\mu}\left(2r_p\,\rho_c r_b - 2r_p\,\frac{PM}{RT}u\right) \tag{7.25}$$

In order to get a pressure dependency of the Reynolds number, some fitting the experimental agglomerate size results were tried.

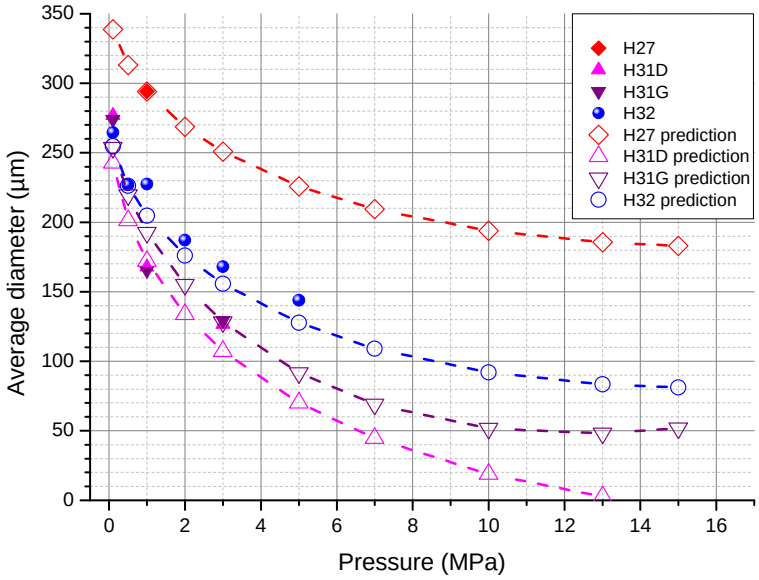

Fig. 7.11. Comparison between observed and predicted agglomerate sizes.

The fitting was done on the results of the ADN/GAP/Al formulation.
A fitting with equation having a similar shape of the function presented in Fig. 7.10 was tried unsuccessfully, so it was decided to get a polynomial fitting with a second order equation

$$d_p = 0.1(\,aP^n)^2 - a^2P^n + d_0 \tag{7.26}$$

where d_0 is the diameter measured at 0.1 MPa and d_p is the expected agglomerate size for ADN/GAP/Al formulation.
The heuristically proposed Eq. 7.26 fits relatively well the observed agglomerate diameter and leads to an extrapolation of size for higher pressure, as shown in Fig. 7.11.
Substituting the Eq. 7.26 into the Eq. 7.25, it is possible to get a Reynolds number in function of pressure (considering also u=0),

$$Re = \left\{\frac{1}{\mu}[0.1(aP^n)^2 \; - a^2P^n + d_0]\,\rho_c aP^n\right\} \tag{7.27}$$

and applying the hypothesis of fully reacted gas to calculate the viscosity, an estimation of the Reynolds number is possible.
The Sutherland's formula acts decreasing the estimated Reynolds with increase temperature (see Fig. 7.12).

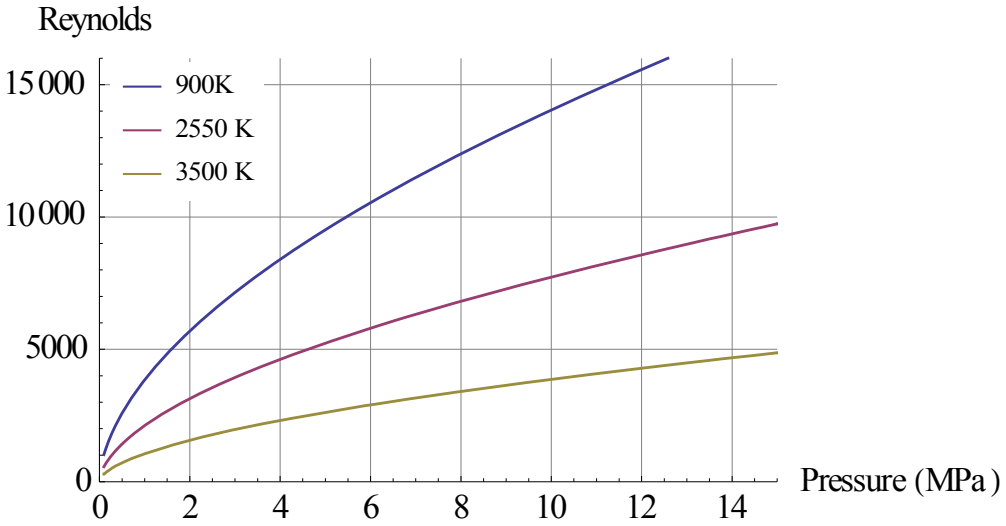

Fig. 7.12. Reynolds number for zero velocity agglomerate at different temperatures

7.2.2 Discussion of the Results

The results obtained were far from both the hypothesis of low and high Reynolds numbers since Reynolds seems to be always higher than 100 and may reach values higher than 10^4. This regime stays in between the laminar and the turbulent flow, and therefore different empirical equations for the drag coefficient should be used. However, the Stokes's solution seems to offer a reasonable estimate since it somehow reflects the behaviour experimentally observed and gives size results in the same order of magnitude of the observations. So the empirical drag coefficient should have an inverse dependency from Reynolds.

Looking at Fig. 7.13, which shows the behaviour of drag coefficient in function of Reynolds number for an isolated sphere, it would seem logical to assume a drag coefficient close to one for the calculated regime. However, this would result in a behaviour similar to that observed with Oseen model, with an expectation of detachment size increase with increasing pressure.

The solutions obtained require strong assumptions (perfect and fully reacted gas, homogeneous phase, isolated particle, validity of Sutherland law, polynomial extrapolation) but lead to an estimation of the Reynolds number which is definitively out of the usual hypothesized Reynolds range.

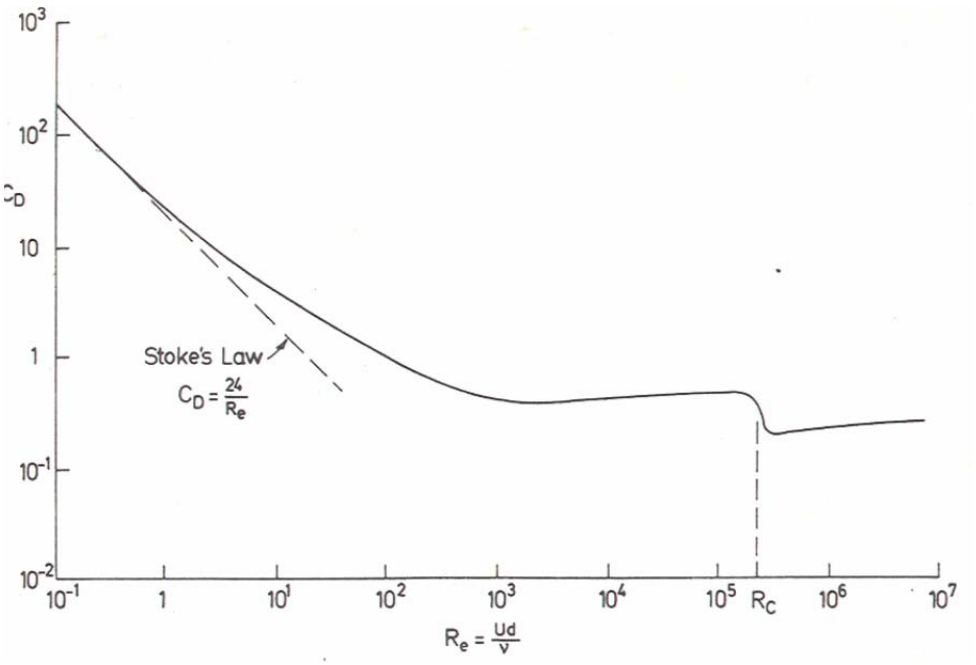

Fig. 7.13. Drag coefficient vs. Reynolds number for isolated sphere

The three expressions of drag coefficient considered cover two different Reynolds ranges, and the calculated Reynolds seems to fall in the range of the fourth order approximation model. Anyway, the best results are surprisingly obtained using the Stokes's expression that should be not valid over the Reynolds range calculated for the agglomerate. This means that a further empirical expression of the drag coefficient of the "Stokes-type" should be used.

For all the tested models a quadratic tendency of increasing particle sizes for increasing burning rate and a linear correlation between the considered temperature and the estimate size were observed.

It has to be pointed that these models are extremely simple, and they do not take into account some important feature like the real shape of the agglomerate, the strong reactive media in which they are immerse, the possible existence of a vaporised aluminium boundary layer, the retainment forces and the real temperature of the flowing gases.

7.3 Concluding Remarks

Different drag coefficient models were investigated in order to get a rough estimation of the expected agglomerate size that can detach from the burning surface. Within the validity of the assumptions made, it was possible to estimate the Reynolds number of the hot gases around the agglomerate. This results in a flow regime where the standard Stokes

equation is no longer valid. Despite that, the most realistic trends were obtained with the use of such a model, especially if the volumetric solid fraction Z is explicitly taken into account (see below).
The other tested models (Oseen and fourth order approximation), which in principle should fit better than Stokes, results in trends opposite to those experimentally observed and overestimate the dimension of the detaching particles.
The most consistent trends were obtained using the two-phase flow model (Eq. 7.24 and Fig. 7.10) proposed by Pai. This result in the same pressure dependence observed for the standard Stokes model, and in a size range closer to that experimentally obtained. As a matter of fact, both the simple Eq. 7.12 (for Z = 0) or Eq. 7.23 (for Z = finite) results in a range of agglomeration size that is close to the one experimentally observed for the tested ADN/GAP/Al formulations. A further and probably more important result is the obtained dependence of agglomerate size on pressure: compare Fig. 7.4 (Z = 0) and Fig. 7.10 (Z = finite) with the experimental trend shown in Fig. 7.11.
Actually, the above conclusion was unexpected since the Pai model is valid for Reynolds number lower than 0.1 and for volumetric solid fraction of the combustion products higher than 0.1. Yet, over the investigated pressure range of the tested formulations and for volumetric solid fractions of the same order of the calculated for AND/GAP/Al formulation (0.048), it turned out to be the best performer.
All this implies that, under the investigated operating conditions and within the invoked assumptions, the drag coefficient is much larger than the corresponding value for isolated inert spheres immersed in a viscous flow.

Chapter 8

Conclusions and Outlook

8.1 General Remarks

Several burning tests were carried out for the selected compositions, including ADN/GAP with and without aluminium or alane. A good evaluation of the burning rates and flame temperatures has been discussed deeply for the first characterization of this new kind of green propellants.
These formulations promise specific impulse higher than the widely used AP/HTPB/Al propellants (Tab 3-3), with potential enhancement of payload mass of more than 30% for launchers like Vega, and about 30 kg mass saving for a intended mars ascent vehicle (with an estimation cost reduction between 150000$ and 225000 $ [5]). However, these estimations were based on ideal thermochemical calculations.
The behaviour of the burning rate with respect of the ADN prill size has been studied, and a correlation has been observed: the reduction of dimension of ADN prills reduces the burning rate (Fig. 5.4 and Annex 1). Also a maximum dimension of ADN prills is related with a maximum reachable burning rate. Unfortunately, the observed burning rates of 25 to 30 mm/s at 7 MPa (Tab. 5-1, Tab. 5-2 and Tab. 5-4) were very high for the application that is aimed for this work, and also the higher achieved temperatures by this propellant are a weak point (Fig. 5.6, Fig. 5.16-5.18, Fig. 5.35).
The high thermal load provided by this new kind of propellant requires an increased thermal shielding mass, and consequently, an increase of inert mass of the complete system.
The supposed benefit in volumetric specific impulse is less remarkable because of the loading factor of aluminium in AP/HTPB-based formulations, in fact this reference propellants presents a density of 1.759 g/cm^3 against 1.735 g/cm^3 of formulation H32 (Tab. 3-3).
All the propellants do not reach the mechanical property of the reference propellant. But the mechanical properties can be enhanced drastically by using ADN with a lower prill size.

8.2 Agglomeration

Agglomeration measurements have been carried out for all composition containing metals, and results were presented in Chap. 5. All the formulations containing ADN show the tendency to create agglomerates bigger than the commercial propellants (Tab. 5-3 and Tab 5-5), and this could be a problem for the discussed 2P loss. However, has been observed also the tendency of these propellants to reach higher flame temperature, sometime close to the boiling point of alumina (Fig. 6.5 and Fig. 6.11), and this could lead to a complete vaporizations of the agglomerates during their permanence inside combustion chamber.
Since the equation used for the estimation of the 2P loss (Eq 2.3) was validated only for AP/HTPB/Al propellants, it is not possible at this time to predict the 2P loss for these new kinds of formulations. For a correct estimation of this loss medium and full scale tests are required, since the 2P loss is manifested mostly in the nozzle.
Several tests on compositions based on AP/HTPB/Al were performed in order to study the dependency of the agglomeration size with respect to ideal thermodynamic calculation (agglomeration results in Tab. 5-7).
A common trend between formulation with the different oxidizer but same oxidizer prills dimension and same heat of formation has been observed, but conclusions on that are difficult because of the low number of common results. However, a correlation between agglomeration size and flame temperature is found: the increase of temperature leads to an increase of dimension of agglomerates (comparison between Figs. 6.14-6.17). This trend is superposed by the pressure dependency.
It has been demonstrated that the dimension of the agglomerates do not depend only on the metals or oxidiser size and concentration (that control the pocket dimension), temperature and pressure, but also on the type of binder, in fact changing the binder from GAP to GA/BAMO the agglomeration size was reduced (comparison between Formulations A1 and A7 in Fig. 6.17), enhancing also the mechanical properties.
The study conducted on the detachment model results in a good approximation of the experimental results provided by the use of the 2 phase flow drag coefficient approximation. However, the validity of this approximation has to be demonstrated with further investigations since it seems to be used outside the validated range of Reynolds and volumetric solid fraction.

8.3 Outlook and Future Tasks

Small and medium scale test will be performed in future in order to confirm the results obtained from this first lab-level characterization and assess, in particular, 2P flow losses for delivered specific impulse..
Perhaps that a formulation based on a monomodal distribution of small ADN prills dimension (about 40 μm) and nano-aluminium will obtain lower burning rates, lower temperature and lower agglomerations.
A change in binder from GAP to GA/BAMO can enhance the mechanical property and reduce the dimension of agglomerates without changing the combustion behaviour.
Concerning the 2P loss, all the existent methods for the determination of loss, and also for the estimation of agglomerate sizes, are optimized for AP/HTPB/Al formulations so an omni-comprehensive methods which taking into account different binders and different oxidizers must be developed.

References

[1] V. Weiser, A. Franzin, V. Gettwert, and L. T. DeLuca, “Combustion of Metallised ADN/GAP Solid Rocket Propellants with Focus on Agglomeration Effects”, EuCASS-Propulsion Physics, Munich, 2013.

[2] V. Weiser, A. Franzin, L.T. De Luca, S. Fischer, V. Gettwert, S. Kelzenberg, S. Knapp, J. Neutz, A. Raab, E. Roth, “Combustion Behaviour of Aluminium Particles in ADN/GAP Composite Propellants”, HEM Workshop, Tokyo, 2013.

[3] L. T. DeLuca, F. Maggi, S. Dossi, V. Weiser, A. Franzin, V. Gettwert, T. Heintz, “High-energy Metal Fuel for Rocket Propulsion: Characterization and performance”, Chinese Journal of Explosives and Propellants, Vol. 20, N^{o} 6, 2013.

[4] N. Wingborg, “High Performance Solid ADN Propellant for Space Applications”, EuCASS-Propulsion Physics, Munich, 2013.

[5] M. Calabro, “FP7 HISP Program: Selection of Reference Missions and Definition of Propellant Requirements”, EuCASS-Propulsion Physics, Munich, 2013.

[6] H. Arisawa and T. B. Brill, “Thermal Decomposition of Energetic Materials: Structure-Decomposition and Kinetic Relationships in Flash Pyrolysis of Glycidyl Azide Polymer (GAP)”, Combustion And Flame, Vol.112, 1998, pp.533-544.

[7] G. Ampleman, United State Patent number 5.256.804, 1980.

[8] K. Hori, “Combustion Mechanism of Glycidyl Azide Polymer”, Propellant, Explosive, Pyrotechnics, Vol. 21, 1996, pp. 160-165.

[9] N. Kubota, “Propellants and Explosives: Thermochemical Aspects of Combustion”, 2nd edition, Wiley-VCH, 2007.

[10] N. Kubota and T. Sonobe, “Combustion Mechanism of Azide Polymer”, Propellant, Explosive, Pyrotechnics, Vol. 13, 1988, pp. 172-177.

[11] N. Kubota, T. Sonobe, A. Yamamoto and H. Shimizu, “Burning Rate Characteristics of GAP Propellants”, Journal of Propulsion, Vol. 6, 1990, pp. 686-689.

[12] C. Tang, Y. Lee and T. A. Litzinger, “Simultaneous Temperature and Species Measurements of the Glycidyl Azide Polymer (GAP) Propellant During Laser-Induced Decomposition”, Combustion and Flame, Vol.117, 1999, pp. 244-256.

[13] M. B. Frankel, L. R. Grant, and J. E. Flanagan, “Historical Development of Glycidyl Azide Polymer”, Journal of Propulsion and Power, Vol. 8, 1992, pp. 560-563

[14] E. W. Price, S. R. Chakravarthy, J. M. Freeman, and R. K. Sigman, "Combustion of Propellants with Ammonium Dinitramide", AIAA Paper No. 3387, 1998.

[15] S. R. Chakravarthy, J. M. Freeman, E. W. Price, and R. K. Sigman, "Combustion of propellants with Ammonium Dinitramide", Propellant, Explosive, Pyrotechnics, Vol. 29, 2004, pp. 220-230.

[16] A. I. Atwood, T. L. Boggs, P. O. Curran, T. P. Parr, D. M. Hanson-Parr, C. F. Price, and J. Wiknich, "Burning Rate of Solid Propellant Ingredients, Part 1: Pressure and Initial Temperature Effects", Journal of Propulsion and Power, Vol. 15, 1999, pp. 740-747.

[17] A. I. Atwood, T. L. Boggs, P. O. Curran, T. P. Parr, and D. M. Hanson-Parr, C. F. Price, and J. Wiknich, "Burning Rate of Solid Propellant Ingredients, Part 2: Determination of Burning Rate Temperature Sensitivity", Journal of Propulsion and Power, Vol. 15, 1999, pp. 748-752.

[18] F. Volk, H. Bathelt, "User's Manual for the ICT-Thermodynamic Code", Vol.1, Report 14/88, Fraunhofer-ICT, Pfinztal.

[19] A. E. Fogelzang, V. P. Sinditskii, V. Y. Egorshev, A. I. Levshenkov, V. V. Serushkin, and V. I. Kolesov, "Combustion Behavior and Flame Structure of Ammonium Dinitramide", 28th International Annual Conference of ICT, Karlsruhe, 1997, p. 99.

[20] V. P. Sinditskii, V. Y. Egorshev, A. I. Levshenkov, and V. V. Serushkin, "Combustion of Ammonium Dinitramide, Part 1: Burning Behavior", Journal of Propulsion and Power, Vol. 22, 2006, pp. 769-776.

[21] V. P. Sinditskii, V. Y. Egorshev, A. I. Levshenkov, and V. V. Serushkin, "Combustion of Ammonium Dinitramide, Part 2: Combustion Mechanism", Journal of Propulsion and Power, Vol. 22, 2006, pp. 777-785.

[22] S. Venkatachalam, G. Santhosh, K. N. Ninan, "An Overview on the Synthetic Routes and Properties of Ammonium Dinitramide (ADN) and other Dinitramide Salts", Propellants, Explosive and Pyrotechnics, Vol. 29, 2004, pp. 178-187.

[23] W. Kim, S. Hang, Y. Kwon, Y. Jo, Y. C. Park, "Yield and Purity of ADN Depending on Potassium Sulfamate", 44th International Annual Conference of ICT, Karlsruhe, 2013, p. 1.

[24] T. Heintz, H. Pontius, J. Aniol, C. Birke, K. Leisinger and W. Reinhard, "Ammonium Dinitramide (ADN) – Prilling, Coating, and Characterization", Propellants, Explosive and Pyrotechnics, Vol. 34, 2009, pp. 231-238.

[25] U. Teipel, T. Heintz, H.H. Krause, "Crystallization of Spherical Ammonium Dinitramide (ADN) Particles", Propellants, Explosive and Pyrotechnics, Vol. 25, 2000, pp. 81-85.

[26] M. Johansson, J. de Flon, A. Pettersson, M. Wanhatalo, and N. Wingborg, “Spray Prilling of ADN, and Testing of ADN-Based Solid Propellants”, 3rd International Conference on Green Propellants for Space Propulsion, ESA, Poitiers, 2006.

[27] Z. P. Pak, “Some Ways to Higher Environmental Safety of Solid Rocket Propellant Application”, AIAA Paper No. 93-1755, 1993.

[28] V. Weiser, N. Eisenreich, A. Baier, W. Eckl, “Burning Behaviour of ADN Formulations”, Propellants, Explosive, Pyrotechnics, Vol. 24, 1999, pp. 163-167.

[29] E. Landsem, T. L. Jensen, F. K. Hansen, E. Unneberg, and T. E. Kristensen, “Mechanical Properties of Smokeless Composite Rocket Propellants Based on Prilled Ammonium Dinitramide", Propellants, Explosive and Pyrotechnics, Vol. 37, 2012, pp. 691-698.

[30] N. Kubota, T. Sonobe, “Burning Rate Catalyst of Azide/Nitramine Propellants”, 23rd international Symposium on Combustion, The Combustion Institute, Pittsburgh, 1990, pp. 1331-1337.

[31] K. Menke, T. Heintz, W. Schweikert, T. Keicher, H. Krause, “Formulation and Properties of ADN/GAP Propellants”, Propellants, Explosive, Pyrotechnics, Vol. 34, 2009, pp. 218-230.

[32] V. Gettwert, S. Fischer, K. Menke, “Aluminized ADN/GAP Propellants – Formulation and Properties”, 44th International Annual Conference of ICT, Karlsruhe, 2013, p. 57.

[33] G. P. Sutton and O. Biblarz. “Rocket propulsion elements”, John Wiley &Sons, Hoboken, NJ, USA, 7th edition, 2001.

[34] L. T. De Luca, “Problemi energetici in propulsione aerospaziale, Appunti per studenti”, Politecnico di Milano, Milano, Italia, 2007.

[35] R. W. Humble, G. N. Henry, and W. J. Larson, “Space Propulsion Analysis and Design”, McGraw-Hill, 1995.

[36] A. Larsson and N. Wingborg, “Green Propellants Based on Ammonium Dinitramide (ADN)”, Advances in Spacecraft Technologies, Dr Jason Hall (Ed.), 2011.

[37] V. M. Gremyachkin, A. G. Istratov and O. I. Leipunskii, “Model for the Combustion of Metal Droplets”, Translated from Fizika Goreniya i Vzryva, Vol. 11, 1974, pp. 366-373.

[38] M. W. Beckstead, “A Summary of Aluminum Combustion”, NATO RT-EN-23, 2002.

[39] S. Dossi, “Effetti della Struttura di Fiamma sull’Agglomerazione nei Propellenti Solidi Eterogenei Alluminizzati”, Politecnico Di Milano, 2010.

[40] J. K. Sambamurthi, E. W. Price and R. K. Sigman, “Aluminium Agglomeration in Solid-Propellant Combustion”, AIAA journal, Vol. 22, 1983, pp. 1132-1138.

[41] N. S. Cohen, “A Pocket Model for Aluminium Agglomeration in Composite Propellants”, AIAA Journal, Vol. 21, 1983, pp. 720-725.

[42] L. T. DeLuca, “Burning of Aluminazed Solid Rocket Propellants: from Micrometric to Nanometric Fuel Size”, Theory and Practice of Materials, IASPEP, Vol. 6, Xi'an, 2007.

[43] V. Weiser, W. Eckl, N. Eisenreich, S. Kelzenberg, Y. Plitzko, S. Poller, E. Roth, “Burning Behaviour of aluminised Composite Propellants Including Nanoparticle”, 3rd European Combustion Meeting, ECM, 2007.

[44] A. A. Gromov, E. M. Popenko, “Aluminium Nanoparticle burning-Still a Puzzle?”, Progress in Propulsion Physics, Vol.1, 2009, pp.17-30.

[45] N. Wingborg, M. Wanhatalo, A. Petterson, “Solid Propellants Containing Activated Aluminum”, 3rd International Conference on Green Propellant for Space Propulsion, ESA, Poitiers, 2006, p. 635.

[46] A. Hahma, A. Gany, and K. Palovuori, “Combustion of activated aluminium”, Combustion and Flame, Vol. 145, 2006, pp. 464–480.

[47] L. Facciolati, “Mechanical Activation of Energetic Materials”, Politecnico di Milano, 2013.

[48] S. Dossi, F. Maggi, L. Facciolati and L. T. De Luca, “Activation of Micrometric Aluminum – Metal Oxide Mixtures by Mechanical Milling”, EuCASS-Propulsion Physics, Munich, 2013.

[49] V. Weiser, N. Eisenreich, A. Koleczko, E. Roth, “On the Oxidation and Combustion of AlH_3 a Potential Fuel for Rocket Propellants and Gas Generators”, Propellants, Explosives, Pyrotechnics, Vol. 32, 2007, pp. 213-221.

[50] L. T. DeLuca, L. Rossettini, C. Kappenstein and V. Weiser, “Ballistic Characterization of AlH_3-Based Propellants for Solid and Hybrid Rocket Propulsion”, 45th Joint Propulsion Conference & Exhibit, AIAA, Denver, 2009.

[51] L. T. DeLuca, L. Galfetti, F. Severini, L. Rossettini, L. Meda, G. Marra, B. D’Andrea, V. Weiser, M. Calabro, A. B. Vorozhtsov, A. A. Glazunov, G. J. Pavlovets, “Physical and Ballistic Characterization of AlH_3-based Space Propellants”, Aerospace Science and Technology, Vol.1, 2007, pp.18-25.

[52] V. A. Babuk, V. A. Vasilyev, and M. S. Malakhov,” Condensed Combustion Products at the Burning Surface of Aluminized Solid Propellant”, Journals of Propulsion and Power, Vol. 15, 1999.

[53] V. A. Babuk, “Study of Metal Agglomeration and Combustion”, project SPC-97-4033-1, Final Report, Baltic state University, 1998.

[54] E. W. Price, R. K. Sigman, J. K. Sambamurthi and, C. J. Park, “Behavior of aluminum in solid propellant combustion”, Georgia institute of technology, School of aerospace engineering, 1982.

[55] O. G. Glotov, “Condensed Combustion Products of Aluminized Propellants. II. Evolution of Particles with Distance from the Burning Surface”, Combustion, Explosion, and Shock Waves, Vol. 36, 2000.

[56] D. Reydellet, “Performance of rocket motors with metallized propellants”, in AGARD Advisory Report AR-230, AGARD PEP WG-17, Paris, 1986.

[57] R. W. Hermsen, “Aluminum oxide particle size for solid rocket motor performance prediction”, AIAA JSR Journal, Vol. 18, 1981, pp. 483-490.

[58] L. T. De Luca, E. Marchesi, M. Spreafico, A. Reina, F. Maggi, L. Rossettini, A. Bandera, G. Colombo, and B. M. Kosowski, “Aggregation versus Agglomeration in Metallized Solid Propellants”, Journal of Energetic Materials and Chemical Propulsion, Vol. 9, 2010, pp. 91-105.

[59] M. Calabro, “Selection of reference missions and definition of propellant requirements”, Delivery No. D1.1, FOI-2010-1487, HISP European Commission, 2011.

[60] C. Boyars and K. Klager, “Propellants Manufacture, Hazards, and Testing”, American Chemical Society, No. 88, Washington, DC, 1969.

[61] W. Kim, S. Hang, Y. Kwon, Y. Jo, Y. C. Park, “Yield and Purity of ADN Depending on Potassium Sulfamate”, 44th International Annual Conference of ICT, Karlsruhe, Germany, 2013, paper 1.

[62] J. P. W. McCarthy and H. M. Whitehead, “Decomposition and combustion of ammonium perchlorate” Chemical Reviews, Vol.69, 1969, pp. 551-590.

[63] L. J. Shannon and E. E. Petersen, “Deflagration Characteristics of Ammonium Perchlorate Strands”, AIAA Journal Vol.2, 1969, pp. 168-169.

[64] V. Gettwert, unpublished results.

[65] V. Weiser, H. Ebeling, M. Weindel, W. Eckl, T. Klahn, “Non-intrusive burning rate measurement under pressure by evaluation of video data”, 35th International Annual Conference of ICT, Karlsruhe, 2004, p. 6.

[66] C. B. Ludwig, W. Malkmus, J.E. Reardon, J. A. L. Thomson, “Handbook of Infrared Radiation from Combustion Gases”, Report NASA-SP-3080, 1973.

[67] G. Herzberg, “Molecular Spectra and Molecular Structure, I. Spectra of Diatomic Molecules”, Second Edition 1950.

[68] V. Weiser, N. Eisenreich, “Fast Emission Spectroscopy for a Better Understanding of Pyrotechnic Combustion Behaviour”, Propellants, Explosive, Pyrotechnics, Vol. 30, 2005, pp. 67-78.

[69] L. T. DeLuca, L. Galfetti, F. Maggi, G. Colombo, A. Reina, S. Dossi, D. Consonni, and M. Brambilla, "Innovative Metallized Formulation for solid or Hybrid Rocket Propulsion", Chinese journal of energetic materials, Vol. 20, 2012, pp. 465-474.

[70] K. Fujisato, "Combustion characteristics of ADN-based solid propellants", Europyro2011, 2011, p. 64.

[71] N. Wingborg, S. Andreasson, J. de Flon, M. Johnsson, M. Liljedahl, C. Oscarsson, A. Pettersson, and M. Wanhatalo, "Development of ADN-based Minimum Smoke Propellants ", AIAA, 2010, p. 6586.

[72] F. Maggi, A. Bandera, L. T. DeLuca, V. Thoorens, J. F. Trubert and T. L. Jackson, "Agglomeration in Solid Propellants: Novel Experimental and Modelling Method", Progress in propulsion Physics Vol. 2, 2011, pp. 81-98.

[73] S. Knapp, D. Bieroth, S. Kalzenberg, A. Raab, V. Weiser, W. Eckl, "New Approach for Simple Temperature Measurements of Metals Combustion", 44th International Annual Conference of ICT, Karlsruhe, 2013, p. 67.

[74] R. Clift, J. R. Grace, M. E. Weber, "Bubbles, Drops, and Particles", Academic Press, Inc., 1978.

[75] B. Veyssiere, B. Khasainov, "A Model for Steady, Plane, Double-Front Detonations in Gaseous Explosive Mixture with Al Particles in Suspension", Combustion and Flame, Vol.85, 1991, pp. 241-253.

[76] A. L. Kuhl, J. B. Bell, V. E. Beckner, "Heterogeneous Continuum Model of Aluminium Particle combustion in Explosions", Combustion, Explosion and Shock Wave, Vol. 46, 2010, pp. 433-448.

[77] S. I. Pai, "Two-Phase Flows", Vieweg, Braunshweig, Germany, 1977, pp. 122.

Appendix 1

Average of the burning rate measured for the different formulations

Tab. 1 Mean of the burning rate of ADN/GAP formulations

Pressure [MPa]	H55 ADN 212 µm [mm/s]	H56 ADN 153 µm [mm/s]	H57 ADN 55 µm [mm/s]	H59 ADN 40 µm [mm/s]	H60 Raw ADN [mm/s]
1	9.78	8.5	10.06	8.92	10.52
2	13.12	--	--	--	--
4	19.35	21	22.06	19.77	27.49
7	28.33	26.25	28.76	27.21	41.68
10	40.07	44.61	29.36	31.83	64.57
13	--	43.86	33.34	31.44	81.39

Tab. 2 Mean of the burning rate of ADN/GAP/Al and ADN/GAP/Alane formulations

Pressure [MPa]	H31G [mm/s]	H31D [mm/s]	H32 [mm/s]	H27 [mm/s]	H53 [mm/s]	H54 [mm/s]
0,1	--	--	2.35	--	5.36	6.24
0,5	--	--	6.48	--	--	--
1	9.31	11.06	7.47	9.3	10.97	13.24
2			13.07	13.015	--	--
3	19.69	18.82	16.96	--	15.07	1.92
4	--	--	--	18.26	--	--
5	--	--	22.78	--	19.01	--
7	36.22	28.4	29.57	28.23	22.52	24.16
10	37.89	38.31	35.58	33.98	28.51	30.81
11	--	--	34.14	--	--	--
13	--		34.53	39.61	31.04	37.99
14	--	--	45.31	38.43	--	--
15	--	--	39.26	--	33.93	--

Tab. 3 Formulation's compositions

Label	ADN [%]	GAP [%]	Al [%]	Alane [%]
H31G	60 (208 µm)	24	16	--
H31D	60 (208 µm)	24	16	--
H32	60 (208/55 µm)	24	16	--
H27	60 (228 µm)	24	16	--
H53	60 (208/55 µm)	24	--	16
H54	52 (208/55 µm)	22	--	26